



Norwegian University of
Science and Technology

Stability assessment of the underground powerhouse cavern for the Sach Khas hydroelectric project in Himachal, India

Ajender Rathore

Hydropower Development

Submission date: June 2016

Supervisor: Krishna Kanta Panthi, IGB

Norwegian University of Science and Technology
Department of Geology and Mineral Resources Engineering



Your ref.: MS/I12T36/IGB/ARKKP

Date: 08.01.2016

TGB4910 Rock Engineering - MSc thesis
for
Ajender Rathore

STABILITY ASSESSMENT OF THE UNDERGROUND POWERHOUSE CAVERN FOR THE
SACH KHAS HYDROELECTRIC PROJECT IN HIMACHAL, INDIA

Background

The Chenab River Basin in North Western part of Himachal Pradesh offers attractive sites for the Hydropower Projects. Many hydropower projects are being implemented in this river valley and one of such projects under the process of implementation is 260 MW Sach Khas Hydroelectric Project. This project will utilize the drop between Purthi (EL 2219 masl) and Cheni Nala (EL 2149 masl) by constructing a 90m high concrete gravity dam located approximately 8 km downstream of Purthi Village. Then the water will be discharged from the dam to the underground power house through three underground settling basin and 3 penstock lined pressure shafts of 5.8m diameter.

The length of the underground cavern is 130m and is 23m wide and 47m high. The cavern is located at relatively shallow depth varying between 45m (minimum) and 70m (maximum). Geologically, the underground powerhouse cavern is placed in fine grained massive quartzite with schistose phyllitic veins representing weakness planes. Therefore, stability situation in the underground cavern is a real challenge for underground cavern excavation.

MSc thesis task

Hence, this MSc thesis is to focus on the documentation, overall evaluation of the Sach Khas Hydroelectric Project with particular focus on the detailed stability assessment of the underground powerhouse and service hall with a focus on following issues:

- Review existing theory on the stability connected to the large underground caverns.
- Briefly describe Sach Khas Hydroelectric Project including review on the geological condition at the project area and extent of engineering geological investigations carried out during planning.

- Document engineering geological and mechanical properties of the rock mass at underground powerhouse
- Document rock support principles and excavation philosophy to be used for the powerhouse
- Carry out stability assessment of the powerhouse cavern using empirical and analytical approaches.
- Assess stability condition of the underground powerhouse using Wedge-Unwedge
- Assess stability condition of the underground powerhouse using RS2 (Phase2) and RS3 approaches.
- Discuss the analysis results from empirical, analytical and numerical approaches
- Conclude the work and give recommendation.

Relevant computer software packages

Candidate shall use *roc-science package, auto-CAD* and other relevant computer software for the master study.

Background information for the study

- Relevant information about the project such as reports, maps, information and data collected by the candidate.
- The information provided by the professor about rock engineering and hydropower.
- Scientific papers, reports and books related to the Himalayan geology and tunnelling.
- Scientific papers and books related to international tunnelling cases.
- Literatures in rock engineering, rock support principles, rock mechanics and tunnelling.

The project work is to start on January 11, 2016 and to be completed by June 10, 2016.

The Norwegian University of Science and Technology (NTNU)
Department of Geology and Mineral Resources Engineering

January 08, 2016



Dr. Krishna K. Panthi
Associate Professor of geological engineering, main supervisor

PREFACE AND ACKNOWLEDGEMENT

This master thesis has been conducted at the Department of Geology and Mineral Resources Engineering, as a part of the Master's Degree Programme, Hydropower Development conducted by Department of Hydraulic and Environmental Engineering, Norwegian University of Science and Technology (NTNU). Associate Professor Krishna Kanta Panthi has been my main supervisor.

The work presented here is my own and the sources used for the background and theory behind the work is duly acknowledged.

This thesis work has been done under the guidance of Associate Prof. Dr. Krishna Kanta Panthi. His good guidance has been an essential contribution to this task, to this I owe my gratitude for his guidance. I would also like to extend my thanks to friends and fellow students for helping in the working process.

Ajender Rathore

Trondheim, June 2016

ABSTRACT

Chenab basin in state of Himachal Pradesh has been opened for detailed study and development of hydropower projects. The government of Himachal Pradesh awarded development of the 260+7 MW Sach Khas project to L&T Himachal Hydropower Limited (L&T HHL) on competitive bidding to develop the project on Build, Own, Operate and Transfer (BOOT) basis. It is a dam toe project with underground power house. This work aims to access placement, optimize orientation and perform stability assessment of caverns placed close to toe slope of the valley. To achieve this objective, engineering geological conditions including rock mass properties and stress situation in the Sach Khas project area have been evaluated.

Original placement and orientation of the caverns from the background information is assessed. In addition, an alternative orientation is proposed to reduce the length of the appurtenant tunnel system and minimize the impact of structurally induced instability. The two cases are compared throughout the thesis.

An in-depth stability assessment of the underground caverns is carried out, with scope of evaluating possible structurally induced instability and stress induced instabilities for the caverns. The analysis includes analytical, empirical and numerical methods. The analysis detected low cumulative probability for block fall, brittle failure in the cavern roof and tensile fracturing in the cavern walls extending towards slope face due to magnitude and anisotropy in the redistributed stresses. The stress induced instabilities are more extensive than structurally induced instabilities in both cavern alignments due to its placement, orientation, shape and size.

Probabilistic Unwedge analysis is done to assess the structurally induced stability problems. Analytical and empirical studies involve Kirsch's equations and Hoek and Brown (1980) methods to assess the redistribution and concentration of stresses in the cavern contour. Spalling potential and depth of brittle failure is estimated based on cavern span, rock mass spalling strength and tangential stresses. The results are compared to estimation of failure depth from numerical analysis using analysis of strength factor with Hoek-Brown brittle parameters in 2D finite element program, Phase2. 3D finite element analysis (RS³) is carried out for the final selected cavern alignment. Reasonable difference between analytical/empirical and numerical approach is found considering caverns location in low rock cover and near tow slope.

Support measures are proposed based on empirical relations, recommendations from the RMR, Q-system and analysis of yielding and deformation from the numerical results.

From assessment of engineering geological conditions and in-depth stability analysis, it is considered feasible to obtain a satisfactory level of stability for original alignment, considering the rock mass properties and stress conditions that are most likely to occur. However, the numerical analysis carried out for worst case scenario showed significant stability problems. If such conditions prevail in the area, placing large scale cavern may be challenging regarding stability during construction and long term stability aspects.

TABLE OF CONTENT

PREFACE AND ACKNOWLEDGEMENT.....	I
ABSTRACT.....	II
TABLE OF CONTENT	III
1 INTRODUCTION.....	1
1.1 Background.....	1
1.2 Objective and scope of study.....	2
1.3 Approach	3
2 STABILITY ASSESSMENT OF UNDERGROUND CAVERNS	6
2.1 Structurally controlled instability	6
2.2 Tensile failure	8
2.3 Compressive failure.....	8
2.4 Failure criterion	9
2.5 Stability issues in caverns.....	11
2.6 Considerations regarding large scale caverns.....	18
3 SACH KHAS HYDROELECTRIC PROJECT	23
3.1 Project Description	23
3.2 Engineering Geological Investigations.....	25
3.3 Underground powerhouse cavern.....	30
3.4 Placement and orientations of underground caverns.....	35
4 MECHANICAL PROPERTIES OF ROCK IN PROJECT AREA	37
4.1 Introduction	37
4.2 Test results.....	37
5 STABILITY ANALYSIS METHODS AND ROCK SUPPORT PRINCIPLES	39
5.1 Estimating stress distribution.....	39
5.2 Classifying rock mass quality.....	41
5.3 Predicting failure extent.....	46

5.4	Estimating rock support.....	50
5.5	Numerical methods.....	52
6	STABILITY ANALYSIS.....	54
6.1	Stress Distribution	54
6.2	Rock Mass Quality	55
6.3	Predicting Failure extent.....	56
6.4	Support.....	57
7	NUMERICAL MODELLING	61
7.1	Unwedge analysis	61
7.2	Phase2 Analysis.....	71
7.3	RS ³ analysis	95
8	DISCUSSION	107
8.1	Stress situation.....	107
8.2	Placement and Orientation of caverns	107
8.3	Stability analysis.....	108
9	CONCLUSION, RECOMMENDATIONS AND LIMITATIONS	113
9.1	Conclusions	113
9.2	Recommendations	114
9.3	Limitations.....	115
10	BIBLIOGRAPHY	116
	ANNEXURES.....	121

1 INTRODUCTION

1.1 Background

With consequent increase in transmission and distribution (T&D) systems in India, the installed capacity of power generation has risen from 1.3 GW at the time of independence(1947) to almost 290 GW at present (Ministry of Power, 2016).

Despite this seemingly impressive increase, the states have been facing shortages. India is one of the countries where the present level of electricity consumption, by world standards, is very low. The per capita consumption of electricity is about 1010 kWh (International energy agency, 2015; Ministry of Power, 2016). As compared to this, the electricity consumption in some of the other countries is of the order of over 8000 for Japan, about 14000 for USA, and over 17000 kWh for Canada. Even our neighbouring China has reached a per capita electricity consumption of about 2500 kWh, just below the world average of about 2800 kWh. In terms of per capita electricity consumption, India is far behind the world average. India is targeting a growth rate of 9 – 10%, having already reached a level of almost 8%. Hence, to sustain this grown rate, energy generation has to be enhanced.

In the profile of energy sources in India, coal has a dominant position. Coal constitutes about 56 % of India's primary energy resources followed by Hydro (19 %), Renewable energy sources (12 %), Natural Gas (9 %), and Nuclear (2.3 %) (Ministry of Power, 2016).

The share of Hydro capacity in the total generating capacity has declined from 34 % to 19 % by the end of the 11th plan. Suitable corrective actions have been initiated to improve the share which is likely to achieve 40 % by the end of 2026. Considering the above mentioned figures, regional/national importance and demand/supply gap, Chenab basin in Himachal Pradesh has been opened for detailed study and development of hydropower projects (Larsen and Toubro(PDL), 2012c).

Govt. of Himachal Pradesh awarded the development of 260+7 MW Sach Khas project to L&T Himachal Hydropower Limited (L&T HHL) on competitive bidding to develop the project on Build, Own, Operate and Transfer (BOOT) basis. L&T HHL has prepared the DPR for the project. Once implemented the Sach Khas project will give design energy, in 90% dependable year with 95% of installed capacity, about 970 GW.

Sach Khas HPP (260+7 MW) is one of the four cascade projects to be developed in the Chenab basin inside the state of Himachal Pradesh. It utilizes a head of 70 meters between 2219 and 2149 m.a.s.l approximately. The powerhouse for the Sach Khas plant will be placed

underground with surface transformer building with indoor gas insulated substation (GIS) and pothead yard on the left bank. Optimal location and orientation of the powerhouse cavern is crucial to a successful execution of this project.

As a result, this thesis will assess these parameters, in addition to an in-depth stability analysis. Also, the main engineering geological challenges related to the establishment of underground caverns in the area of Sach Khas HEP are young Himalayan geology, topographical stresses and low cover varying between 59m (minimum) and 70m (maximum) with rock cover of 45m (minimum) and 48m (maximum) respectively, which can cause severe stability problems during construction. In addition, practical and economic conditions have to be taken into account when evaluating location and orientation of the underground cavern.

1.2 Objective and scope of study

This MSc thesis will focus on the documentation and overall evaluation of the Sach Khas Hydroelectric Project with particular emphasis on the detailed stability assessment of the underground powerhouse cavern.

The scope of the thesis can be listed as follows:

- Review existing theory on the stability issues connected to the large underground caverns.
- Briefly describe Sach Khas Hydroelectric Project, review geological condition at the project area and extent of engineering geological investigation carried out during planning.
- Document engineering geological parameters, mechanical properties of the rock mass and in-situ stress conditions in and around underground powerhouse location.
- Document rock support principles and excavation philosophy used in the powerhouse cavern.
- Carry out assessment on orientation and placement of the powerhouse cavern.
- Carry out stability assessment of powerhouse cavern using empirical and analytical approaches.
- Analyse structurally controlled instability in powerhouse cavern using Unwedge.
- Assess global stability condition of the powerhouse using RS2 (Phase2) and RS³ numerical approaches.
- Discuss the analysis results from empirical, analytical and numerical approaches.
- Conclude the work, give recommendation and highlight limitations.

1.3 Approach

The methodology in the work has principally followed the structure described as:

1.3.1 Literature review

The literature reviews are based on theory and methods utilized in this thesis. Literature and Scientific articles constitute the majority of the references which were found through databases (Oria.no) in the university library of the Norwegian University of Science and Technology. Google Scholar and search engine in the Ei Compendex (<https://www.elsevier.com/>) have also been used regularly to methodically narrow down the search to the most relevant scientific articles and journals. The main topics for the literature reviews have been:

- Stability issues for large underground caverns (located at shallow depth in particular).
- Structurally controlled instability problems in the underground caverns.
- Failure mechanism in brittle rocks.
- Analytical and empirical methods to assess stability of underground excavations.
- Support principles for underground caverns.
- Himalayan Geology (North western Sector).
- Case studies of numerical analysis carried for underground caverns.

1.3.2 Study of Sach Khas HPP

An overview of the project has been studied through reports and project descriptions with special consideration to the powerhouse complex area. The assessment of Cavern placement, orientation and stability, evaluation of engineering geological reports, collecting data from geological field and lab reports have been of utmost importance. Furthermore, project layout and the topography in powerhouse complex area has been of equal importance to get an overview of the project. All this has been done to make sure all options regarding placement and orientation of powerhouse are available without interfering with the practicability.

1.3.3 Cavern placement and orientation

Due to limitations in options available for placement selection, reason one being land accusation already done for the project, reason two being project layout which is already selected from techno economical evaluation of four other alternatives, it is a dam toe project with underground power house, no head race tunnel in water conductor system. Combination of these two factors limits the location change. However, lateral movement deep into the mountain side is discussed in detail after stability assessment.

In this thesis two different alternatives of orientation have been analysed without changing the placement of cavern. One orientation is based on the studies done by project authorities Larsen & Toubro Power Development Ltd. referred to as Original alignment. The other alternative is the solution proposed by the author where cavern length axis is orientated in N200E – S200W direction, rather than N550E-S550W direction which is the original orientation. This other orientation will be referred as “Alternative alignment” and stability assessment is carried out for both orientations discussed in this thesis.

1.3.4 Stability assessment

Analytical, Empirical and Numerical methods are used to carry out stability assessment of the cavern. The Analytical and Empirical methods have been summed up in one chapter as they are often a combination of analytical and empirical approaches.

The stability assessment of the powerhouse cavern uses the following techniques:

- To estimate the redistribution of the stresses around the excavation contour, Kirsch’s equation and empirical approaches introduced by Hoek and Brown (1980) have been utilized.
- Q-system, RMR calculated from geological and field reports, GSI calculated from RMR values are used to describe rock mass quality.
- Classification developed by Hoek and Brown (1980), based on the UCS and major principle stress is used to estimate the extent of the brittle failure.
- Methods from Diederichs (2007), Martin and Christiansson (2009) and Cai and Kaiser (2014) are used to estimate spalling potential.
- Formula given by Martin and Christiansson (2009) is used to calculate the depth of brittle failure.
- Bolt lengths are estimated using collection of empirical formulas based on cavern span.
- Support system is proposed by using Q-System and RMR calculated from geological and field reports, later modified after numerical analysis.

Both elastic and plastic material properties are used in carrying out Numerical analysis. Information about distribution of secondary stresses, stress concentration and strength factor is gathered by analysing elastic model. Prediction of deformation, yielded elements and estimation of rock support is predicted by using plastic model. Hoek-Brown brittle parameters and the deviatoric stresses criterion is used to analyse depth of spalling.

1.3.5 *Limitations*

Main focus of the thesis is on the assessment of structurally controlled instabilities and stress induced stability issues in original and alternative alignment. Due to the reasons discussed under section 1.3.3. Focus of finding new location for alternative alignment is declined, instead lateral placement i.e. placing cavern deep into the mountain is discussed in detail (Section 7.2.4).

2 STABILITY ASSESSMENT OF UNDERGROUND CAVERNS

Failure modes in underground caverns are the result of in-situ stress magnitude & characteristics of rock mass (Martin et al., 1999) (Figure 2-1). Stability assessment is done by different methods depending upon the type of failure. Influence of surface topography on in-situ stress field has to be considered in deciding the location of underground powerhouse and assess the stability condition (Hoek and Moy, 1993).

In this thesis we will assess the cavern orientation/location and stability of Power House in relatively shallow depth at toe slope of valley.

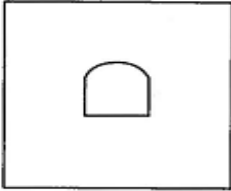
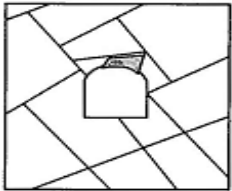
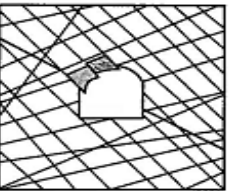
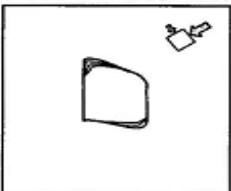

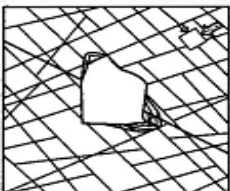
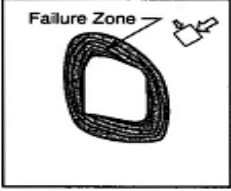
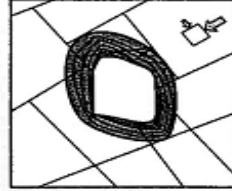
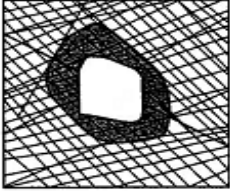
	Massive ($RMR > 75$)	Moderately Fractured ($50 > RMR < 75$)	Highly Fractured ($RMR < 50$)
Low In-Situ Stress ($\sigma_1 / \sigma_c < 0.15$)	 <p>Linear elastic response.</p>	 <p>Falling or sliding of blocks and wedges.</p>	 <p>Unravelling of blocks from the excavation surface.</p>
Intermediate In-Situ Stress ($0.15 > \sigma_1 / \sigma_c < 0.4$)	 <p>Brittle failure adjacent to excavation boundary.</p>	 <p>Localized brittle failure of intact rock and movement of blocks.</p>	 <p>Localized brittle failure of intact rock and unravelling along discontinuities.</p>
High In-Situ Stress ($\sigma_1 / \sigma_c > 0.4$)	 <p>Failure Zone</p> <p>Brittle failure around the excavation.</p>	 <p>Brittle failure of intact rock around the excavation and movement of blocks.</p>	 <p>Squeezing and swelling rocks. Elastic/plastic continuum.</p>

Figure 2-1. Examples of instability and brittle failure (grey squares) as a function of Rock Mass Rating (RMR) and the ratio of the maximum far-field stress to the unconfined compressive strength, Modified after Martin et al. (1999).

2.1 Structurally controlled instability

There are two distinct types of failures that occur in the roof and walls of the Power House cavern. Failure of the rock mass surrounding the excavation is the dominant failure mode in

weak or heavily jointed rock or massive hard rock subjected to very high stresses. Wedge failure is most common type of failure in hard rock excavation in shallow depths defined by intersecting structural discontinuities i.e. three structural planes intersecting form a block with excavation boundary as the fourth plane (Hammett and Hoek, 1981). If the loose wedges are allowed to fall, the stability of the cavern will deteriorate rapidly, causing further complications leading to reduction in restraint and interlocking of rock mass. This effect will cause the other wedges to be destabilized and the failure process will continue until natural arching stage is reached. Orientation of discontinuities, the shape of the cavern and condition of the structural feature i.e. friction and weathering will influence the structurally controlled instability. Influence of the in-situ stresses is neglected as it is considered prudent during the analysis i.e. to ensure conservative support design (Hoek, 2007). Figure 2-2 shows potentially unstable rock blocks around the underground cavern with failure modes depending on the location of the wedge.

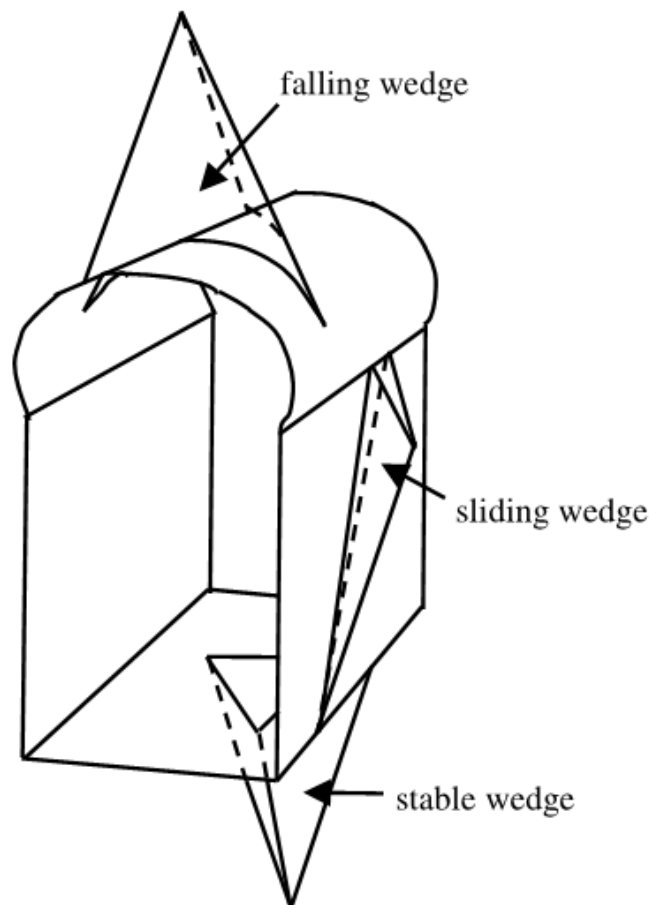


Figure 2-2. Sketch of potentially unstable rock blocks around the underground chamber of the Rio Grande hydroelectric power plant (Cordoba district – Argentina) (Oreste and Cravero, 2008).

Dynamic support design is required for supporting blocks and wedges, i.e. rock bolts and cables are installed to support the weight of the possible loose wedge or block.

The steps required to deal with such problems are:

- Determination of average dip and dip direction of significant discontinuity sets.
- Identification of potential wedges which can slide or fall.
- Calculation of the factor of safety for these wedges, depending upon the mode of failure.
- Calculation of amount of reinforcement required, to bring the factor of safety of individual wedges up to an acceptable level.

(Hoek, 2007).

Although the steps above can be performed manually, it is efficient to utilize the computer program such as UNWEDGE, developed specifically to deal with such problems. This methodology will be used in this thesis.

2.2 Tensile failure

Due to rock's discontinuous character and brittle nature, it can resist little tensile stresses. Tensile stresses can develop on the powerhouse cavern wall, near crest and toe of the slope due to cavern geometry. This can lead to tensional cracks on the wall of the powerhouse cavern, crest and toe of the slope. Tensional jointing might develop when cavern orientation is aligned with major principal horizontal stress.

2.3 Compressive failure

When the tangential stresses in hard rock exceeds the strength of the rock mass, the result will be a fracture parallel to the cavern contour (Nilsen and Palmström, 2000). Often the fracturing process will cause a loud noise from the rock, called rock burst. If the stress levels are moderate, fracturing will result in the loosening of the thin slabs, often referred to as rock slabbing or spalling. Very high tangential stresses may cause large rock slabs to pop with considerable force and speed. The intensity of the rock burst activity is high immediately after excavation. Area close and around working face is the most exposed to such failures (Nilsen and Thidemann, 1993).

An effective way of reinforcing the excavation where rock burst and rock spalling or slabbing is an issue, is by pinning the slabs together i.e. providing rock bolts normal to the cavern contour.

In soft rocks, the failure mechanism is plastic in nature rather than brittle. The plastic deformation is called squeezing, causing convergence resulting in reduction of excavation diameter to several tens of centimetres (Nilsen and Palmström, 2000).

2.4 Failure criterion

Over the years a number of failure criteria explaining or predicting failure in materials have been developed. Examples such as Mohr-Coulomb, Tresca-Criterion and Von Mises are some of the familiar ones. Theories linked to these criteria are based on assumptions that failure occurs due to particular mechanism exceeding particular mechanical property.

The simplest and one of the most widely used theoretical failure criteria in rock engineering is the Mohr-Coulomb and Hoek-Brown failure criterion, discussed as follows:

Mohr-Coulomb Criterion

The strength criterion is linear approximation variation of peak stress with confining pressure, it suggests that shear strength of the rock material is made of constant cohesion and friction angle varying with the normal stress. The shear strength (τ) is given by Eq- 2.1.

$$\tau = c + \sigma_n \tan \phi \quad \text{Eq- 2.1}$$

Where, c is the cohesion, σ_n is the normal stress acting on the plan of failure and ϕ is the angle of internal friction (Zhao, 2000).

Hoek-Brown Failure Criterion

The Hoek-Brown criterion is an empirical strength criterion, developed as a result of research work done on brittle failure of intact rock and model studies of jointed rock (Hoek et al., 2002). Based on research data and model studies, the empirical relationship between the principal stresses associated with rock failure can be described by Eq- 2.2.

$$\sigma'_1 = \sigma'_3 + \sigma_{ci} \left(m_i \frac{\sigma'_3}{\sigma_{ci}} + s \right)^{0.5} \quad \text{Eq- 2.2}$$

Where σ'_1 is maximum effective principal stress at failure, σ'_3 is minimum effective principal stress at failure, σ_{ci} is uniaxial compressive strength of the intact rock, m_i is material constants and s is equal to 1 for Intact rock.

(Hoek et al., 2002)

Over the years, additions have been made to the Hoek-Brown criterion and several parameters introduced, as for practical application a failure criterion for the entire rock mass is often more useful. Hence, it is appropriate to apply the generalised Hoek-Brown criterion:

$$\sigma_1' = \sigma_3' + \sigma_{ci} \left(m_b \frac{\sigma_3'}{\sigma_{ci}} + s \right)^a \quad \text{Eq- 2.3}$$

Where m_b is the reduced value of the Hoek-Brown constant m_i for rock mass, s and a are constants depending on the rock mass characteristics. The rest of the parameters are similar to Eq- 2.2 (Hoek et al., 2002).

The geological strength index (GSI) was introduced to relate the failure criterion to geological observations in the field, in particular for weak rock mass (Figure 5-4). Factor D was added, which depends on the degree of disturbance in terms of blast damage and stress relaxation (Appendix A). The range varies from 0 for undisturbed in situ rock masses to 1 for very disturbed rock masses (Hoek et al., 2002). The relationships for m_b , s and a are given by:

$$m_b = m_i \exp \left(\frac{GSI - 100}{28 - 14D} \right) \quad \text{Eq- 2.4}$$

$$s = \exp \left(\frac{GSI - 100}{9 - 3D} \right) \quad \text{Eq- 2.5}$$

$$a = \frac{1}{2} + \frac{1}{6} \left(e^{\frac{-GSI}{15}} - e^{\frac{-20}{3}} \right) \quad \text{Eq- 2.6}$$

(Hoek et al., 2002; Hoek and Marinos, 2007)

Residual parameters must be calculated to model post peak behaviour of rock mass, based on the same concept valid for failed rock masses at the residual strength state. Residual Hoek-Brown parameters are determined from residual GSI value (GSI_r) (Cai et al., 2007). The equation is suitable for rock masses with GSI values ranging from 40-80, which is suitable for the case under study in this thesis, where the GSI ranges from 48-58, it is always better to give a range of GSI value and it is hard to predict a single value of GSI.

$$GSI_r = GSI e^{-0.0134GSI} \quad \text{Eq- 2.7}$$

$$m_r = m_i \exp \left(\frac{GSI_r - 100}{28} \right) \quad \text{Eq- 2.8}$$

$$s_r = \exp\left(\frac{GSI_r - 100}{9}\right) \quad \text{Eq- 2.9}$$

$$a_r = 0.5 + \frac{1}{6}\left(e^{\frac{-GSI_r}{15}} - e^{\frac{-20}{3}}\right) \quad \text{Eq- 2.10}$$

(Cai et al., 2007).

In this thesis the Generalised Hoek-Brown criterion will be used for stability assessment.

2.5 Stability issues in caverns

Underground cavern stability is governed by several factors, most of which are significant for excavation in rocks. Certain points to consider when dealing with large scale underground excavations are listed as following:

2.5.1 Rock type

Rock mass is a heterogeneous medium with many connected variables, a building material for the underground excavations. Rock mass quality and the mechanical processes acting on it are the main features that characterize the rock mass, describing its ability to withstand stress and deformation (Panthi, 2006). Figure 2-3 shows that stability of tunnels and underground caverns is a function of mechanical processes and rock mass quality.

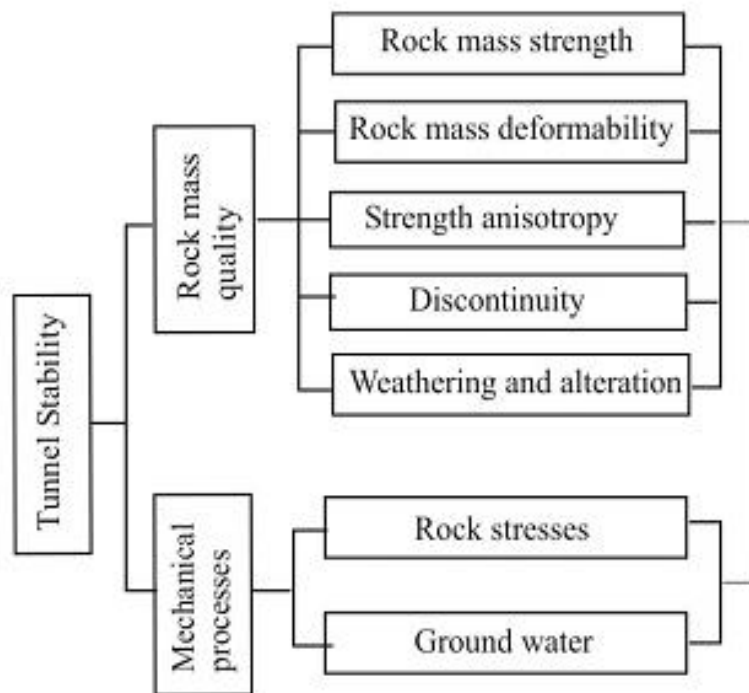


Figure 2-3. Factors influencing on tunnel & cavern stability(Panthe, 2006).

2.5.2 Rock Mass Quality

Rock mass strength, deformability properties, strength anisotropy, degree of weathering and mechanical characteristics of the discontinuities govern the rock mass quality. The most commonly used rock mass classification system described in section 5.2.

2.5.2.1 Strength anisotropy

Directional stress history and preferred orientations of minerals are the main reasons for strength anisotropy. Sedimentary and metamorphic rocks due to their bedding, schistosity and foliation have a very distinct anisotropy (Goodman, 1989). The Himalayan rocks are highly directional regarding strength and deformability (Panthi, 2006). The direction values of the stress conditions are used in this thesis and discussed in detail in section 7.2.1.3.

2.5.2.2 Rock mass strength

It is difficult to estimate rock mass strength directly in the field or laboratory testing, hence, many authors have suggested empirical formulae for estimation of rock mass strength (Panthi, 2006). In this thesis RocData software package from Rocscience is used to calculate the rock mass strength which uses Generalized Hoek-Brown strength criteria to calculate rock mass parameters. This data is then transferred to Phase2 and RS³ numerical analysis packages.

2.5.2.3 Rock mass deformability

The *Modulus of deformation* (E_{rm}), a ratio of stress to corresponding strain during loading of the rock mass, together with elastic and inelastic behaviour and *modulus of elasticity* (E_i), a ratio between applied stress and corresponding strain inside the elasticity limit, is described by the commission of Terminology of ISRM (1975) (Panthi, 2006).

The use of term the modulus of deformation rather than the modulus of elasticity or Young's modulus is because of the fact that the jointed rock mass does not behave elastically (Bieniawski, 1978). The deformation modulus of jointed rock as compared to elasticity modulus of intact rock is very low, it can reach as low as 10 percent of the elastic modulus of the intact rock specimen (Hudson and Harrison, 1997).

There are several field methods to determine the deformation modulus, however, all the methods are time consuming and costly with operational difficulties. Also test values obtained from these methods differ considerably (Nilsen and Palmström, 2000), hence there are many empirical equations available for estimating the rock mass deformation modulus (Panthi, 2006).

It is really important to gather information about elasticity of the rock mass in order to predict the failure mode. High E-modulus produces stiff rock, hence brittle failure mode. Low E-modulus produces more deformation, hence squeezing is possible. All this has influence on the post-failure behaviour. In order to estimate the permanent rock support, it is important to gather information about post-failure behaviour. The stress-strain diagrams in Figure 2-4 show typical post-failure behaviour for different rocks.

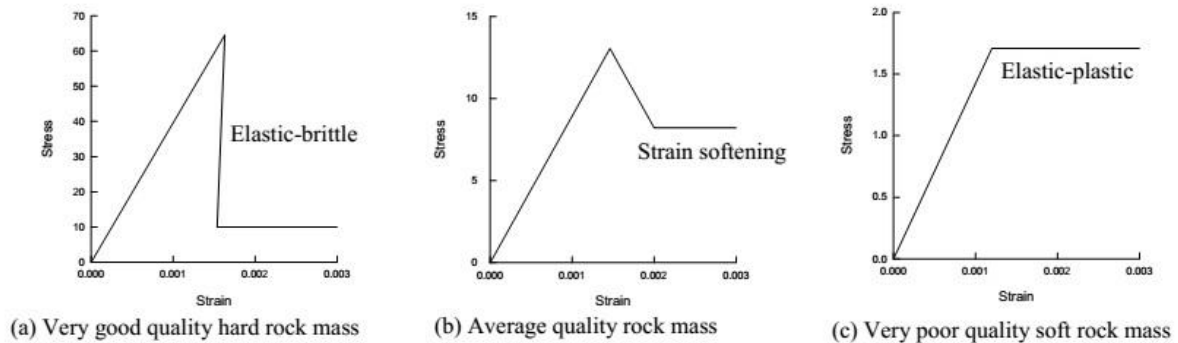


Figure 2-4. Stress-strain diagrams of typical post-failure behaviour for different quality rock. Modified after Hoek (2007)

In this thesis Roc Data software package is used to calculate modulus of deformation for rock mass (E_m), which utilises Hoek and Diederichs (2006) method for estimation of rock mass modulus.

2.5.2.4 Discontinuity

Properties of discontinuities govern the properties of the in-situ rock mass. “Discontinuities” is the collective term used for most types of bedding planes, joints, schistosity planes, foliation planes, fault zones and weakness zones (Nilsen and Palmström, 2000). It is crucial to understand the discontinuities/jointing in order to understand the behaviour of the rock mass (Nilsen and Thidemann, 1993).

Roughness, alteration, weathering, spacing and persistence represent the mechanical characteristic of the discontinuity surface (Barton et al., 1985; Hudson, 1989). The Figure 2-5 illustrates the ten parameters recommended by ISRM (1978) considered for describing the discontinuity characteristics.

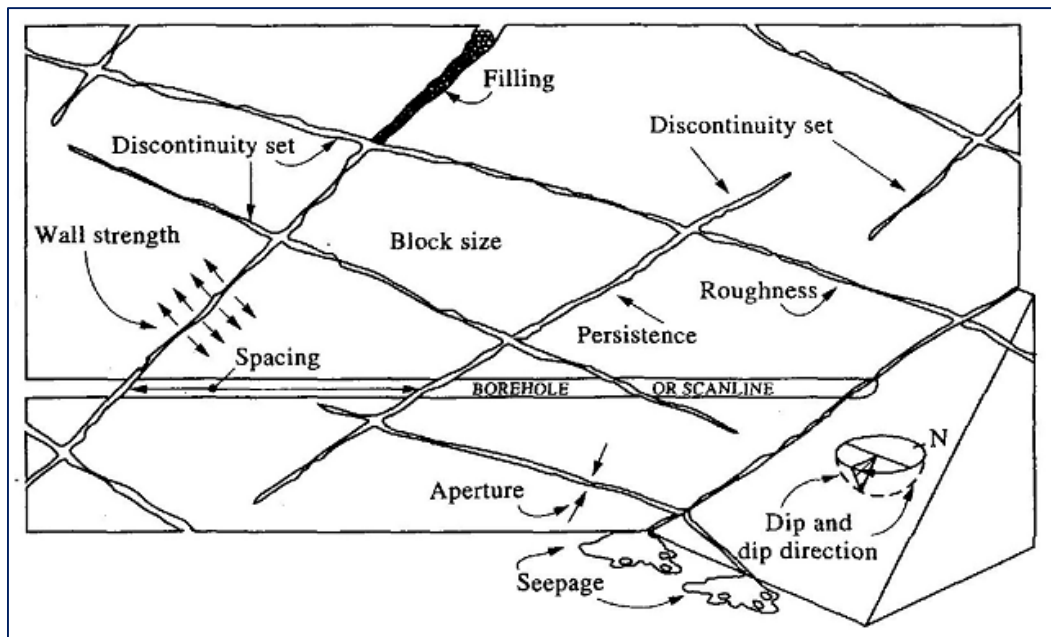


Figure 2-5. Discontinuity characteristics in the rock mass (Hudson and Harrison, 1997)

It's really important to know the information about the degree and characteristics of joints. There are several methods to measure the degree of jointing, such as joint spacing, density of joints, block size on surface and rock quality designation (RQD) in drill cores. Joint characteristics such as surface roughness, alteration, infilling, wall strength, spacing and block size influence the stability of the rock mass, in turn affecting the shear strength of the joints as well as the quantity of water which can flow through the rock mass (Nilsen and Palmström, 2000). These properties and characteristics will differ from one type of discontinuity/joint to another due to their fundamentally different history, formation and age of development. When characterizing the rock masses for the practical applications, special attention should be paid to the discontinuities/joints because of their influence on rock mass behaviour (Palmstrom and Stille, 2010).

Appendix F shows the prominent joint sets in power house complex area along with joint characteristics.

Weakness Zones

During planning stage, when deciding the location of the underground cavern it is very important to avoid weakness zones. Weakness zones contain two main groups in terms of engineering geological context: Tectonic faults and weak rock layers (Figure 2-6) (Nilsen and Broch, 2009). Stability problems in weakness zones are associated with rock squeezing and tunnel collapse of the roof and side walls, the reason is that there are very weak bonds that decrease the self-supporting capacity of rocks.

Weakness zones and fault zones, form the weakest parts in the rock mass and are a reason for severe stability problems in any kind of excavation. Depending on their type and origin, their mechanical and engineering behaviour varies. The Sach Khas HEP project area does not contain any major weakness zones, confirmed by various geological sections available from 100 m upstream to 280 m downstream of dam axis at every 20 m interval (Larsen and Toubro(PDL), 2012b).

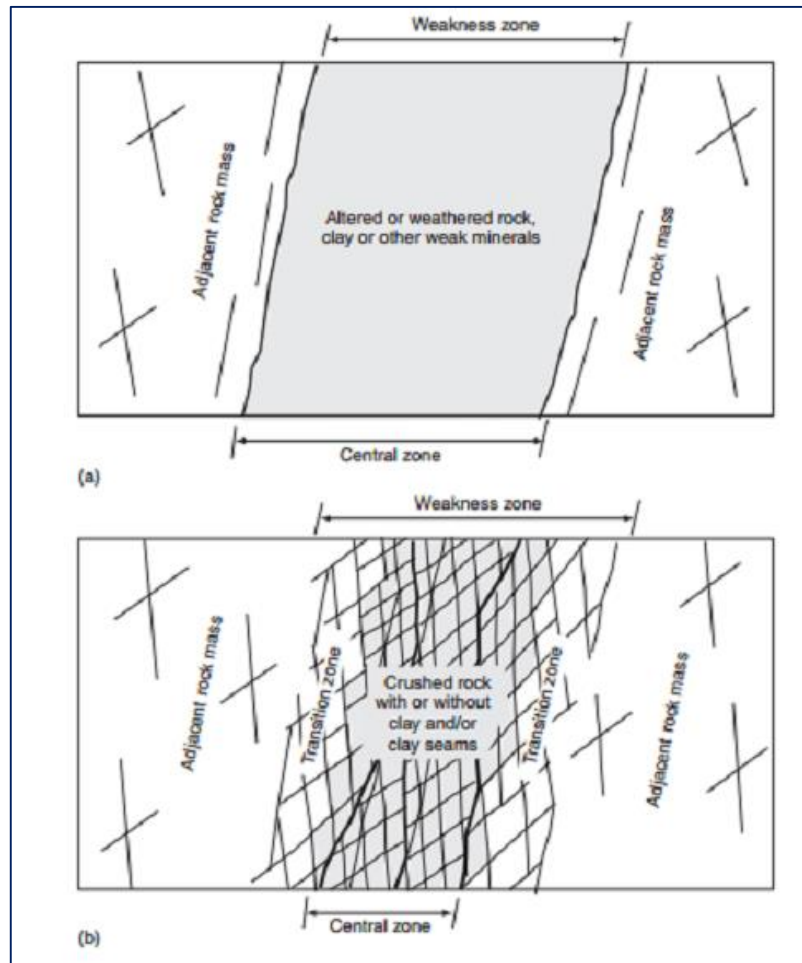


Figure 2-6. Weakness zones divided into two main groups: weak rock layers (a) and tectonic faults (b) (Palmstrom and Stille, 2010).

2.5.2.5 Rock weathering

As a result of natural processes and the response of dynamic earth to changing environment, weathering in a rock mass start from discontinuities and continues to the rock mineral. There exists a considerable variation in the degree of weathering of rock mass and in weathering zones (Panahi, 2006). The variability can be assessed by classification of weathering grade in rock mass.

Weakness and fault zones influence weathering. Being formed by fracturing, shearing and hydrothermal alteration, the weakness and fault zones provide excellent conditions for intensified weathering, acting as medium for ground water flow. Weathering changes the properties of the rock mass such as rock mass strength, deformability, frictional resistance and slaking durability, increasing the permeability significantly at the same time.

Weathering has significant effect on the underground excavation stability in the Himalayas, hence it has to be addressed in rock mass quality evaluation and stability analysis of the underground excavations (Panthi, 2006).

Weathering is discussed in detail in the geological report prepared by project authorities, as the project belongs to the region where weathering is a major issue considering long term stability of the cavern at shallow depth.

2.5.3 Rock stresses

Rock stresses are one of the reasons for significant stability problems, also significant in terms of vitality to obtain a self-bearing construction where rock can support itself as building material. The conventions used are, compressive stresses are positive and tensile stresses are negative.

For stress analysis the principal stresses are of importance in terms of their magnitude and directions, i.e. normal stresses on the planes with no shear stress. Information about the in-situ stresses in the rock mass along with the statistics available about the opening geometry can give information about magnitude and directions of the redistributed stresses adjacent to the opening. It is possible to access potential stress induced stability problems if the information about the rock mass properties are known at first hand. Therefore, giving a fair amount of chance to predict rock support and possibilities to optimize the excavation geometry (Nilsen and Palmström, 2000).

The gravity, plate tectonics, surface topography and residual stresses are the principle reasons for origin of the virgin in-situ stresses (Nilsen and Thidemann, 1993).

Hoek and Brown (1980) found that the ratio (k) between horizontal and vertical in-situ stresses differ significantly and the average horizontal stresses near the surface in most cases is greater than the vertical stresses (Figure 2-7). The ratio (k) is greater than one at shallow depths, less than one and approaches constant value when the depth increases (McCutchen, 1982). The magnitude of the average horizontal stress (σ_h), to a great extent is influenced by the plate tectonic moments (Panthi, 2006).

Horizontal stress induced by gravity normally contributes only a little part of the total horizontal stress (Nilsen and Palmström, 2000), greater part is influenced by plate tectonic moments.

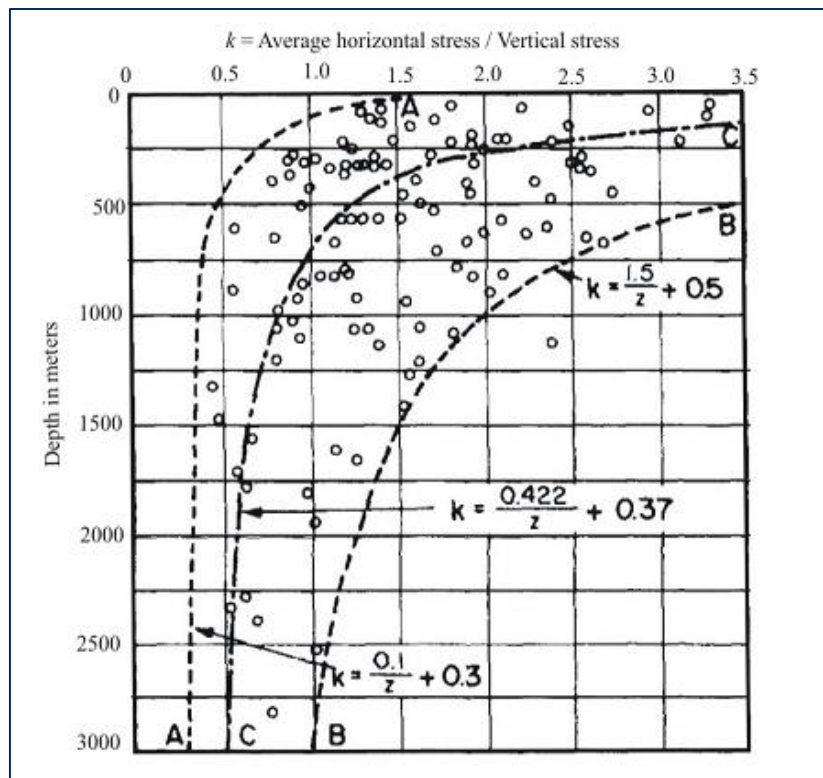


Figure 2-7. Variation of ratio of average horizontal stress to vertical stress with depth below surface
(Panthi, 2006)

In dipping surfaces, stress situation is influenced by topographic stresses, i.e. in high valley sides, topographic effect near the surface will dominate the stress situation, the situation being dealt with in this thesis. Largest principle stress will be more or less parallel to the surface slope (Nilsen and Palmström, 2000).

The earlier stage of the geographical history is responsible for locked residual stresses in the rock mass variation. Variation in cooling of rock melt at early stage in rock history can lead to residual stresses (Nilsen and Palmström, 2000), making them hard to predict without clear stress measurements (Section 3.3.4 and section 7.2.1.3).

2.5.4 Ground water

The rock mass is a jointed aquifer where groundwater freely moves through permeable discontinuities or through open channels along them, below ground water table. A large amount of subsurface water consists of groundwater. Altogether, it is observed that the rock mass close to the surface is more jointed and the joints are more open as compared to ones at greater depth. Visual observations in ungrouted underground excavations show that the most of the water

leakage occurs in parts close to the surface, confined in fractures, weathered zones and faults (Karlsrud and Kveldsvik, 2002; Nilsen and Thidemann, 1993). Freely moving groundwater affects the underground excavation conditions the most, along with long term stability considerations (Palmstrom and Stille, 2010).

Being a part of the hydrological cycle, the groundwater travels long distances through rock masses. Hence, making it important for consideration in regional geology and groundwater patterns when analysing probable water problems or at planning stage.

Strength of rock material and shear strength of the discontinuities are reduced to certain extent by groundwater affecting the stability of the excavations. The reduction of friction and strength will be significant in swelling clays. In this thesis the saturated condition value for uniaxial compressive strength (UCS) is used as input for material properties (Section 4.2.2).

In underground excavations the failure due to joint water pressure is rare but it may contribute to instability, especially in weak rock masses. Hence, it is important to evaluate the impact of groundwater pressure when it is potentially significant (Nilsen and Palmström, 2000). Not much leakage is observed in the exploratory drift for the underground powerhouse, not even the piezometric line is defined in reports, hence, numerical modelling is done without modelling ground water.

2.6 Considerations regarding large scale caverns

There are many considerable factors that make it challenging to excavate large scale caverns. Factors such as large span, orientation and pillar stability etc. are some of the important issues which need considerable caution. A careful and systematic design approach is needed to avoid or reduce stability problems.

A general design recommendation for underground caverns can be divided in the following stages:

- Select an optimal location as this is important from stability point of view and engineering geological condition of the area.
- Orientate length axis of cavern to give minimum stability problems and outbreaks.
- Keep in view mechanical properties, jointing of the rock mass and local stress conditions, decide the shape of the cavern.
- Dimension the cavern complex components to give best economical arrangement.

(Edvardsson and Broch, 2003).

2.6.1 Large span

Large span caverns require constructive confining pressure. Due to low gripping tension there can be wedge failure leading to destabilization of the excavation i.e. the increase in span will expose large blocks and allow them to be relieved. Stability problems increase with increase in cavern span. It is recommended to meet the need for the increased volume to extend the length of cavern than to increase the span (Nilsen and Thidemann, 1993). The cavern under study has a span of 23 m, which is quite large.

2.6.2 Location

Stability of cavern and construction material selection make the site location an important task. Unfavourable types of rock mass should be avoided. Weak, porous rock and heavily jointed rock are not favourable for the selection of a location. Construction material (aggregate) quality should be taken into consideration while selecting a site location, it can reduce the net cost of the project in broad terms. The location of access tunnels, waterway hydraulic conditions and other economically determined conditions limit the possibility of site location to a smaller area (Edvardsson and Broch, 2003).

The stability of the cavern also depends on the assessment of overburden. Hence the cavern should be placed deep enough in order to give considerable amount of normal stress for self-supporting roof. As most of the hydroelectric projects are located in mountainous area, as it is in our case, influence of the topographic stresses has to be taken into account in deciding the exact location (Hoek and Moy, 1993). Avoid weakness zones and heavily jointed rock mass. Evaluation and mapping of weakness zones and joints are important pre-construction phase activity (Edvardsson and Broch, 2003). All the situations discussed in this section will come into play in deciding the final location at the end of the stability assessment.

2.6.3 Orientation

The orientation of the local joint sets is the deciding factor for the cavern orientation, preferably the length of the cavern should be orientated along the bi-section line of the maximum intersection angle between two major dominating joint sets, foliation or bedding directions illustrated in the Figure 2-8. However, orientation shouldn't be parallel to the third or fourth joint set direction (Edvardsson and Broch, 2003).

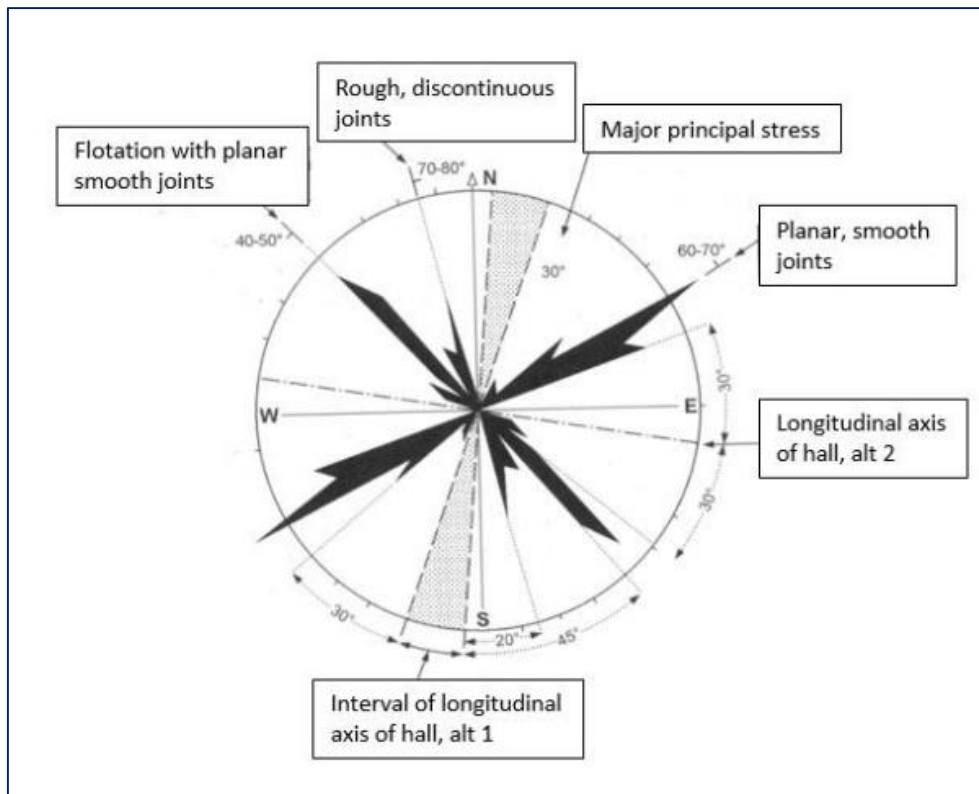


Figure 2-8. Typical rosette plot and favourable orientation of caverns with respect to joints and stress directions (Edvardsson and Broch, 2003)

To obtain the most stable situation regarding stress induced instability i.e. in areas with high anisotropic stresses, cavern length should be orientated in an angle 15° - 25° to the horizontal projection of major principal stress (Edvardsson and Broch, 2003).

2.6.4 Cavern shape

The conventional shape of powerhouse cavern shown in Figure 2-9 is preferred in the strong rock masses. Arched roof helps distribute the rock stresses and provides convenient head space for overhead crane. Its cross section with straight walls makes it preferable in term of stability and ease of excavation. Elliptical shape shown in Figure 2-9 is favourable in weak rock masses, preventing the wall to deflect inwards because of tensile failure. Although from stability point of view the elliptical shape is preferred, it has disadvantages in some practical aspects such as that the construction has to be carefully executed as compared to the conventional shape and items, i.e. cranes and service items, have to be custom designed to fit in to the elliptical shape (Hoek, 2000).

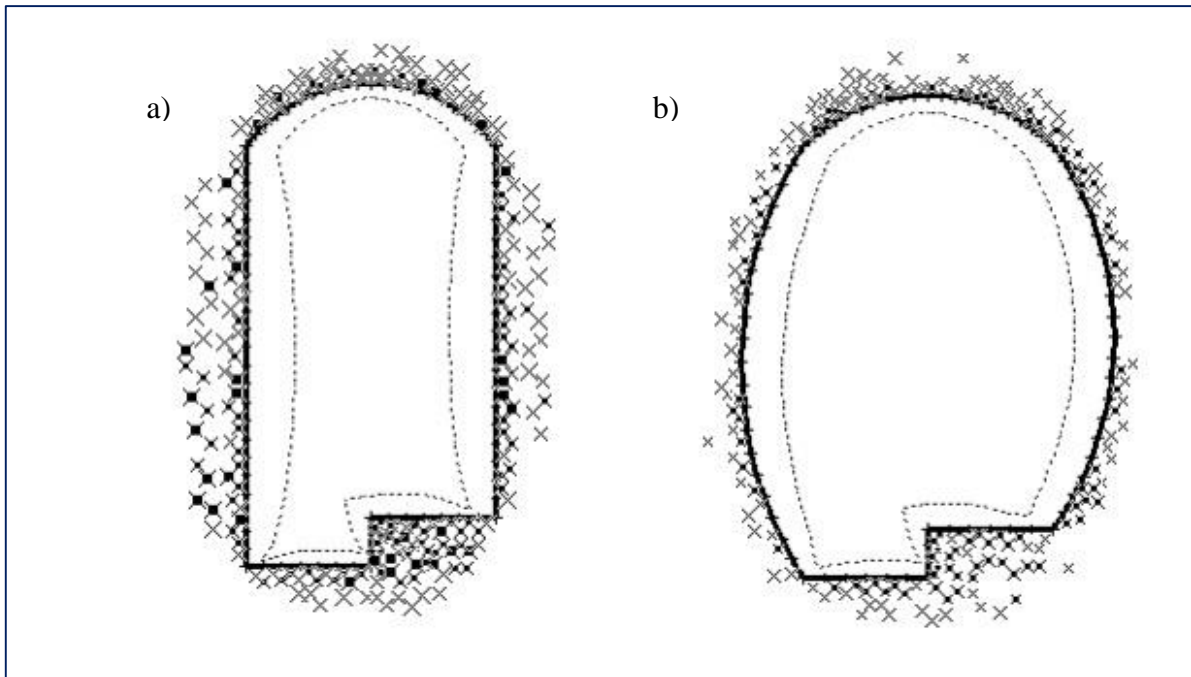


Figure 2-9. Comparison of zones of failure for conventional straight-walled cavern (a) and elliptical shaped cavern (b) (Hoek, 2000).

Ideally, from a geomechanical perspective, the rock mechanical properties and stress conditions should be directly related to ideal cavern shape, however, the reality is different as neither geomechanical conditions, nor rock parameters show dependency on the cavern shape. Some of the cavern shapes and their applicability according to rock mass properties and stress conditions are shown in (Marcher and Saurer, 2013). The cavern shape, i.e. circular, is used by project planning authorities.

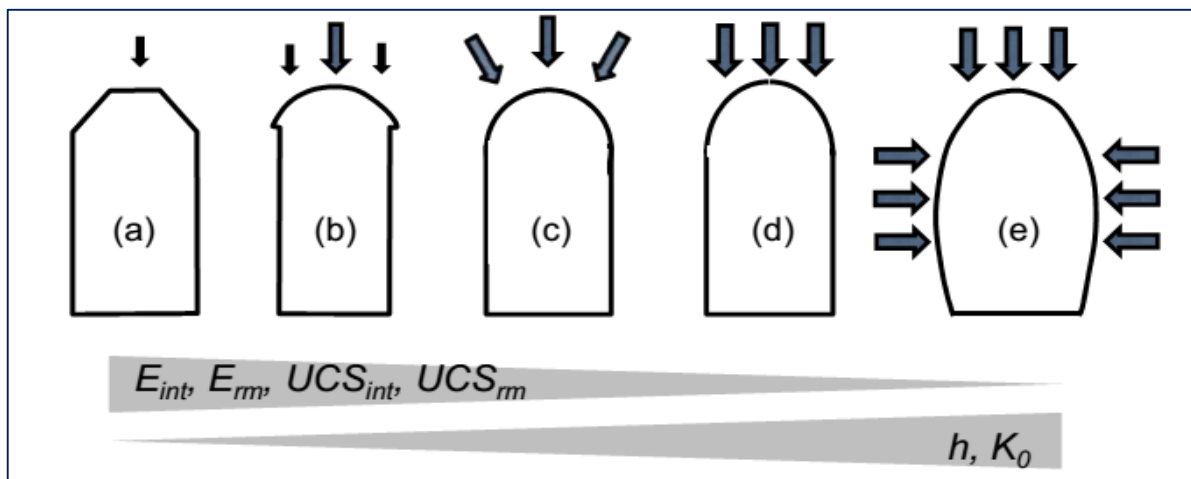


Figure 2-10. Different cavern shapes and their applicability according to rock mass properties and stress conditions: (a) trapezoidal (b) mushroom (c) circular shape (d) bullet shape (e) horse shoe (Marcher and Saurer, 2013).

2.6.5 Pillar width

Often, parallel to the powerhouse cavern is a smaller cavern, i.e. transformer hall, has the advantage of isolating the transformers in case of fire and reduce the span of the powerhouse cavern. In order to minimize the length and cost of the bus duct tunnel, that link transformer to generator, it is important to place the two caverns as close to each other as possible (Hoek, 2000). But in the case under study, the transformers are located on the surface with a bus duct tunnel connecting the transformer to the generator. Hence much detail about the pillar width won't be discussed further.

3 SACH KHAS HYDROELECTRIC PROJECT

3.1 Project Description

Proposed Sach Khas hydroelectric project is located on Chenab river in the Pangi valley, Chamba District of Himachal Pradesh and lies between longitudes 76° 25' 30.143" E to 76°25' 3.8" E and latitudes 32° 57' 55.123" N to 32° 58' 7.5"N.

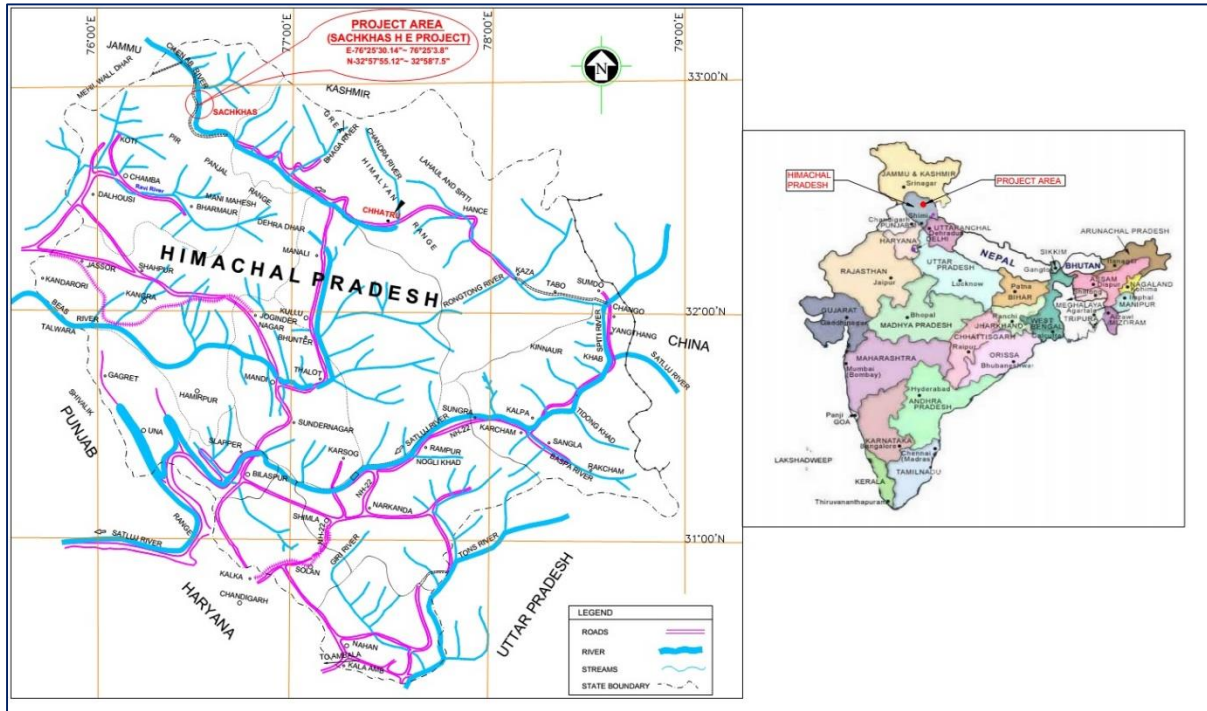


Figure 3-1. Project area location map (Larsen and Toubro(PDL), 2012b)

The project area is located about 14.3 kms upstream from the town of Killar. The project is envisaged as a dam–toe scheme with dam and underground powerhouse sites approximately 3~3.5 km downstream of Purthi / Ajog village.

Chenab is one of the major rivers in the Indus basin. Sach Khas project identified under the Govt. of India’s 50,000 MW initiative, is located across this major river just upstream of confluence of Cheni nala with Chenab River. Line schematic of the projects in cascade development u/s and d/s of Sach Khas Hydro-electric project is shown in Figure 3-2.

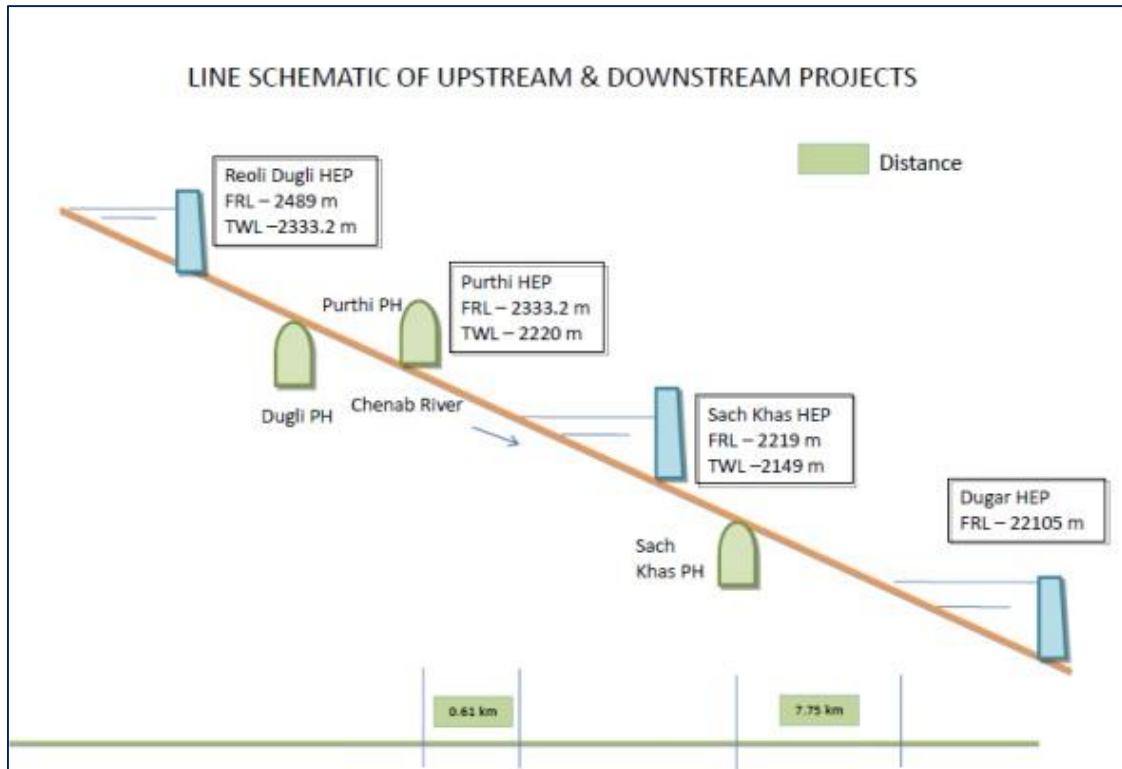


Figure 3-2. Line schematic of hydro projects u/s & d/s of Sach Khas HEP (Larsen and Toubro(PDL), 2012b)

Proposed Sach Khas HEP parameters are shown in Table 3-1 and project layout features are mentioned in Appendix N.

Table 3-1. Project Parameters

Installed Capacity	260 + 7 MW
FRL	2219 m
MDDL	2209.3 m
TWL	2149m
Design discharge	428.5 cumec

3.1.1 Powerhouse complex design

The Powerhouse complex includes:

- Powerhouse cavern comprising
 - Machine hall
 - Service bay
 - Control Block
- Surface Transformer Building with indoor GIS

- Bus duct/Bus shaft connecting PH cavern to transformer building at surface
- Pothead yard on left bank
- Main Access Tunnel (MAT) to the power house cavern
- Ventilation cum Construction adit to power house

Cross section of the powerhouse cavern in Sach Khas HEP, size 126m (L) x 23m (W) x 48.5m (H) is shown in Appendix B. The three generating units are spaced at 21.5 m c/c. The 35 m long Service bay is located at the northern end, and the 15 m long Control Block is located at the southern end of the machine hall.

Information about typical proposed support are given in Appendix C. Rock bolts and steel fibre reinforced shotcrete will be installed. Heavier support like lattice girder and steel ribs have been taken into consideration for poor and very poor rock condition shown in Appendix D.

3.2 Engineering Geological Investigations

3.2.1 Introduction

In order to utilize the full potential between (EL 2219.0m) and (EL 2149.0m) keeping in view the environmental and ecological balance, various schemes namely Alternative I, Alternative II, Alternative III, Alternative III-A and Alternative IV have been investigated.

Geotechnical mapping and sub-surface investigations carried out to evaluate various alternative layouts is shown in Table 3-2.

After studying all the alternative layouts, the project authorities based on years of discussion and studies that were carried out, selected alternative IV with underground Power House as final layout.

In addition, the following tests were carried out in the final selected layout:

- In situ rock mechanics test in left and right abutment drifts for determination of C and ϕ values.
- Various physical and rock mechanics parameters on drilled core samples viz. unconfined compressive strength, tri-axial, C and ϕ and poison's ratio.
- Petrological analysis of rock and silt samples.
- Identification of Quarry Sites with Quality Assessment Report.
- Seismic Study Report.
- ODC Report.

Table 3-2. Geotechnical mapping and sub-surface investigations carried for various alternative layouts.

(1)	Geological mapping of dam site, head race tunnel, power house, tail race tunnel and diversion tunnel on 1:2000, 1:1000 and 1:500 scale	Cumulative 6000 × 600m
(2)	Drill hole core logging	Cumulative 1343.27 m
	Alternative II	50.50 m
	Alternative III	319.10 m
	Alternative III-A	50.50m
	Alternative IV	923.17 m
(3)	Drift logging	Cumulative 320 m
	Alternative III	100 m
	Alternative IV	220 m

3.2.2 Regional geology

Sach Khas Project area constitutes a part of the Pangri Valley and is characterized by rugged terrain comprising high ranges, deep valleys, escarpments and cliff faces. The area constitutes a part of great Himalayan range, older folded cover sequence and crystalline complex overprinted by Himalayan fold thrust movement, covering a stretch of Chandra-Bhaga Valley. The altitude of the area varies from 2150m and 6000m.

The Himalayas are a product of collisional tectonics, where the Indian plate collided with the Eurasian plate, around 55-50 Ma. Since the work of Gansser (1964), most workers have divided the Himalayas into a series of longitudinal lithostratigraphic domains separated by major dislocation zones/ tectonic elements shown in Figure 3-3, (Najman, 2006).

The Himalayan belt can be divided into four major structural elements shown in Figure 3-3. The main frontal thrust (MFT), main boundary thrust (MBT), main central thrust (MCT) one of the most important tectonic elements associated with Himalayan orogeny as it separates high grade metamorphic rocks of High Himalayan Crystalline sequence from weak metamorphosed series of the lesser Himalaya (Dezes et al., 1999) and south Tibetan detachment system (STDS) also known as North Himalayan shear zone (NHSZ), representing north dipping structural detachments at the boundary between High Himalayan Crystalline Sequence (HHCS) and Tethys Himalaya (Dezes et al., 1999).

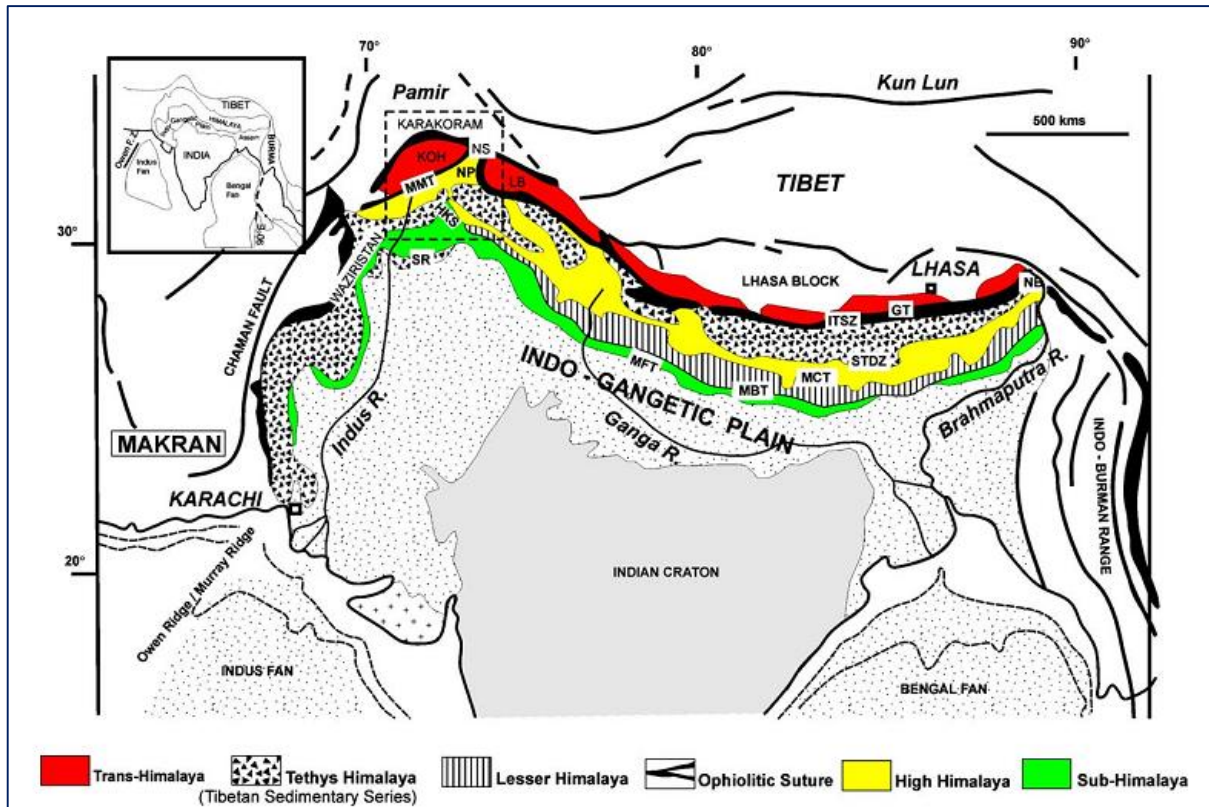


Figure 3-3. Location map of Himalaya region showing broad litho-tectonic units, MBT- Main Boundary Thrust, MCT- Main Central Thrust, MFT- Main Frontal Thrust, ITSZ- Indus-Tsangpo Suture Zone, STDZ- South Tibetan Detachment Zone, MMT- Main Mantle Thrust, NB- Namcha Barwa, GT- Gangdese Thrust, HKS- Hazara Kashmir Syntaxis, NP- Nanga Parbat, NS- Northern Suture, SR- Salt Range, LB- Ladakh batholith (Najman, 2006).

The Sach Khas project area falls in the Tethyan Himalayas having Higher Himalayan Crystalline Sequences as basement, which is extended from Pangri Valley, Chamba in the northwest to Kinnaur in the southeast. The project geology belongs to Precambrian (Chlorite - biotite Zone) as shown in Figure 3-4.

A large number of lineaments has been identified and mapped by the Geological Survey of India (Shanker et al., 1989). No profound effect of the lineaments in the project vicinity area is mentioned in reports on the project components.

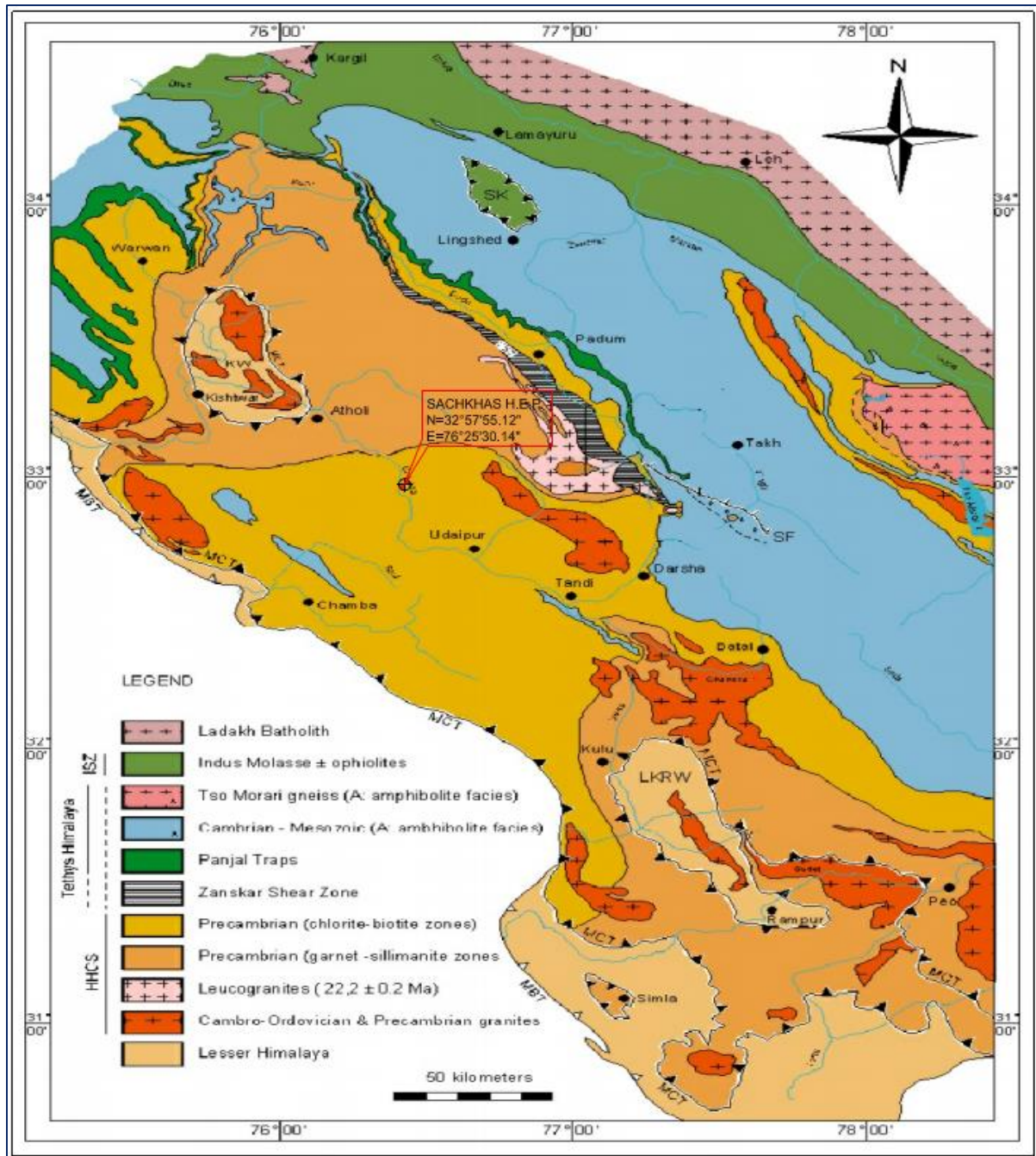


Figure 3-4. Regional Geological map of Chamba Basin with marked project location

(Larsen and Toubro(PDL), 2012b)

The project area is in seismically active regions of the Himalayas. It is continuously under stress and has been experiencing frequent crustal adjustment since the last phase of the Himalayan Orogeny. These crustal movements are identifiable in the form of reactivation of some of the existing major tectonic lineaments and the development of the cross faults along which block movements are taking place (Larsen and Toubro(PDL), 2012b). Figure 3-5 shows Seismotectonics domain of NW Himalayas.

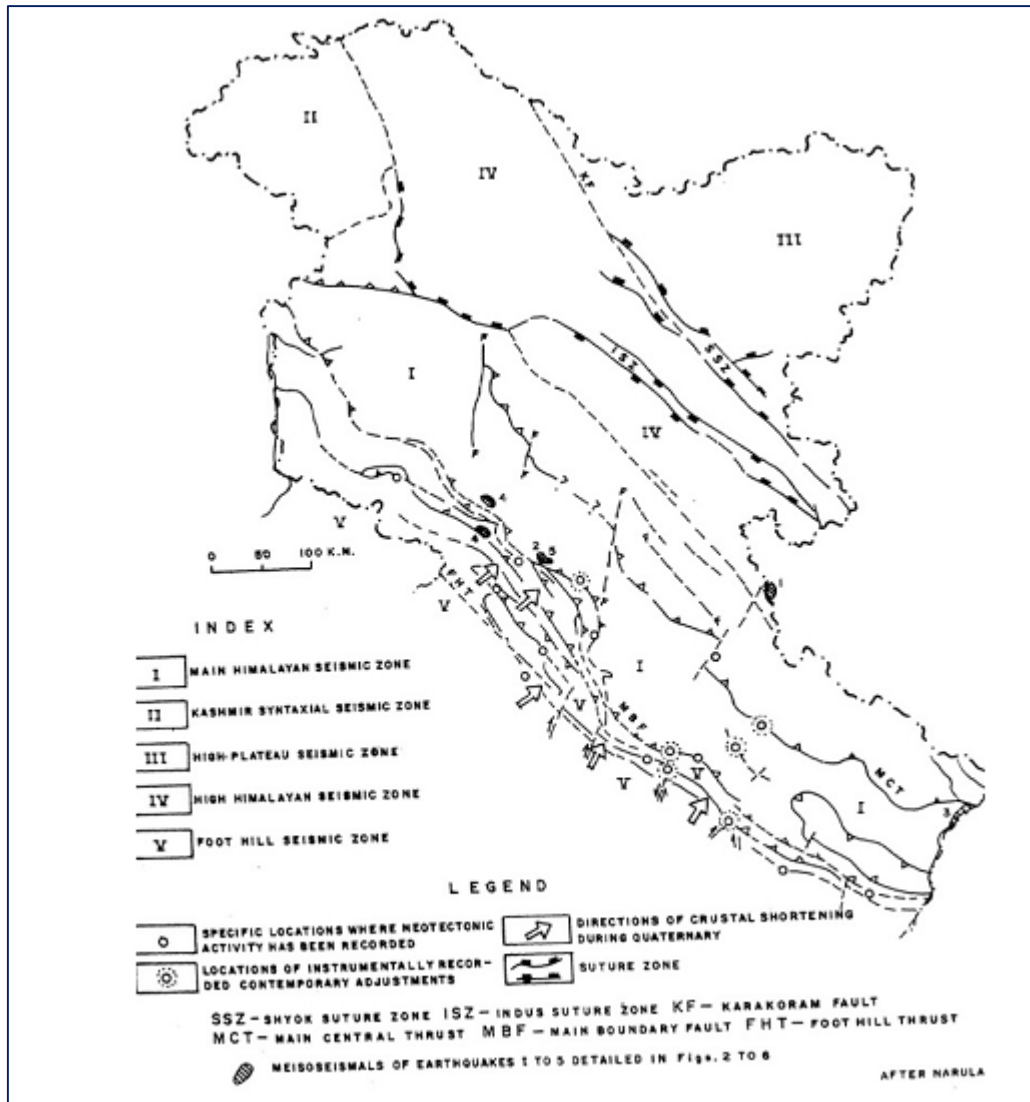


Figure 3-5. Seismotectonics domain of NW Himalayas (Larsen and Toubro(PDL), 2012b)

3.2.3 Surface and Sub surface exploration

In order to know the thickness of the overburden, nature of the rock mass, location of weak zones and slumped rock mass zones, surface and sub surface exploration drilling and drifting were carried out.

Figure 3-6 shows the plan for surface and sub surface geological explorations.

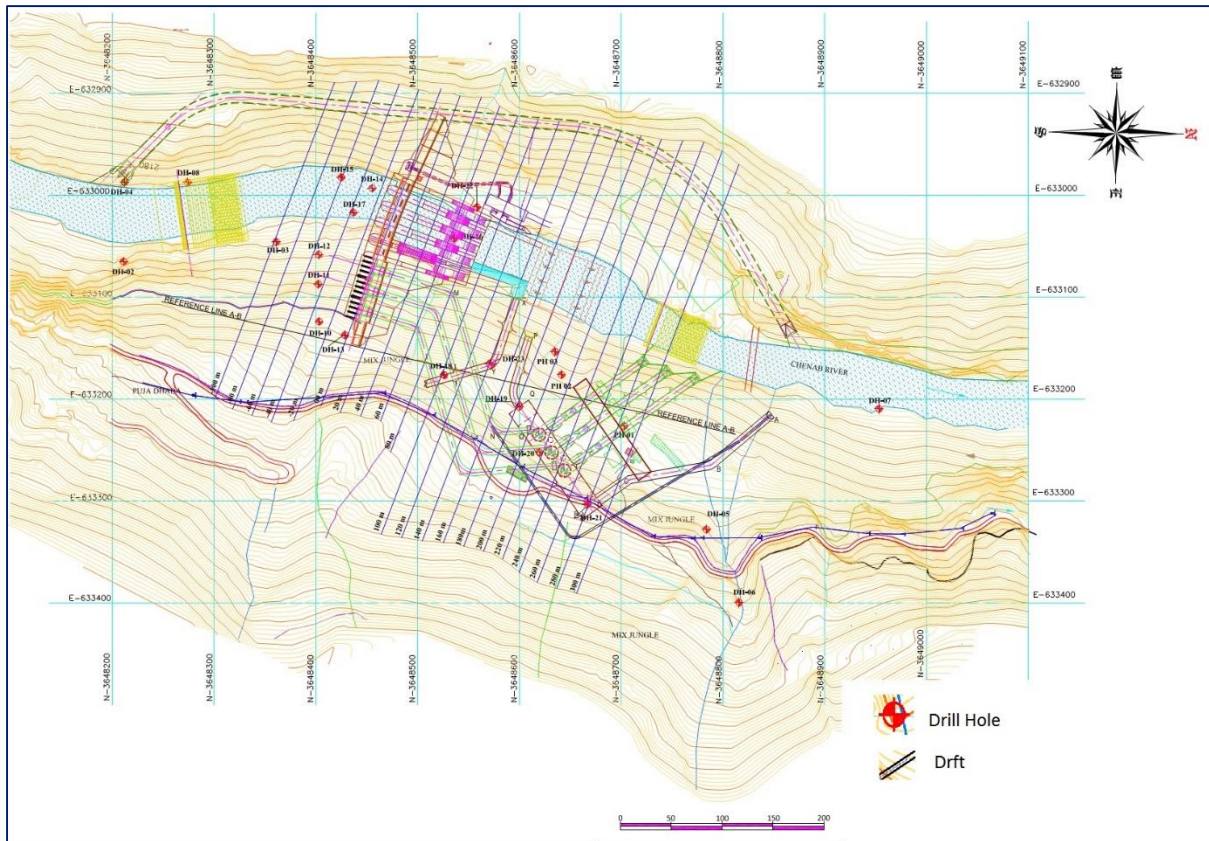


Figure 3-6. Plan surface and sub-surface geological explorations (Larsen and Toubro(PDL), 2012b)

3.2.4 Project geology

In Chenab Valley, especially in the Pangi and Pattan area, i.e. the project area, the stratigraphic column is essentially composed of a thick and monotonous series of upper Proterozoic to Cambrian detrital sediments belonging to Haimanta Group (Section 3.2.2). These rocks are essentially alternatively thick beds of clastic rock such as dark grey quartzite, quartzitic phyllite, phyllitic quartzite, slates, pelites diamictites and bands of dolomites. In the Sach Khas area sandier lithology dominates over the pelitic sediments. The regional strike of these formations trend NW-SE dipping 45° to 85° SW directions with local variation due to folding. Surface geological mapping is carried out in the entire project area under appropriate scale.

3.3 Underground powerhouse cavern

The underground power house (126mX23mX48.5m) has been proposed to be located in the north-south trending ridge forming right abutment about 300m downstream of the dam axis. The cavern has been explored by 4 drill holes, which established the vertical rock cover of the order of 45m and exploratory drift (300m) long.

The area encompassing the underground power house and appurtenant structures is covered with reworked fluvio glacial deposits, talus and scree, and exhibits luxuriant growth of tall fern

trees and deciduous forest. The area hasn't shown any creep movement, as evident from the stability of the slope.

Observations made from the investigations in and around the Underground Power house cavern site during exploration study are shown in Appendix E.

3.3.1 **Rock Type**

Rock masses encountered in the drift and in the drill holes are hard and fresh, grey colour quartzite, diamictite and phyllite interbands with two plus random joint sets.

The proposed power house cavern is likely to encounter fresh and hard quartzite (55% to 60%), diamictite and phyllitic quartzite (30% to 35%) in 80 to 85% reach, phyllite in 10% reach and sheared and shattered rock mass in 5% reach (Larsen and Toubro(PDL), 2012b), as per the exploration made through drift tunnelling and the drill holes.

The underground cavern will be located in grey quartzite, diamictite and phyllitic quartzite bands. The general trend of foliation is N125°E with 35° – 76° SW dip.



Figure 3-7. Rock face at RD 114.0m in power house drift (PH-1) Alternative IV

(Larsen and Toubro(PDL), 2012b)

3.3.2 **Jointing**

Rosettes are plotted based on values from outcrops and drift logs database. Figure 3-8 (left) shows rosette plot of all the joint measurements from the outcrops and drifts logs in the whole

project area and Figure 3-8 (right) shows joint measurements in & around the underground Powerhouse complex.

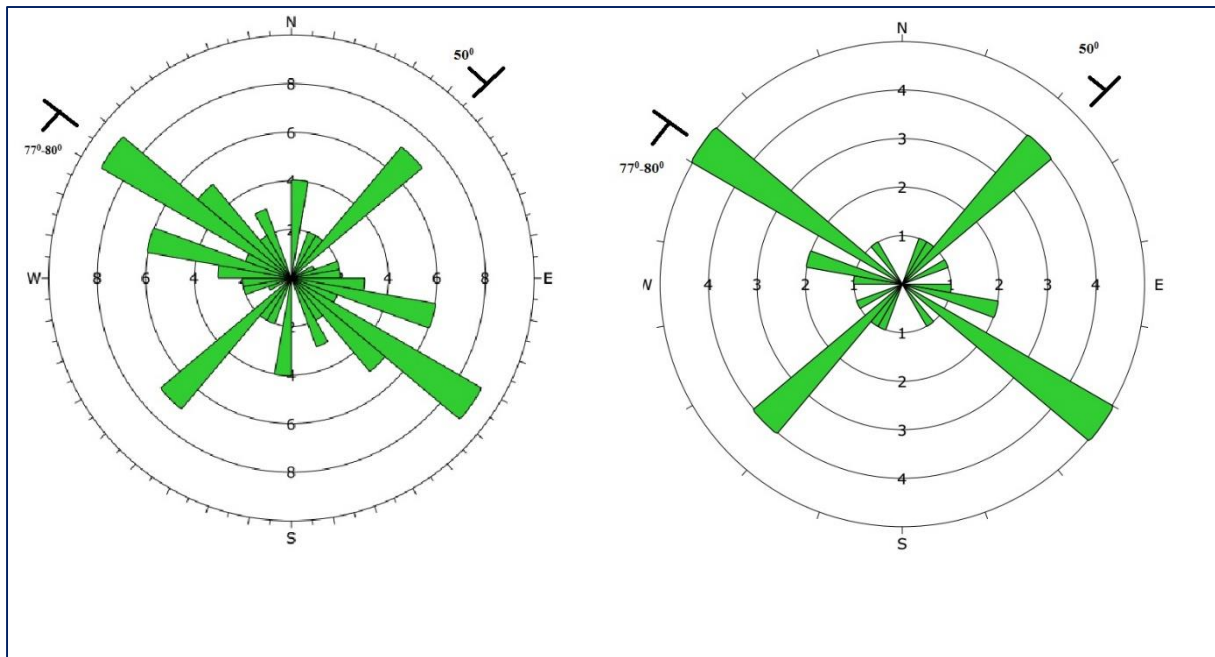


Figure 3-8. Rosette plots of the joint measurements (exploratory drifts) whole project area (left) and in powerhouse caverns(Power House Drift) (right).

Appendix F shows the orientation of prominent joint sets of the Sach Khas underground power house cavern along with joint characteristics.

3.3.3 Weakness zones

The geological L-section through water conductor system (Appendix G) shows that the area of the powerhouse complex avoids conflicts with any weakness zones.

3.3.4 Stress situation and executed measurements

The project is located in highly seismic central Himalayas, the region is continuously under stress and experiencing frequent crustal adjustment (Section 3.2.2).

In-situ stress measurement in the powerhouse cavern area is done by hydraulic fracturing test. Figure 3-9 shows a typical hydraulic fracturing schematic (Haimson and Lee, 1984). test procedure is carried out by sealing a section of the borehole with packers (Inflatable rubber), and pressurising the section until tensile failure occurs, which gives us the fracture initiation pressure (P_f). By stopping the pressurizing process, the shut-in pressure (P_s) is reached, yielding the pressure where the fracture is sealed. Re-pressurisation process is used to determine fracture reopening pressure (P_r) and repeated measurements of the shut-in pressure (Figure 3-10). The

direction of the hydro fracture is obtained by use of oriented impression packer (AECS Engineering and Geotechnical Services Pvt. Ltd, 2014).

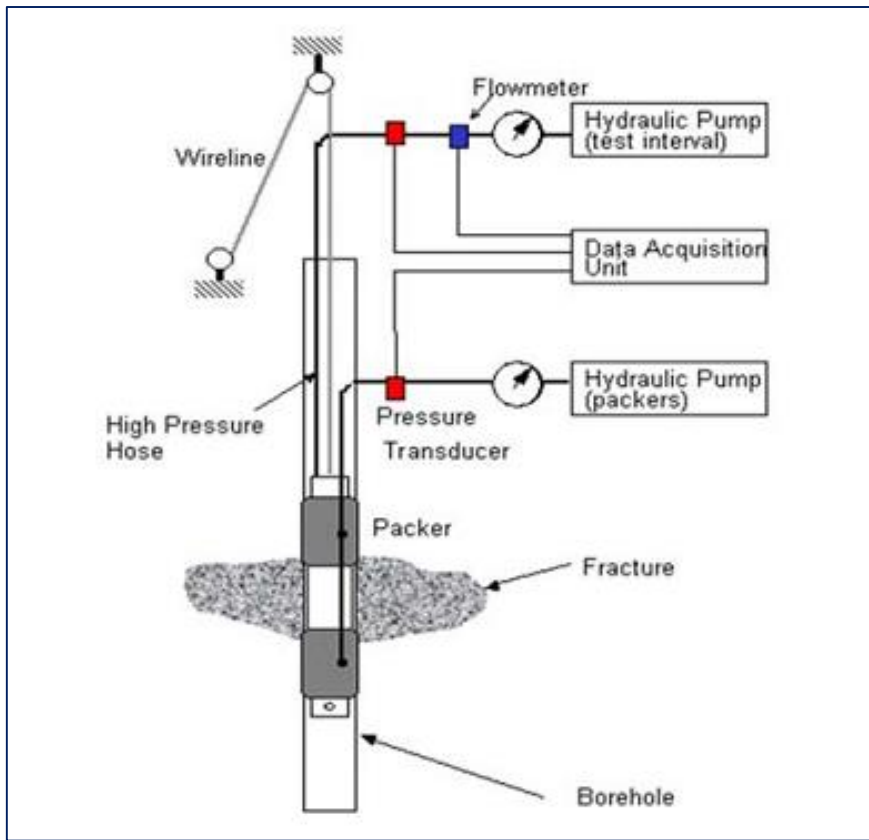


Figure 3-9. A Typical Hydraulic Fracturing System Schematic (Haimson and Lee, 1984).

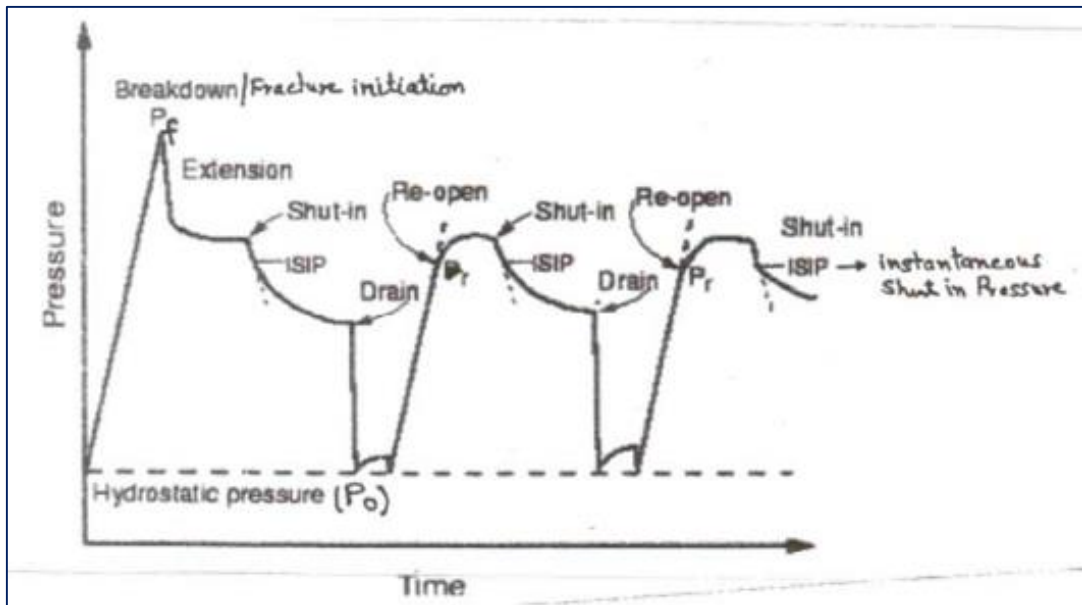


Figure 3-10. Pressure-Time plot of typical hydraulic fracturing experiment showing three pressurisation cycles. During shut in phase, the instantaneous shut-in pressure is observed, which is identical to the least secondary principal stress. Modified after (Brudy, 1995).

Minimum horizontal principal stress magnitude and direction:

$$\sigma_h = P_s \quad \text{Eq- 3.1}$$

Where σ_h is the minimum horizontal stress, P_s is the shut in pressure and the direction of σ_h is obtained directly from the azimuth of the HF.

Maximum horizontal principal stress magnitude and direction:

In case of fracture initiation cycle, the calculation for σ_H is made by using Eq- 3.2.

$$\sigma_H = T + 3\sigma_h - P_f - P_o \quad \text{Eq- 3.2}$$

Where σ_H is the maximum horizontal principal stress, T is Tensile strength of the tested rock, P_f is Fracture initiation pressure or break down pressure & P_o is initial pore water pressure. The direction of the maximum horizontal stress is perpendicular to the σ_h direction. Eq- 3.2 is used for initial pressurization cycle.

In case of subsequent pressure cycles, the calculation for σ_H is made using Eq- 3.3.

$$\sigma_H = 3(\sigma_h) - (P_r) - P_o \quad \text{Eq- 3.3}$$

Where P_r is the fracture reopening pressure obtained from pressure-time plot of the HF test.

Vertical Stress:

The vertical stress is estimated from the overburden (Table 7-5).

The calculation of maximum principal stress contains a relatively large uncertainty, hence should be verified by other stress measurements methods for example overcoring method.

After analysing all max. and min. horizontal stresses and the corresponding orientations, the average values of maximum principal stress (σ_H) and minimum principal stress (σ_h) is considered appropriate for design of power house cavern (AECS Engineering and Geotechnical Services Pvt. Ltd, 2014). The orientation of σ_H based on tests in vertical hole. Table 3-3 shows the in-situ stress results.

Table 3-3. In-situ stresses at power house site (AECS Engineering and Geotechnical Services Pvt. Ltd, 2014)

Results	Values (MPa)		Remarks
In-situ Vertical Stress (σ_v)	1.60-2.04 (Original Alignment)	1.74-1.79 (Alternative Alignment)	Based on overburden range from 59m-75m (Original Alignment) and 68m-64m (Alternative Alignment). Average rock density of 2.72T/m ³ .
Maximum Horizontal principal stress (σ_H)	10		Orientation of σ_H varies N50°E to N86°E.
Minimum Horizontal principal stress (σ_h)	5.88		

3.4 Placement and orientations of underground caverns

3.4.1 Original placement and orientation

The planned location of the cavern is shown in Appendix M, the cavern is located in low cover varying between 59m (minimum) and 70m (maximum) with rock cover of 45m (minimum) and 48m (maximum) respectively.

The alignment of the power house cavern was tentatively selected taking into consideration the geometry of the structural discontinuities in the rock. For a better stability of the roof and wall and to have minimum problems of over breaks, the long axis of the underground cavern should be as much oblique to the strike direction of the major discontinuity planes as possible. Since it was not possible to keep the alignment in a direction normal to the strike direction of all the discontinuities, an alignment had to be found which was best oriented with respect to all structured features present in the area. The best orientation of power house cavern according to project authorities was found to be in N55°E direction (Figure 3-11). This orientation was selected without taking into consideration of the in-situ stress measurement and stress directions. It is almost parallel to the secondary joint set and in line with the directional range of σ_H (max. horizontal principle stress) which can cause tensional cracks on the roof along the length. Figure 3-11 illustrates the cavern orientation with respect to measured joint orientation and major horizontal stress.

3.4.2 Alternative placement and orientation

The project authorities haven't changed the alignment after the submission of hydraulic fracturing test by the concerned agency. However, an alternative orientation of the cavern is proposed as a part of this thesis. The length axis of the new proposed orientation is aligned in N20°E (Section 2.6.3). Figure 3-11 shows the orientation of cavern in the rosette plot, together with original orientation and major horizontal stress. There will be slight change in the length of the pressure shafts and degree of bends which will influence the head loss and effect power output. Changes due to penstock alignment are not discussed in this thesis.

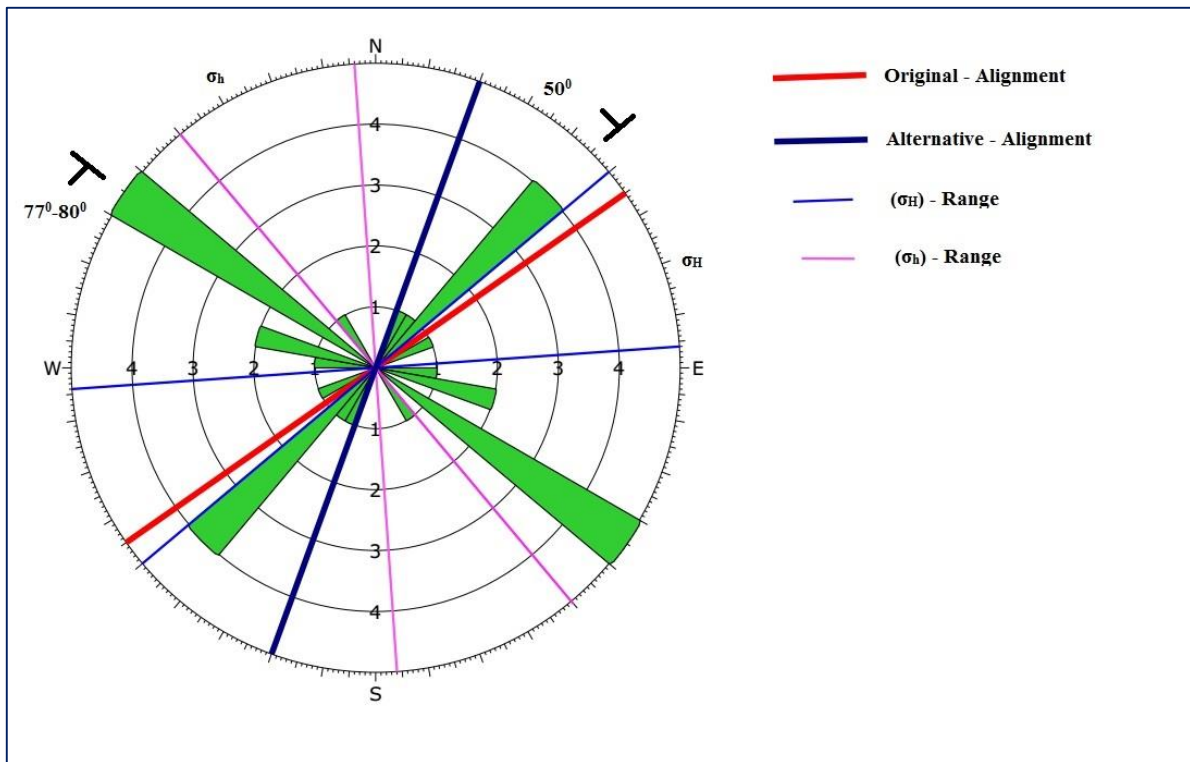


Figure 3-11. Rosette plot of the joint measurements in and near powerhouse complex. Length axis for the caverns for both alternatives are indicated together with directions for range of major and minor horizontal stresses from the hydraulic fracturing measurements.

4 MECHANICAL PROPERTIES OF ROCK IN PROJECT AREA

4.1 Introduction

List of in-situ tests carried out at the project site are described below:

- Measurement of In-situ Deformability of rock mass by Cyclic Plate Load Test (Rigid Plate Method)
- Hydraulic Fracturing (HF) Test for determination of in-situ stresses at the power house site.

The following laboratory tests were conducted on the rock core samples:

- Index Tests
 - Bulk Density
 - Water Content at Saturation
 - Specific Gravity
 - Porosity
- Uniaxial Compressive Strength
 - Dry Condition
 - Saturated Condition
- Tensile Strength (Brazilian Test)
- Elastic Parameters-Modulus of Elasticity & Poisson's Ratio
- Dynamic Modulus
- Triaxial Compression Test for $C - \phi$ Parameters

4.2 Test results

4.2.1 *In-Situ Test Results*

In-situ deformability of rock mass by Cyclic Plate Load Test (Rigid Plate Method) has been taken from the right bank dam exploratory drift, which is about 300 metre above the power house site with similar rock conditions.

Table 4-1. In-situ Deformability of rock mass (Larsen and Toubro(PDL), 2012a; Larsen and Toubro(PDL), 2012b)

Location	Direction	Modulus of Deformation (GPa)	Stress Level (MPa)
Dam Site (Right Bank Drift)	Vertical	3.25	3.54
	Horizontal	3.50	

In-situ stresses at power house site are shown in Table 4-2 and discussed in section 3.3.4.

Table 4-2. In-situ stresses at power house site (AECS Engineering and Geotechnical Services Pvt. Ltd, 2014)

Results	Values (MPa)		Remarks
In-situ Vertical Stress (σ_v)	1.60-2.04 (Original Alignment)	1.74-1.79 (Alternative Alignment)	Based on overburden range from 59m-75m (Original Alignment) and 68m-64m (Alternative Alignment). Average rock density of 2.72T/m ³ .
Maximum Horizontal principal stress (σ_H)	10		Orientation of σ_H varies N50°E to N86°E.
Minimum Horizontal principal stress (σ_h)	5.88		

4.2.2 Laboratory Results

Rock core samples from different bore holes of Sach Khas project were collected by project authority and transported to laboratory for carrying out the requisite laboratory test (Section 4.1) Laboratory test results are shown in Table 4-3.

Table 4-3. Laboratory test results (Larsen and Toubro(PDL), 2012a; Larsen and Toubro(PDL), 2012b)

Tests		Values	Units
Index Tests	Bulk Density	2.72	t/m ³
	Water Content at saturation	0.20 – 0.32	%
	Porosity	0.51	%
Uniaxial Compressive Strength	Dry Condition	54 – 85	MPa
	Saturated condition	53 – 83	MPa
Tensile Strength		10 – 13	MPa
Modulus of Elasticity		45 – 67	GPA
Poisson's Ratio		0.20	
Cohesion (c)		5 – 10	MPa
Friction angle (Φ)		46-51	Degree

Saturated condition values for Uniaxial Compressive Strength (UCS) will be used as input in the empirical and numerical analysis (Panthi, 2016).

5 STABILITY ANALYSIS METHODS AND ROCK SUPPORT PRINCIPLES

5.1 Estimating stress distribution

Predicting in-situ stress redistribution is important in terms of assessing stability around excavations. It is a complex task limited to simplified two – dimensional problems when approached analytically. Stress situation close to the excavation contour is of particular significance. These stresses depend on in-situ stress field and excavation geometry (Palmstrom and Stille, 2010). Idealised analytical equations for homogeneous materials are presented in this thesis as in reality the joints and discontinuities will influence the stress distribution.

Stresses around a circular opening in an Isostatic stress condition ($\sigma_h = \sigma_v = \sigma$) depend on the distance (r) from the opening centre. In absence of external forces on the excavation surface, radial (σ_r) and tangential (σ_θ) stress magnitude is given by Eq- 5.1 & Eq- 5.2, illustrated in Figure 5-1.

$$\sigma_r = \sigma_o \left(1 - \frac{r^2}{R^2} \right) \quad \text{Eq- 5.1}$$

$$\sigma_\theta = \sigma_o \left(1 + \frac{r^2}{R^2} \right) \quad \text{Eq- 5.2}$$

Where, σ_0 is virgin stresses, r is opening radius and R is radial distance (Palmstrom and Stille, 2010; Panthi, 2006).

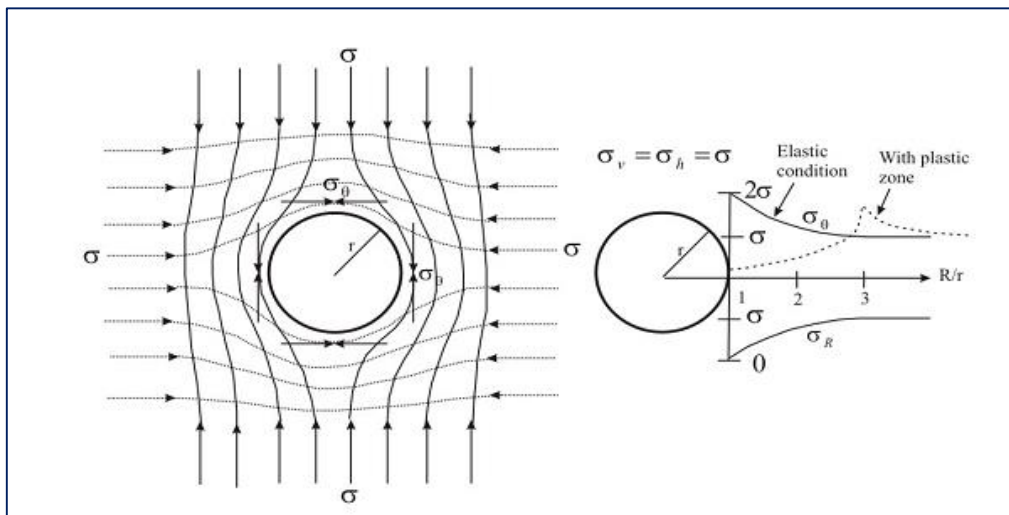


Figure 5-1. Stress trajectories in surrounding a circular opening (left) and tangential and radial stress distribution in elastic and non-elastic conditions (right) (Panthi, 2006).

In anisotropic stress conditions the tangential stresses will vary around the periphery of the circular opening. According to Kirsch's solution, tangential stress will reach its maximum value

($\sigma_{\theta max}$) where maximum principle stress (σ_1) is tangent to the excavation contour and its minimum value ($\sigma_{\theta min}$) where the minimum principal stress (σ_3) is tangent to the excavation contour. The actual values according to Kirsch's equations:

$$\sigma_{\theta max} = 3\sigma_1 - \sigma_3 \tag{Eq- 5.3}$$

$$\sigma_{\theta min} = 3\sigma_3 - \sigma_1 \tag{Eq- 5.4}$$

Eq- 5.1, Eq- 5.2, Eq- 5.3 & Eq- 5.4 are valid for homogeneous, isotropic and elastic rock mass having wide spaced and tight joints. In weak and anisotropic rocks, steady reduction in strength by tangential stresses drives the zone of broken rock deeper, forming a plastic zone. In such rock mass (Figure 5-1 (right) dotted lines), maximum tangential stresses are moved further, until the elastic zone is reached (Panthi, 2006). A solution for stresses and displacements derived from the theory of plasticity may provide a useful basis for the analysis in such rock mass condition (Goodman, 1989).

Kirsch's equation is strongly influenced by the degree of stress anisotropy i.e. large stress anisotropy might cause negative tangential stresses resulting in tensional jointing. In theory, the stress magnitude depends on shape and not on the size of excavated opening. Nevertheless, the zone of influence will increase with larger openings (Palmstrom and Stille, 2010).

Kirsch's equation calculates tangential stresses at four points around a circular opening. To apply stress analysis for caverns, it's important to calculate the tangential stresses around different shapes.

Empirical approaches are used to estimate the magnitude of tangential stresses for different excavation shapes. Based on a large number of boundary element analyses, Hoek and Brown (1980) developed a method to calculate the magnitude of tangential stresses in roof ($\sigma_{\theta r}$) & wall ($\sigma_{\theta w}$) in massive rocks.










									
A	5.0	4.0	3.9	3.2	3.1	3.0	2.0	1.9	1.8
B	2.0	1.5	1.8	2.3	2.7	3.0	5.0	1.9	3.9

Figure 5-2. Values for the factors A and B for various excavation shapes(Nilsen and Palmström, 2000)

$$\sigma_{\theta r} = (A \times k - 1)\sigma_z \quad \text{Eq- 5.5}$$

$$\sigma_{\theta w} = (B - k)\sigma_z \quad \text{Eq- 5.6}$$

Where A and B are factors for excavation geometry (Figure 5-2), k is the horizontal/vertical stress ratio and σ_z is the vertical stress (Nilsen and Palmström, 2000).

5.2 Classifying rock mass quality

Rock mass strength, deformability properties, strength anisotropy, mechanical characteristics of discontinuities and degree of weathering are factors influencing the quality of rock mass (Panthi, 2006), making potential stability problems difficult to quantify. Hence, subjective judgements and practical experiences help evaluate stability & rock support. Classification systems are helpful, as they relate decisions to the experiences gained on other sites (Nilsen and Thidemann, 1993).

The purpose of a classification system is to identify features/parameters of significance and perform assessment. The system describes properties of parameters, assigns values to respective structure, composition and properties (Palmstrom and Stille, 2010). Following are the aims of the classification system:

- Identify similar geomechanical characteristics zones of material.
- Predict stability indications for excavation of any given size.
- Appropriate support strategy selection.
- Suggest in-situ rock mass strength, modulus of deformability etc.

(Palmstrom and Stille, 2010)

Several classification systems have been developed over the years, the ones involving rock support estimates are relevant in terms of stability assessment. Q system, RMR and GSI will be used in this thesis and discussed in detail. Use of two rock mass classification schemes side by side is recommended (Hoek, 2007).

5.2.1 Q-system

The Q-system was developed based on analysis and evaluation of several tunnel cases, by Barton et al (1974) of Norwegian Geotechnical Institute (NGI). It gives a useful relationship between Q-value and tunnel rock support. The system went through updates in 1993 (Grimstad and Barton, 1993). The numerical value of the index Q varies on a logarithmic scale from 0,001 – 1000.

Q-system is based on numerical assessment of six different input parameters defined by Eq- 5.7.

$$Q = \frac{RQD}{J_n} \times \frac{J_r}{J_a} \times \frac{J_w}{SRF} \quad \text{Eq- 5.7}$$

Where RQD is the rock quality designation, J_n is the joint set number, J_r is the joint roughness number, J_a is the joint alteration number, J_w is the joint water reduction factor, and SRF is the stress reduction factor (Barton et al., 1974; Hoek, 2007).

These parameters are measures of block size (RQD/J_n), Inter-block shear strength (J_r/J_a) & Active stress (J_w/SRF) (Palmstrom and Broch, 2006).

Together Q-value, span (or wall height) of the excavation and excavation support ratio (ESR), Q-system recommended the amount of support in the Q-value chart (Appendix I). Bieniawski (1989) (Eq- 5.8) and Barton (1995) (Eq- 5.9) published formulas to calculate Q-value from RMR.

$$RMR = 9 \times \ln Q + 44 \quad \text{Eq- 5.8}$$

$$RMR = 15 \times \ln Q + 50 \quad \text{Eq- 5.9}$$

(Panthi, 2006).

In the thesis, Eq- 5.8 & Eq- 5.9 will be used to confirm RMR value calculated from the data available from drill holes and exploratory drifts using guidelines given in Appendix H.

5.2.2 **Rock Mass Rating (RMR)**

Bieniawski (1976) developed rock mass classification called the Geomechanics Classification or Rock Mass Rating (RMR) system. Classification system has been modified over the years as more case histories have become available (Hoek, 2007). Last modification was made in 1989 (Bieniawski, 1989) and is the basis for study in this thesis. The RMR-system uses the following six parameters to classify a rock mass:

- Uniaxial compressive strength of the rock
- Rock quality designation (RQD)
- Spacing of discontinuities
- Condition of discontinuities
- Ground water conditions
- Orientation of discontinuities

Rock mass is divided into a number of structural regions and each region is classified separately in RMR classification. Region boundaries coincide with major structural features e.g. faults. The RMR system with recommendation for rock support is presented in Appendix H. The guidelines have been published only for a 10 m span drill and blast horseshoe shaped tunnel in rock mass subjected to a vertical stress < 25 MPa (Hoek, 2007; Palmstrom and Stille, 2010). In the 1989 version of Bieniawski's classification, RMR value has a groundwater rating set to 15 and the adjustment for joint orientation is set to zero (Appendix H) (Hoek and Brown, 1997). Main strength of the RMR-system is its relationship with the stand-up time as shown in Figure 5-3.

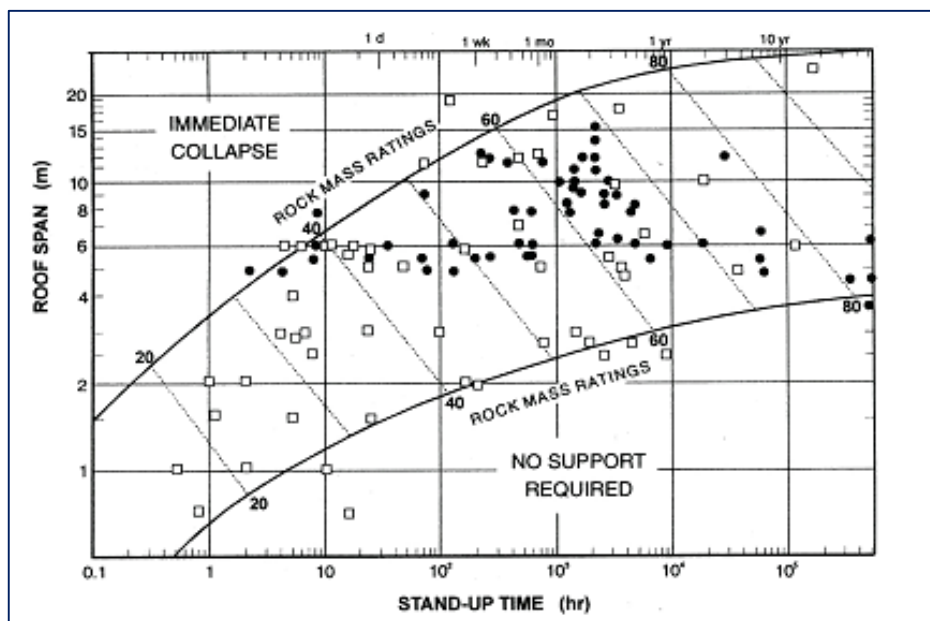


Figure 5-3. Stand-up time of an underground opening as a function of roof span and RMR value (Bieniawski, 1989)

The RMR and GSI values are linked by the following relationship:

$$RMR = GSI + 5 \quad \text{Eq- 5.10}$$

5.2.3 Geological strength index (GSI)

Geological Strength Index (GSI) estimates the strength of jointed rock masses based on the assessment of the interlocking and condition of the surface between the rock blocks (Marinos and Hoek, 2000). Today GSI represents the most universally used engineering index for classifying rock mass quality and is used as input for continuum numerical analysis codes and closed form solutions based on the Hoek–Brown failure criterion (Morelli, 2015). Bieniawski's RMR is difficult to apply to very poor quality rock mass and a nonlinear relationship existed

between RMR and m and s at very low ranges, hence, GSI was introduced (Hoek, 1994; Hoek et al., 1995; Hoek and Marinos, 2007). GSI provides a value which, when combined with the intact rock properties, estimates the reduction in rock mass strength of different geological conditions (Hoek, 2007).

GSI permits the manifold aspects of rock to be quantified, hence enhancing geological logic and reducing engineering uncertainty, making it easy to assess the variables that make up rock mass, giving it an advantage of adjustments for its ratings to cover a wide range of rock masses and conditions (Marinos et al., 2005). Figure 5-4 shows the general GSI chart, which is relevant for the further analysis in this thesis.

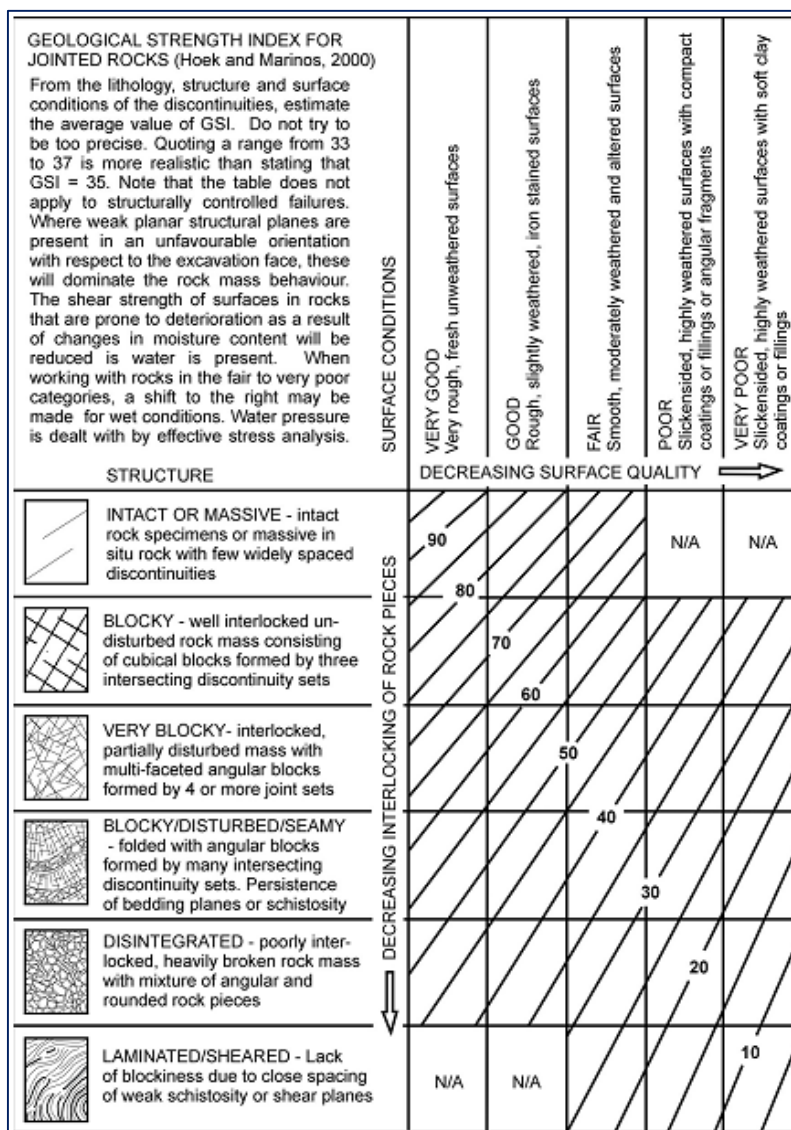


Figure 5-4. General chart for GSI estimates from the geological observations (Marinos et al., 2005)

The major strong point of the GSI system is its interconnection with rock mass strength (σ_{cm}), rock mass deformation modulus (E_{rm}) and constants m and s of Hoek-Brown failure criterion (Panthi, 2006).

5.2.4 Limitations

There are several limitations in empirical methods used for rock mass classification system. The classification systems important in order to describe the stability characteristics of the rock mass. Best application of classification system is in jointed rock mass where instability is caused by block fall (Palmstrom and Stille, 2010).

Classification systems used at present are simplified by overlooking local geometrical and structural features and cover a wide range of conditions giving an averaged value. Significant variation can exist between highest and lowest values, as support charts are derived from cases where the installed supports are based on varying contractual conditions. The excavation methodology and rock support practices used around the world will contribute to these uncertainties (Palmstrom and Stille, 2010). A lot of uncertainties and variations exist between rock mass classification, actual support and between different classification systems shown in the Figure 5-5.

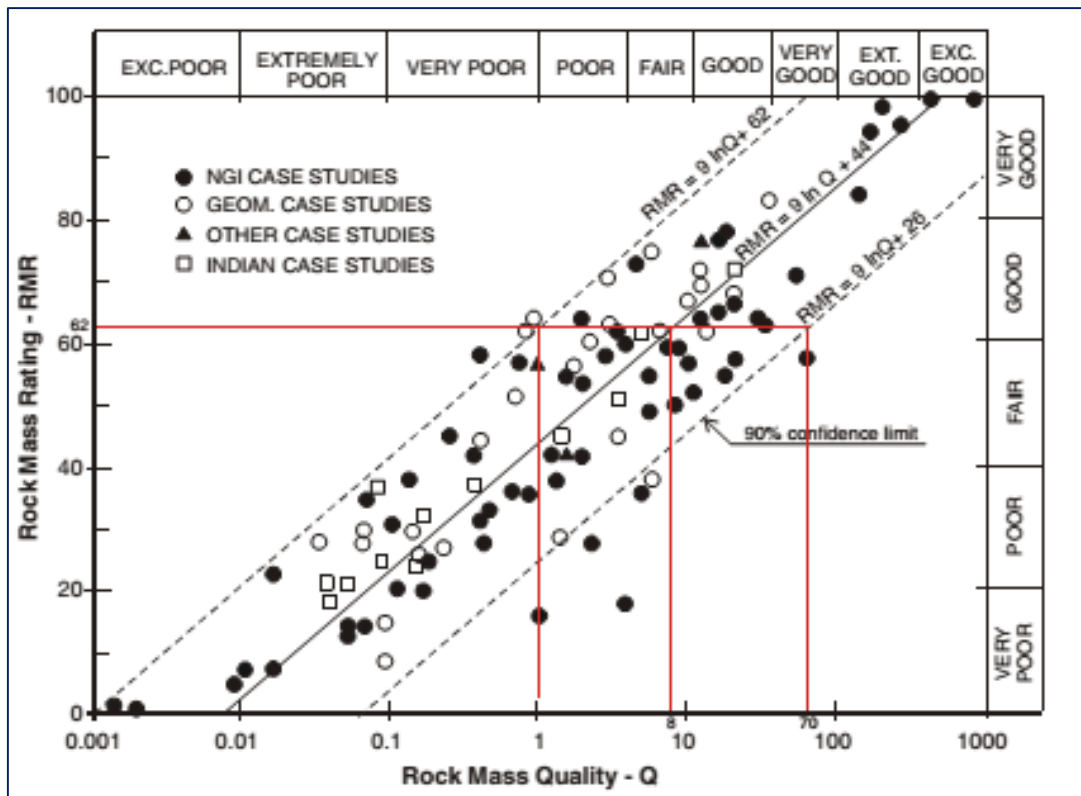


Figure 5-5. The correlation between RMR and Q .Example: for RMR = 62 Q spans from 1 to 70 (very poor/poor to very good) (Palmstrom and Broch, 2006).

While proposing rock support for underground caverns with significantly larger span than 10 meters, RMR system is unfavourable as it has limitations in terms of size and shape of the excavation. It is not optimal when dealing with stress related stability problems, as the rock stresses are not input parameters to the RMR system. SRF makes sure that rock stresses are taken into account in Q system. The SRF is a sort of “correction factor” or “fine tuning factor”, apart from just a factor expressing active stress to get Q-value to estimate appropriate rock support (Palmstrom and Broch, 2006).

Nevertheless, optimisation of the rock support is a complex task. Empirical systems make an important contribution to such optimization and assessment. At least two classification systems should be used when doing rock engineering and designs based on empirical tools (Palmstrom and Stille, 2010).

5.3 Predicting failure extent

Failure is a function of in-situ stress magnitude and characteristics of the rock mass around underground openings. Failure process is controlled by continuity, density and orientation of joints in case of the low in-situ stress magnitudes and is dominated by stress induced fracturing, proliferating parallel to the excavation boundary, with an increase in in-situ magnitudes (Martin et al., 1999).

In-situ rock mass strength called “apparent” rock strength obtained from back analysis, underestimates the actual rock mass strength. But if equivalent simplified excavation boundaries are used, the approach can still be useful in design (Cai and Kaiser, 2014). Hoek and Brown (1980) developed empirical stability classification using back-analyses based on the South African cases for far field stress ratio (K_0) of 0.5 and ratio of far-field maximum stress (σ_1) to the laboratory uniaxial compressive strength (σ_c). Figure 5-6 shows the classification and is briefly described as follows:

$\sigma_1 / \sigma_c \leq 0.1$: a stable unsupported opening

$\sigma_1 / \sigma_c = 0.2$: minor spalling can be observed, requiring light support

$\sigma_1 / \sigma_c = 0.3$: severe spalling, requiring moderate support

$\sigma_1 / \sigma_c = 0.4$: heavy support required to stabilize the opening

$\sigma_1 / \sigma_c = 0.5$: extreme support required, stability of the opening may be very difficult to achieve (Martin et al., 1999)

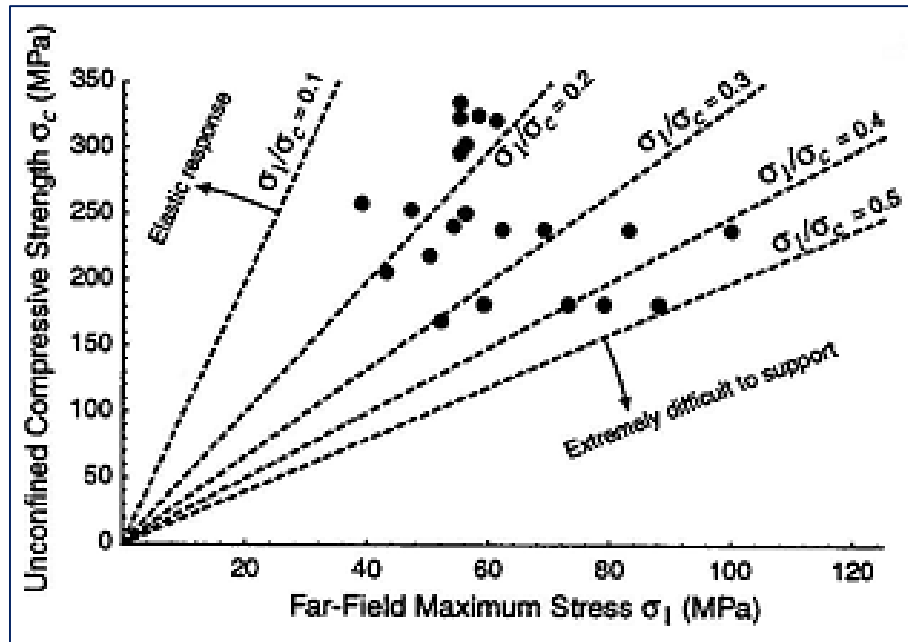


Figure 5-6. Empirical stability classification developed for square tunnels in South Africa ($K_0 = 0.5$)
(Martin et al., 1999)

Before applying the South African classification to any other site, it is crucially important to evaluate the effect of the excavation boundary and changing stress ratios on the maximum tangential stress at the boundary (Martin et al., 1999).

Figure 5-7 illustrates spall and strain burst potential based on the intact rock properties. Squeezing is dominant over bursting at depths where spalling potential is low due to dominating shear forces (Diederichs, 2007). Spalling potential is linked to the brittleness of the rock whereas rock bursting depends on higher energy and strong rocks.

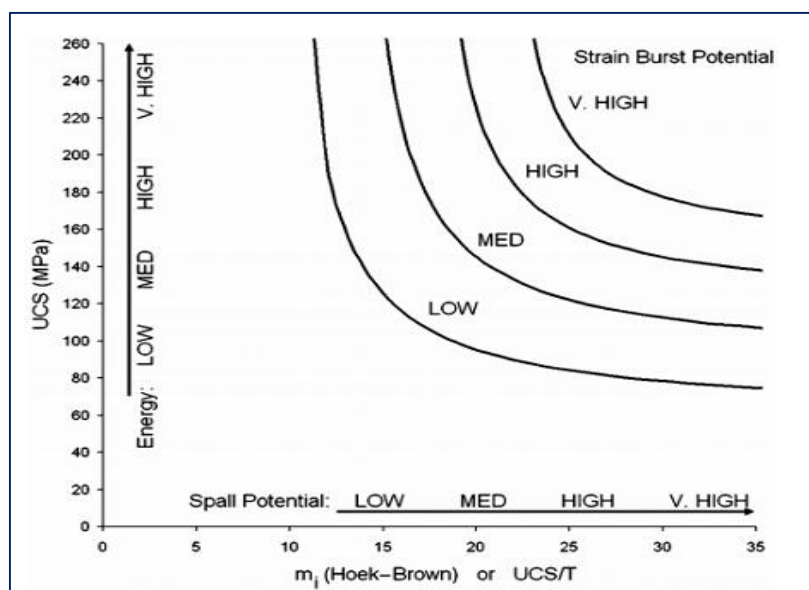


Figure 5-7. Spall potential and strain burst potential as a function of UCS and m_i or UCS/T (Diederichs, 2007)

The relationship between maximum tangential stress on excavation boundary and uniaxial compressive strength of the intact rock has been widely studied over the years. It has been observed through empirical evidence that the initiation of stress induced brittle failure occurs when the damage index exceeds 0.4 ± 0.1 . The damage index is expressed as ratio of max tangential boundary stress to unconfined compressive strength (UCS) (Martin et al., 1999). Rock failure in massive to moderately jointed hard rock in an excavation initiates when maximum tangential stress at the excavation boundary exceeds 0.3 to 0.4 times the rock's UCS (Cai and Kaiser, 2014). The spalling strength in crystalline rocks is commonly between 0.4-0.6 of the rock's UCS (Martin and Christiansson, 2009).

There are many factors that contribute to the low spalling strength as compared to the UCS of the intact rock, such as pre-existing damage, surface interaction effects, stress rotations, loss of effective confinement into the excavation due to progressive slabbing and loading path. Additionally, the difference in geometry between the laboratory tests and in-situ conditions also contributes to the low spalling strength (Cai and Kaiser, 2014).

Cai and Kaiser (2014) maintain that spalling strength of 0.4 ± 0.1 times UCS is overestimating the actual strength of the rock mass, as put forward by Martin et al. (1999). This result is based on the studies of the smooth excavation contours and does not consider excavation boundary irregularities. This leads to local stress concentration yielding higher tangential stresses than the theoretical maximum for the smooth contour.

Cai and Kaiser (2014) maintain that the spalling strength of 0.3-0.4 times UCS can only be used to describe field rock strength when simplified model geometry are used. For analysis in this thesis, simplified model geometry is the case. Hence, in-situ spalling strength of 0.4 times UCS is used for estimation.

There are several failure modes dependent on stress situation and rock mass properties. Figure 5-8 shows different modes for the brittle rock where CI specifies the crack initiation threshold (typically 35-50% of UCS) and CD describes the yield or crack damage threshold (typically 70-90% of UCS) (Diederichs et al., 2010).

Stability analysis is not just predicting potential spalling, rock bursting and squeezing. Information about the depth impact of the failure is of great importance regarding optimization of the support design, e.g. determining the length of the rock bolt. Martin (1997) suggested the deviatoric stress criterion (Eq- 5.11) providing an estimate of radial extent of failure. The criterion is somewhat conservative but still provides a good estimate of the depth of the failure.

At low confining stresses, as around underground excavation, cohesion loss dominates the failing process.

$$\sigma_1 - \sigma_3 = \frac{1}{3} \sigma_c \tag{Eq- 5.11}$$

(Martin, 1997).

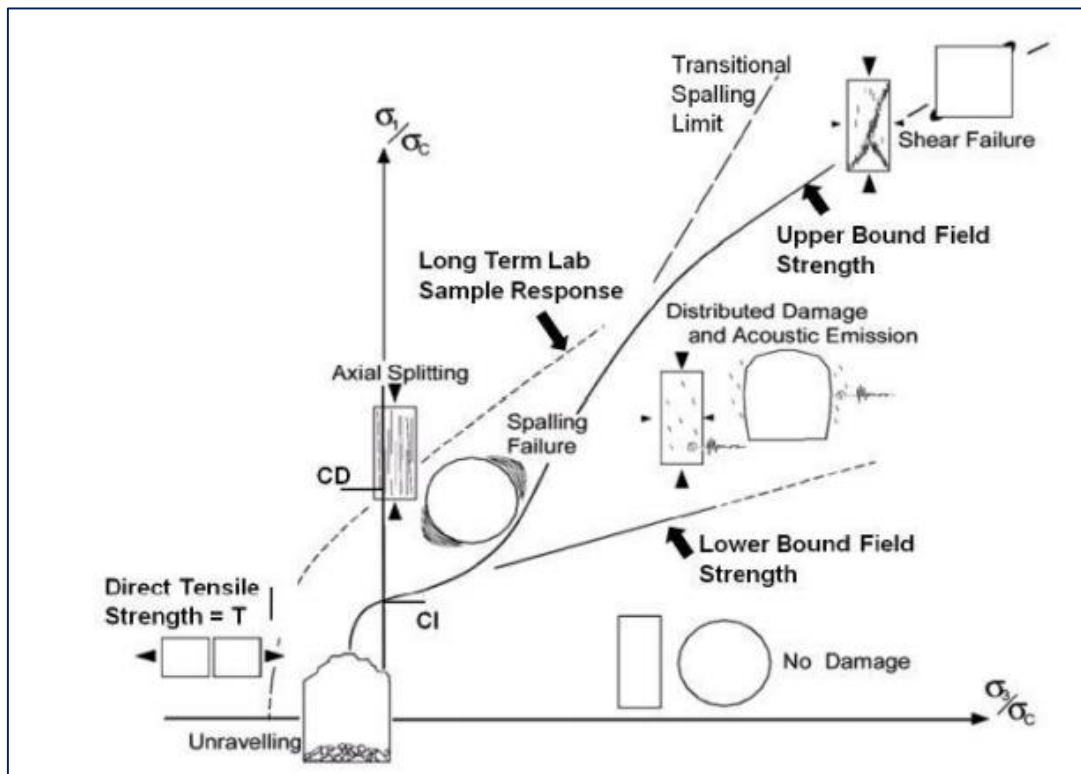


Figure 5-8. Different failure modes for brittle rock (Diederichs et al., 2010)

Several empirical formulas have been developed in order to predict the depth impact of the brittle failure, e.g. by Kaiser (1996), Martin et al. (1999) & Martin and Christiansson (2009). In this thesis empirical formula given by Martin and Christiansson (2009) has been presented.

Opening radius (r), maximum tangential stress ($\sigma_{\theta max}$) and intact rock strength (UCS) or spalling strength (σ_{sm}) are the input parameters. Martin and Christiansson (2009) gave a relationship to calculate the depth-impact (d_f) using spalling strength (σ_{sm}) as input. As discussed previously, spalling strength can be related to strength of intact rock ($\sigma_{sm} = 0.4$ times UCS).

$$d_f = r \times \left(0.5 \times \frac{\sigma_{\theta max}}{\sigma_{sm}} - 0.52 \right) \tag{Eq- 5.12}$$

(Panthi, 2012).

5.4 Estimating rock support

The diameter and spacing of the rock bolt is estimated for the rock pressures in the crown and the side walls as per Barton's Q values.

Table 5-1. Empirical formulas to calculate the design pressure

Description	Formula used
Design pressure on roof	$P_{roof} = \frac{2}{J_r} Q^{-\frac{1}{3}}$
Design pressure on the walls	$P_{roof} = \frac{2}{J_r} Q'^{-\frac{1}{3}}$

Where,

$$Q' = n \times Q \quad \text{Eq- 5.13}$$

n = factor depending on rock mass quality

The support pressure for the rock bolt is computed by the relationship:

$$P = \frac{T}{S} \quad \text{Eq- 5.14}$$

Where P is the rock pressures in the crown/wall, T is the working load of the rock bolt, S is the area supported by each rock bolt (Larsen and Toubro(PDL), 2012c).

Several empirical rules of thumb have been developed over time to determine the length of rock bolts along with their spacing. Table 5-2 shows the Empirical relations found in the literatures to find the length of rock bolts. These rules of thumb for support design have been developed for weak rock as a result of intense jointing or because the rock material itself has a low strength (Hoek, 2007). These empirical rules are developed based on the experience and data gained from mine openings, caverns and tunnels. These guideline should always be used in combination with other design tools (Hutchinson and Diederichs, 1996).

Table 5-2. Empirical formulas, estimating necessary length of rock bolts as a function of cavern span/height. S = span, H = height, S_p = Spacing of primary bolting, B = excavation width and ESR = Excavation Support Ratio

Bolt length	Reference	Comment
$L = 0.67 \times S^{0.67}$	Lang and Bischoff (1984)	
$L = 0.3 \times S$	Farmer and Shelton (1980)	Span > 15m, alternate with secondary bolting
$L = 0.3 \times S_p$	Farmer and Shelton (1980)	Secondary bolting
$L = 2 + 0.15 \times S$	Hoek (2007)	Suited for weak rock masses (roof)
$L = 2 + 0.15 \times H$	Hoek (2007)	Suited for weak rock masses (walls)
$L = 2 + \frac{0.15B}{ESR}$	Barton et al. (1980), Hoek (2007)	ESR = 1 for power house
$L = 1.40 + 0.184 \times S$	Myrvang (2001)	Norwegian approach
$L = \frac{S}{4}$	U.S.C.E	Roof
$L = \frac{H}{4}$	U.S.C.E	Wall

Empirical formulas developed over time to determine the spacing between rock bolts. Table 5-3 shows the empirical relations found in the literatures to determine the spacing between rock bolts.

Table 5-3. Empirical formulas for determining spacing between rock bolts

Spacing	Reference	Comment
$Spacing = \sqrt{\frac{T}{P}}$	Hoek (2000)	T=working load of bolt or cable P=support pressure
$Spacing = 0.5 \times L$	Farmer and Shelton (1980)	Primary bolting
$Spacing = 0.5 \times L(Secondary)$	Farmer and Shelton (1980)	Secondary bolting
$Spacing = 0.5 \times L$	Myrvang (2001)	Applicable to jointed rock mass

5.5 Numerical methods

The analytical methods discussed are appropriate for simple geometries in homogeneous media. Maximum powerhouse caverns have complex geometry and are situated in inhomogeneous rock mass. Moreover, most openings are close to other excavations or toe slope of a mountain as in this thesis, making it too complex to solve by analytical methods. In past decades, there has been development of computer based numerical methods to solve such complex situations. There are two classes for analysing stress driven problems in rock mechanics:

- Boundary discretization methods, in this case the interior of the rock mass is represented as an infinite continuum while the excavation boundary is divided into elements, this division covers elastic analysis.
- Domain discretization methods, in this case the interior of the rock mass, is also divided into elements with presumed properties, resulting in collective behaviour and interaction between these elements, giving rise to a simplified model for complex and inhomogeneous rock mass. The domain method allows analysis of more complex material as compared to boundary method. Finite element and finite difference method techniques treat rock mass as continuum within the domains of the discretization methods. Each individual rock is modelled as a unique element.

The classes discussed above can be combined to form a hybrid model and maximize the effectiveness adding to advantage of both methods (Hoek, 2007).

5.5.1 RocData

RocData is used to determine rock mass strength parameters, based on the generalized Hoek-Brown failure criterion. From the input parameters: UCS, GSI, modulus of elasticity (E_i) intact rock property m_i and disturbance factor (D), RocLab calculates Hoek-Brown criterion parameters (m_b , s , a) and rock mass parameters (Section 2.4).

5.5.2 Unwedge Analysis

Unwedge is a 3D stability analysis and visualization program for underground excavation in rock mass containing structural discontinuities, i.e. to analyse structurally controlled instability, provided by Rocscience Inc. (Rocscience, 2014a).

5.5.3 Rock Science -2D

Phase2 (RS2) is a 2D finite element program used for rock applications where multi stage and complex models can be created and analysed quickly, provided by Rocscience Inc. (Rocscience, 2014b).

5.5.4 Rock Science -3D

RS³ is a 3D finite element program used for rock application i.e. underground excavation, tunnels and support design, provided by Rocscience Inc. (Rocscience, 2014c).

6 STABILITY ANALYSIS

6.1 Stress Distribution

In order to estimate the stress redistribution around the cavern cross section, it is important to evaluate the directions of principal stresses. In both original and alternative alignment of cavern length axis are almost parallel to the valley. This means that maximum tangential stress most likely will appear in the part of the cavern roof facing the valley side. Figure 7-17 shows results from stress modelling, the topographical effect on stress situation is seen clearly near the cavern location (Section 7.2.1.3).

Tangential stresses can be estimated from the Kirsch's equation (Eq- 5.3 & Eq- 5.4). Due to the cavern shape the Kirsch's equation is only applied to the arched roof. Potential tension in cavern walls are difficult to calculate analytically.

The maximum tangential stress value for both alternative and original alignment are shown in Table 6-1. Section 7.2.1.3 describes the calculation and assessment of σ_1 & σ_2 for the cavern cross-section (In-plane stresses). These tangential stress values are applicable only when height and width are approximately the same. In reality, the values increase a bit when benching down to achieve full height.

Table 6-1. Maximum tangential stress on the cavern contour based on Kirsch's equations (Table 7-8).

Description	σ_1 [MPa]	σ_3 [MPa]	$\sigma_{\theta\max}$ [MPa]
Original Alignment	5.91-6.97	1.60-2.04	16.13-18.87
Alternative Alignment	6.90-9.31	1.74-1.79	18.96-26.14

Table 6-2 contains the results for tangential stresses in roof ($\sigma_{\theta r}$) and walls ($\sigma_{\theta w}$) of the caverns as per Eq- 5.5 & Eq- 5.6, along with Figure 5-2. Principle stresses are assumed to be oriented along the horizontal and vertical axes for both the cases when using empirical method developed by Hoek and Brown (1980).

Table 6-2. Tangential stress in roof and walls calculated from the empirical method from Hoek and Brown (1980).

Description	A	B	k	σ_z [MPa]	$\sigma_{\theta r}$ [MPa]	$\sigma_{\theta w}$ [MPa]
Original Alignment	4	1.5	3.7- 3.4	1.60 - 2.04	22.08-25.07	(-3.52) – (-3.87)
Alternative Alignment	4	1.5	4.0- 5.2	1.74 - 1.79	26.1-35.4	(-4.35) – (-6.623)

6.2 Rock Mass Quality

Engineering geological reports (Larsen and Toubro(PDL), 2012a; Larsen and Toubro(PDL), 2012b) use Q-system for rock mass classification. Table 6-3 shows the Q-value in powerhouse complex area.

Table 6-3. Rock mass quality in the area of the powerhouse complex from the Q-system

Rock Type	% reach	Rock mass Quality Index (Q)
Fresh and hard quartzite	55-60	7.8-3.6
Diamictite & phyllitic quartzite	30-35	
Phyllite	5-10	1.6 - <0.5

Rock mass quality index (Q-value) is based on the observation made in the test drifts and borehole logs at the powerhouse cavern site. Still these observations are just an indication for the distribution of rock mass qualities.

RMR is calculated from the data available from drill holes and exploratory drifts using guidelines given in Appendix H, values are confirmed using equations Eq- 5.8 & Eq- 5.9. GSI is calculated by using the relation between RMR and GSI (Eq- 5.10).

Table 6-4. RMR values calculated by using Eq- 5.8 & Eq- 5.9.

Author	Value
Barton (1999)	69-80
Bieniawski (1989)	55-62

Table 6-5 shows the RMR and GSI values used in empirical and numerical analysis.

Table 6-5. Rock mass quality from RMR and GSI values used in Empirical and numerical analysis.

System	Value	Rock Class	Description
GSI	48-58	Blocky	Fair Rock
RMR	53-63	III	Fair Rock

6.3 Predicting Failure extent

The degree of failure can be roughly estimated by the empirical classification developed by Hoek and Brown (1980) (Section 5.3). Table 6-6 shows predicted failure extent. Stresses are averaged to calculate the values of σ_1 / σ_c & K_o .

Table 6-6. Predicted failure extent from the empirical classification developed by Hoek and Brown (1980)

Description	σ_1 (In-Plane) [MPa]	σ_c [MPa]	σ_1 / σ_c	K_o	Predicted extent of failure
Original Alignment	5.91-6.97	53.54-83.02	0.10	0.28	A stable unsupported opening
Alternative Alignment	6.90-9.31	53.54-83.02	0.12	0.21	Minor spalling can be observed, requiring light support

This classification is developed from square mining tunnels in South Africa and far field stress ratio (K_o) of 0.5. A far field stress factor for the Sach Khas HEP (0.2-0.3) and different excavation shape and material properties, make predicting failure extent for Sach Khas HEP uncertain.

Figure 5-7 and section 5.3 are used to estimate potential spalling and strain burst based on the UCS, far field stress (σ_1) and Hoek-Brown parameters (m_i) (UCS = 53.54-83.02 MPa and $m_i = 20$), yielding medium spalling potential and no to low rock burst potential due to varying UCS. Taking conservative assumptions, spalling strength for crystalline rocks (most metamorphic rocks are almost always crystalline) such as hard and fresh quartzite is set to 0.4 times UCS (section 5.3). Table 6-7 gives an estimate of spalling hazard for cavern in both original and the alternative alignment.

Spalling is expected for the alternative alignment of the powerhouse cavern according to the tangential stresses calculated from equations proposed by Hoek and Brown (1980). Tangential stresses are higher in alternative alignment compared to the original alignment.

Table 6-7. Calculation of spalling hazard. Values for $\sigma_{\theta\max}/UCS$ over 0.4 indicates spalling.

Description	$\sigma_{\theta\max}$[MPa] <i>(Kirsch's Equation)</i>	$\sigma_{\theta\max}/UCS$ <i>(Kirsch's Equation)</i>	$\sigma_{\theta\max}$[MPa] <i>(Hoek and Brown, 1980)</i>	$\sigma_{\theta\max}/UCS$ <i>(Hoek and Brown, 1980)</i>
Original Alignment	16.13-18.87	0.26	22.08-25.07	0.35
Alternate Alignment	18.96-26.14	0.33	26.1-35.4	0.45

Eq- 5.12 is used to predict the impact of depth of brittle failure. Results from the calculations using stress values from Kirsch's equation and empirical method from Hoek and Brown (1980) are given in Table 6-8.

Table 6-8. Depth of failure calculated from equation given by Martin and Christiansson (2009) with stress values from Kirsch's equation and Hoek and Brown (1980) as input parameters.

		Depth of failure in the roof (m)	
		<i>Kirsch's equation</i>	<i>Hoek and Brown (1980)</i>
Description	Radius (m)	Eq- 5.12	Eq- 5.12
Original Alignment	11.5	-	-
Alternative Alignment	11.5	-	0.5

Average values of maximum tangential stress ($\sigma_{\theta\max}$) are used to calculate the depth of failure, the values correspond to the magnitude of averaged maximum tangential stresses, and negative values are not mentioned. Spalling is present for the alternative orientation due to increase in in-plane major principal stress (Section 7.2.1.3).

6.4 Support

The support system proposed by project authorities is shown in Appendix C (Typical proposed support in cavern cross section) and Appendix D (Proposed support for crown only in poor (I) and very poor (II) rock conditions).

Table 6-9 proposes rock support spacing and diameter based on empirical approach discussed in section 5.4. A factor of safety of 2.0 (Liu et al., 2004) is used in calculating all the parameters mentioned in Table 6-9.

Table 6-9. Based on the empirical approaches (Section 5.4) following spacing and diameter of rock bolt is been provided for the cavern, length is discussed in Table 6-10.

Support System		Spacing	Crown of powerhouse	Wall of powerhouse
		c/c m	Bolt Dia. (mm)	Bolt Dia. (mm)
Original Alignment	Roof	2.0 x 1.5	32	32
	Wall	2.0 x 1.5	32	32
Alternative Alignment	Roof	2.0 x 1.5	32	32
	Wall	2.0 x 1.5	32	32

Based on empirical relations presented in Table 5-2, Figure 6-1 illustrates the length of rock bolts over a span of 0-30 m for roof and 0-50 for the wall. Project authorities used formulas based on Hoek (2007) & U.S.C.E (1980) to calculate the bolt length (Appendix C).

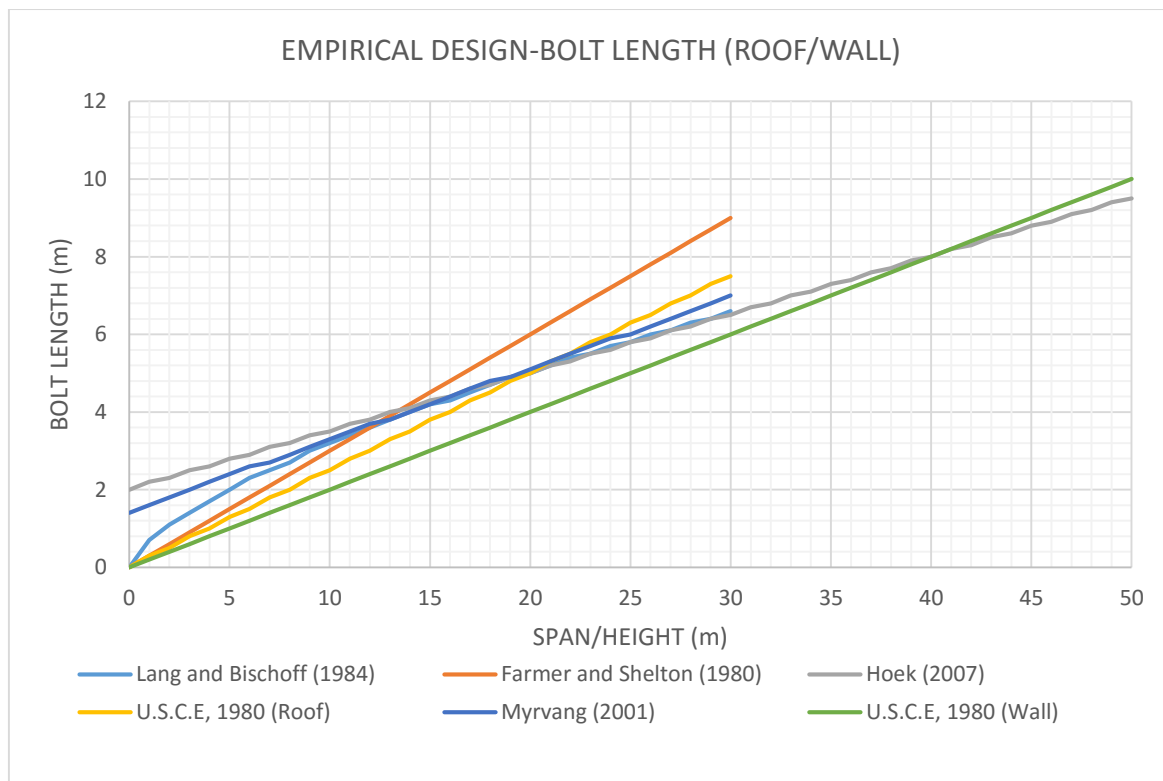


Figure 6-1. Illustration of the formulas in Table 5-2 over a span from 0 to 30 m (roof) & 0 to 50 (wall)

Reading the graph in Figure 6-1, bolt lengths for the cavern are estimated in Table 6-10. Bolt spacing can be approximated to about half of the lengths (Table 5-3).

Table 6-10. Estimation of required bolt length based on empirical formulas illustrated in Figure 6-1

Description		Span (m)	Bolt length (m)
Power House	Roof	23	6
	Wall	48.547	10

Cavern span is used as input for calculating bolt length in Table 6-10. Rock mass quality and stress situation should be evaluated before determining the length of the bolts.

Table 6-8 predicts the depth of failure, suitable for estimating length of rock bolt in the cavern roof. It is recommended to place the rock bolt at least one meter into competent rock. This recommendation is used to set the length of the rock bolt in Table 6-11.

Table 6-11. Recommended bolt length in the cavern roof based on the results presented in Table 6-8.

Description	Bolt length (m) in the cavern roof	
	<i>Kirsch's equation</i>	<i>Hoek and Brown (1980)</i>
Original Alignment	-	-
Alternative Alignment	-	2

RMR provides guidelines for support system shown in Appendix H. From the values in Table 6-5, RMR recommend the following support system (Table 6-12):

Table 6-12. Recommended support from the RMR system (Appendix)

System	Value	Support
RMR	53-63	Systematic bolts, 4 m long; spaced 1,5-2 m in crown and walls with wire mesh in crown. 50-100 mm shotcrete in crown and 30 mm in sides.

Similarly, Q-system (Appendix I) provide guidelines for support system. From the values in Table 6-3, Q-system recommended the following support system (Table 6-13):

Table 6-13. Recommended support from the Q system (Appendix).

Description			Span/ESR	Correction for wall support	Support
Original Alignment	Roof	Fair	23	-	6 m bolts, c/c 2.0 m. E=500J shotcrete: 7 cm
		Poor			6 m bolts, c/c 1.7 m. E=700J shotcrete: 12 cm
	Wall	Fair	48.547	2.5	10 m bolts, c/c 2.5 m. E=700J shotcrete: 7 cm
		Poor			10 m bolts, c/c 2.0 m. E=700J shotcrete: 12 cm
Alternative alignment	Roof	Fair	23	-	6 m bolts, c/c 2.0 m. E=500J shotcrete: 7 cm
		Poor			6 m bolts, c/c 1.7 m. E=700J shotcrete: 12 cm
	wall	Fair	48.547	2.5	10 m bolts, c/c 2.5 m. E=700J shotcrete: 7 cm
		Poor			10 m bolts, c/c 2.0 m. E=700J shotcrete: 12 cm

7 NUMERICAL MODELLING

7.1 Unwedge analysis

UNWEDGE is used for numerical modelling to analyse structurally controlled instability around underground excavation created by intersecting discontinuities and excavated free face. Gravity and other forces induce failure in roof and wall wedges either by falling, sliding or rotating out of their socket (Section 2.1).

7.1.1 Model setup and input data

7.1.1.1 Geometry

The cross section of the cavern is slightly simplified as compared to the original cross-sectional geometry (Appendix B) in order to ease the modelling. Bus duct tunnel and draft tube is excluded. Inclusion of these features is insignificant within the scope of Unwedge analysis. Figure 7-1 shows the simplified geometry used in the modelling. The Power house cavern is 126m long.

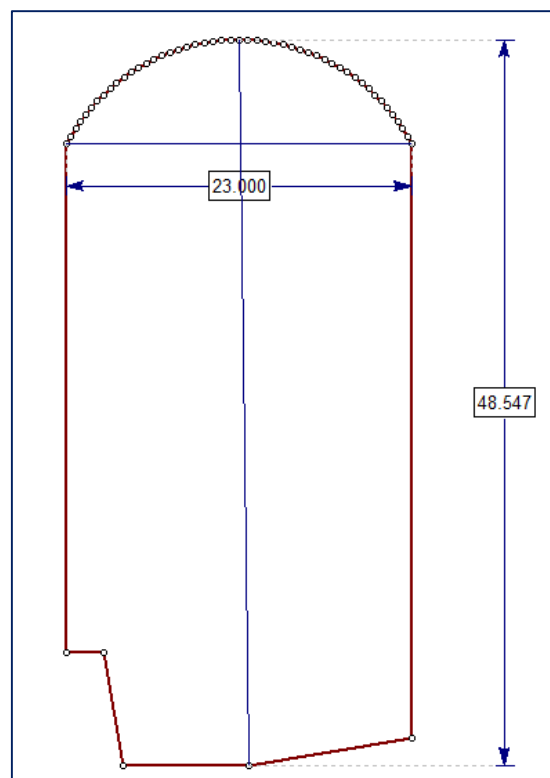


Figure 7-1. Simplified cavern geometry applied in the UNWEDGE analysis.

7.1.1.2 Input data

Input data requires geometric data, rock properties, joint orientations and joint properties. Output of this analysis depends heavily on the joint orientations and joint properties, hence,

proper care is required while gathering information about the joints. Appendix F lists prominent joint sets and their joint characteristics in powerhouse cavern area. There is certain uncertainty in joint characteristic, joint orientations and cohesion (c) (Appendix F). Probabilistic Unwedge analysis is performed in this thesis.

Probabilistic analysis utilizes statistical distribution for input parameters to account for uncertainty in the input values. Range of input values described in the Appendix F are used as input for probabilistic analysis resulting in a distribution of safety factors for each wedge, from which probability of failure is calculated (RocScience, 2016b).

A factor of safety of more than 2 is required for permanent caverns and between 1 and 2 for temporary caverns (Liu et al., 2004). Factor of safety of 2 is used in this analysis.

Default analysis in UNWEDGE is based on the assumption that the wedges are subjected to gravitational loading only, due to wedge weight (RocScience, 2016b). Stress field in rock mass around the excavation is ignored, which can lead to inaccuracy but error is generally conservative giving lower factor of safety (Hoek et al., 2000; Liu et al., 2004).

In this thesis the effect of stress will be ignored as the cavern falls under the category of shallow excavations and to get a conservative factor of safety.

Table 7-1. General Input

Description	Cavern Axis Orientation		Cavern Length (m)	Design factor of safety	Unit weight (MN/m ³)
	Trend	Plunge			
Original Alignment	N55°E	0	126	2	0.0272
Alternative Alignment	N20°E	0	126	2	0.0272

7.1.1.3 Wedge data uncertainty

The Mohr-Coulomb model is used for joint shear strength properties, cohesion (c) and friction angle (Φ) for the discontinuities is taken from Appendix O. Probabilistic input data i.e. joint orientations and joint properties is fed into the analysis using statistics.

The main objective of Unwedge analysis is to assess if wedges are likely to be of concern at the construction stage. Water pressure in the joint properties is considered zero as the ground water level in the area is not known.

7.1.1.4 Severity of wedges

Severity of hazard is a function of excavation size. Size and weight of the wedge is automatically calculated by UNWEDGE and is used to quantify the severity.

7.1.2 Probabilistic analysis

7.1.2.1 Sampling Method

Latin hypercube method is a statistical method for generating samples of probable collection of parameter values from multidimensional distribution (Hoek et al., 2000). In this thesis Latin hypercube method is used for sampling input data.

7.1.2.2 Joint combination

The “all joint combinations analyser” (probabilistic) in the UNWEDGE program allows to carry out an Unwedge analysis when the input data includes more than three possible joint orientations. The combination analyser automatically determines the most critical combinations of joints. The most critical wedge is produced by joint combination 1, 2, 3 for both alignments (Figure 7-2).

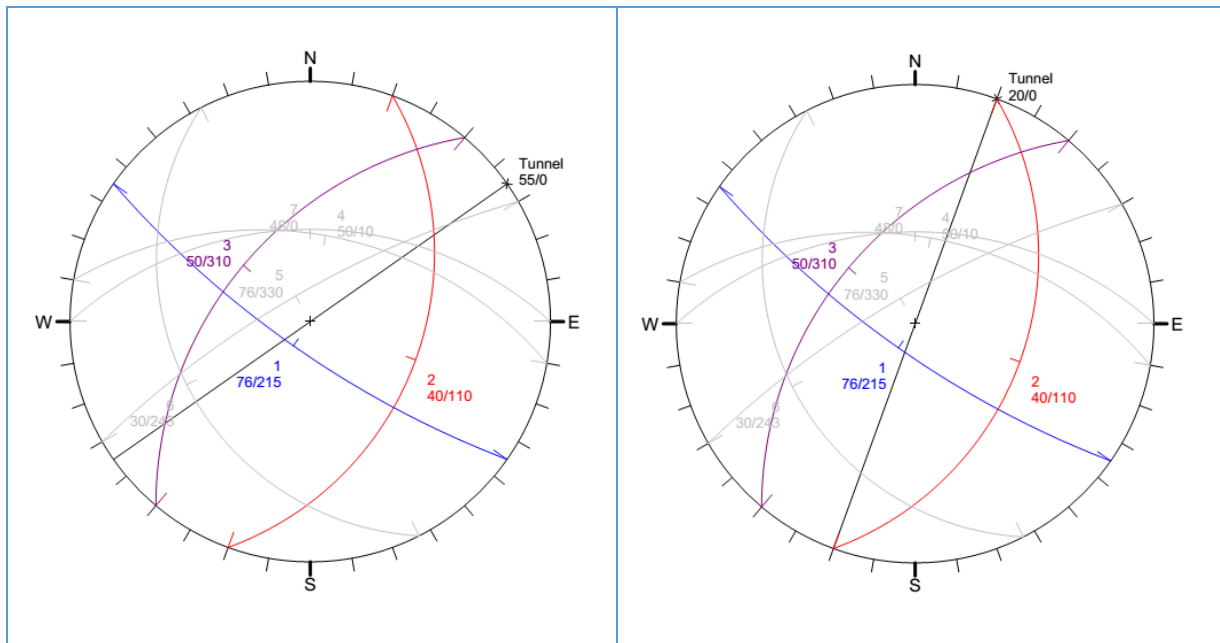


Figure 7-2. Stereonet plot of joint combination (Probabilistic) for Original Alignment $N55^{\circ}E$ (Left) & Alternative Alignment $N20^{\circ}E$ (Right)

The dip/dip direction orientation definition method is used to define the variability of joint orientation in the Unwedge probabilistic analysis. In this method, the dip and dip direction are treated as independent random variables.

7.1.3 Probability Analysis Results

Unwedge results based on findings from maximum support pressure required, maximum wedge depth, minimum factor of safety and probability of failure show that the most critical area in the cavern perimeter and end walls is the crown area. Certain results show very critical values. However, the cumulative probability of such critical values is very low (Appendix K). In this thesis critical values with very low cumulative probability will be used to design the support system.

7.1.3.1 Maximum Support Pressure

Required support pressure gives the starting point for design of actual support systems, i.e. bolts and shotcrete. Applying the required support pressure to the most critical joint combination will produce a safety factor greater than the design factor of safety. Figure 7-3 shows max required support pressure of 0.026 MPa for original alignment and 0.024 MPa for alternative alignment.

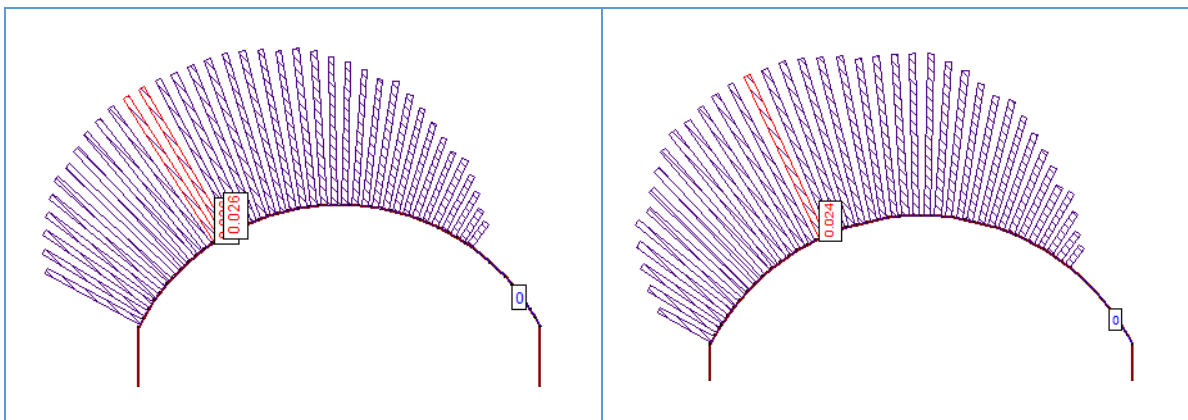


Figure 7-3. Maximum support pressure (MPa) (Probabilistic) for each segment of cavern roof for Original Alignment N55°E (Left) & Alternative Alignment N20°E (Right)

Changing the orientation has shown slight improvement in the required support pressure (0.002 MPa).

7.1.3.2 Maximum Wedge depth

Figure 7-4 shows the maximum wedge depth (m) for each segment for selected trails. Maximum wedge depth of 5.8 m for original alignment and 5.57 m for alternative alignment.

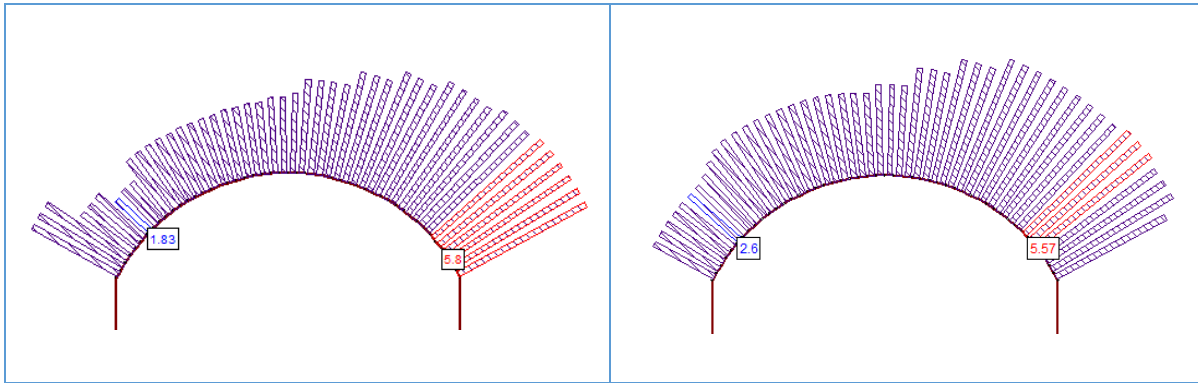


Figure 7-4. Maximum wedge depth (m) (Probabilistic) at each segment for Original Alignment N55°E (Left) & Alternative Alignment N20°E (Right)

7.1.3.3 Maximum Wedge weight

Figure 7-5 shows the maximum wedge weight (MN) for each segment from selected trails. Wedge weight in the roof range from minimum of 0.066 - 0.147 MN for original alignment and 0.063 – 0.133 MN for alternative alignment. The severity of the roof wedge is of critical importance in terms of worker safety and cavern stability.

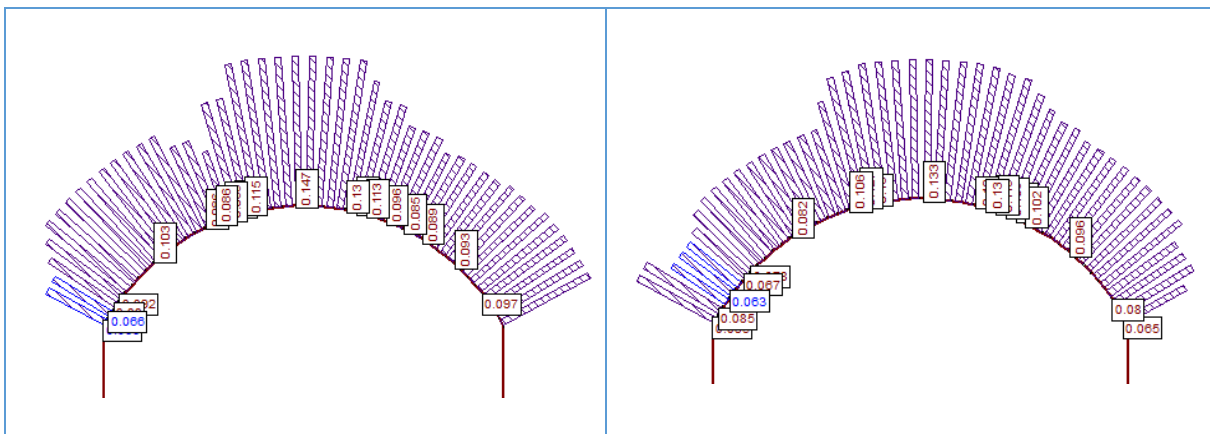


Figure 7-5. Maximum wedge weight (MN) (Probabilistic) at each segment for Original Alignment N55°E (Left) & Alternative Alignment N20°E (Right)

7.1.3.4 Minimum Factor of Safety

Figure 7-6 shows the minimum factor of safety for each wedge on each segment from selected trails. In case of original alignment, the whole roof can be considered critical as the factor of safety for selected trails is either zero or close to the design factor of safety. A similar case is the alternative alignment, except that the upper right corner qualifies the minimum factor of safety mark.

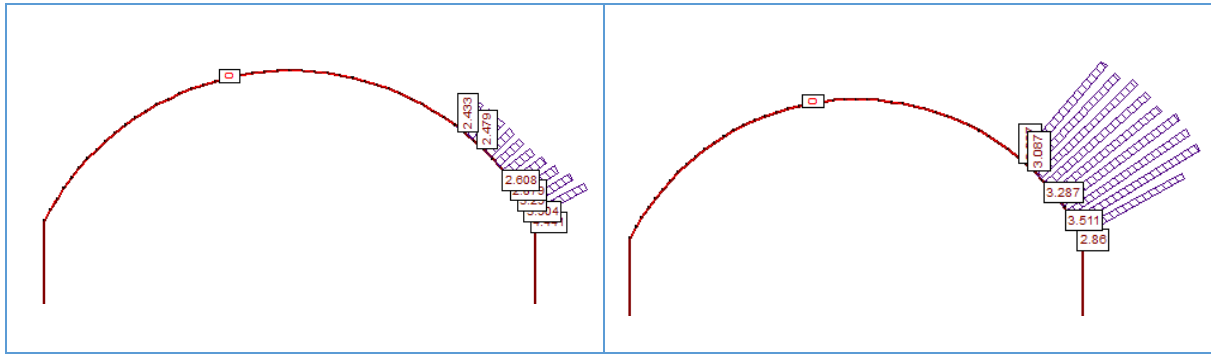


Figure 7-6. Minimum factor of safety (Probabilistic) at each segment for Original Alignment N55°E (Left) & Alternative Alignment N20°E (Right)

7.1.3.5 Probability of failure

Figure 7-7 shows the probability of failure for each segment. Most critical values are marked in red (Figure 7-7). The probability of failure is the ratio of the number of failed wedges to the number of samples. Where the number of failed wedges are valid wedges with a safety factor less than the design factor of safety. The number of samples is specified in the project settings as input. It is the overall probability of wedge failure for the given set of probabilistic input data.

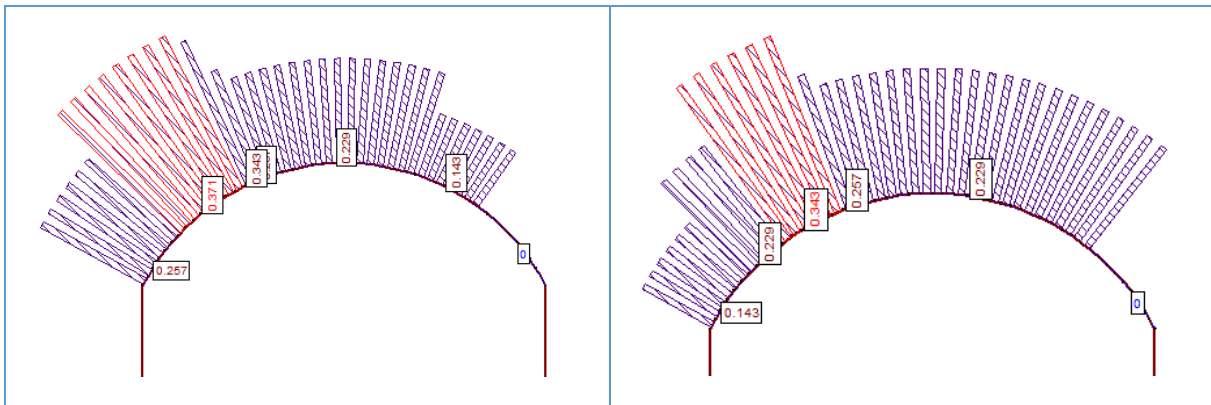


Figure 7-7. Probability of failure (Probabilistic) for each segment for Original Alignment N55°E (Left) & Alternative Alignment N20°E (Right)

7.1.4 Rock Support Design in Unwedge

A rock support system for wedges is designed to provide a stiff response to the block movement i.e. fully tensioned mechanically anchored rock bolts or fully grouted bolts left untensioned, provided movement of blocks hasn't taken place (Hoek, 2007). Support design in the Unwedge analysis is done independent of empirical support design, Rocscience 2D & 3D support design results.

7.1.4.1 *Rock bolt length*

Figure 7-4 & Figure 7-6 show wedges with the maximum depth that have a factor of safety more than the design factor of safety. However, in this thesis the maximum wedge depth will be used as the starting point for selecting suitable length of rock bolt. Table 7-2 show the rock bolt properties.

Table 7-2. Rock bolt properties applied in Unwedge model (www.dsiminingproducts.com, 2016)

Description	Original Alignment	Alternative Alignment
Rock bolt type	Grouted Dowel	Grouted Dowel
Rock bolt length chosen (m)	6	5
Tensile capacity (MN)	0.25	0.25
Yield Strength (MN)	0.14	0.14
Shear Strength (MN)	0.17	0.17
Rock bolt diameter (mm)	21.7	21.7
Plate Capacity (MN)	0.1	0.1
Bond strength (MN/m)	0.34	0.34
Bond length (% of Length)	80	80

7.1.4.2 *Rock bolt pattern spacing*

Figure 7-3 shows the maximum support pressure required. However, the values are really low. A trial and error method is used for finalizing the bolt spacing, keeping in view the bolt spacing density and work conditions. Table 7-3 shows the rock bolt pattern chosen for support design.

Table 7-3. Rock bolt pattern chosen for the support design

Description	Original Alignment	Alternative Alignment
Rock Bolt spacing Pattern	1.5m x 1.5m	2 m x 2m

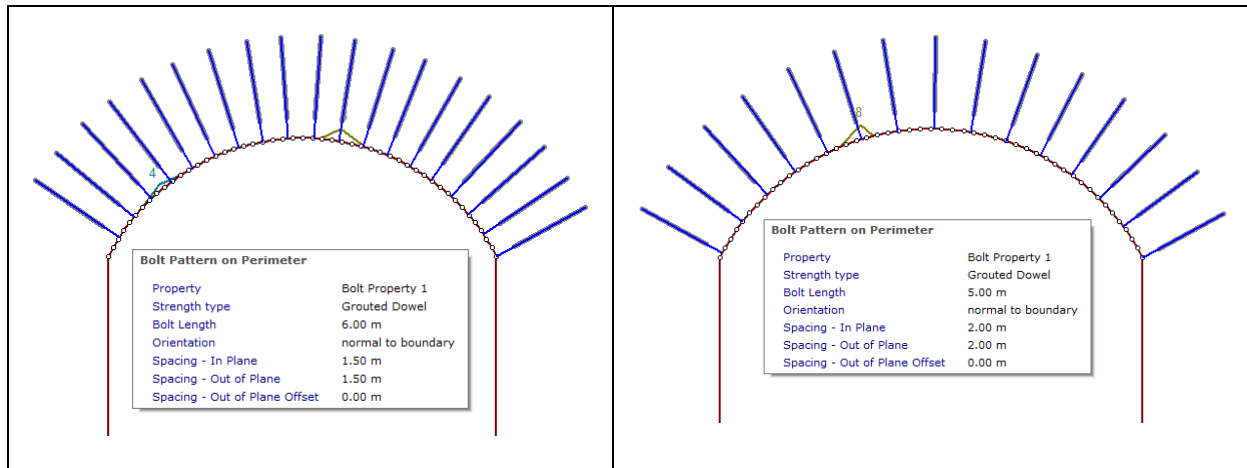


Figure 7-8. Rock bolt pattern used in Original Alignment N55°E (Left) & Alternative Alignment N20°E (Right)

The application of rock bolts increased the factor of safety of most critical wedges above design factor of safety. Figure 7-9 shows the results after applying rock bolts.

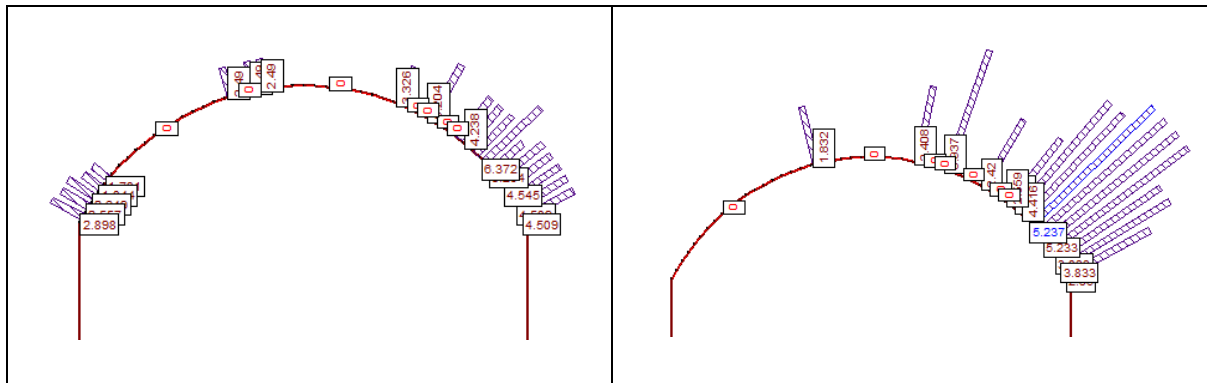


Figure 7-9. Minimum factor of safety in Original Alignment N55°E (Left) & Alternative Alignment N20°E (Right) after providing rock bolts

Figure 7-10 shows the probability of failure for both the cases has decreased considerably. Hence, it conforms that the majority of critical wedges in the sampling trails are safe. Confirming the effectiveness of applied rock bolts.

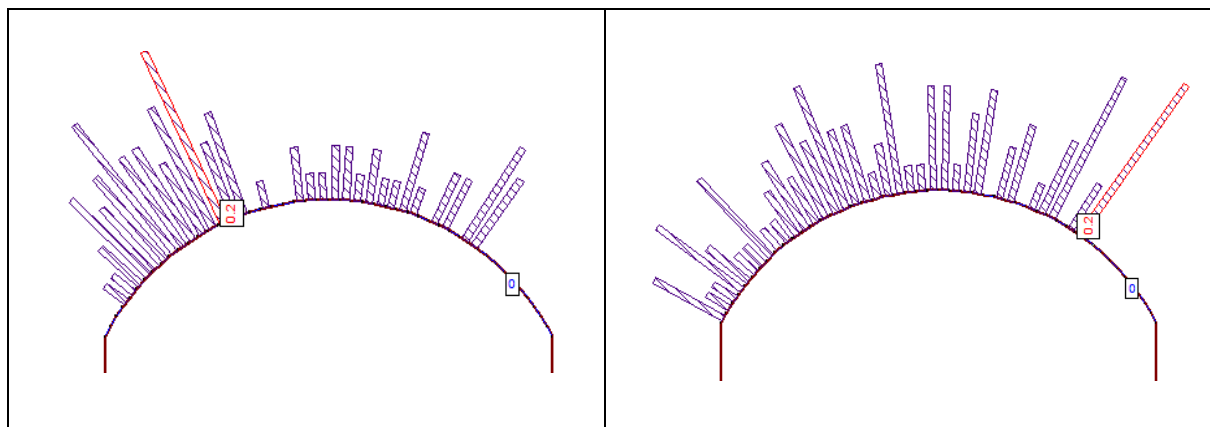


Figure 7-10. Probability of failure in Original Alignment N55°E (Left) & Alternative Alignment N20°E (Right) after providing rock bolts

7.1.4.3 Shotcrete Support

Shotcrete failure mode in Unwedge is direct shear. Hence, shear strength of concrete is important for shotcrete application. Capacity of shotcrete is a function of exposed area perimeter, shear strength and thickness of the shotcrete.

Most reported values for 28-day strength are in the range of 20 to 50 N/mm², strength higher than 25 N/mm² should be used only for most carefully executed shotcrete jobs (BIS, 2002). In this thesis a value of 35 MPa will be used as the compressive strength of shotcrete (Panthi, 2016). Table 7-4 shows shotcrete support input values.

Table 7-4. Shotcrete input values

Description	Original Alignment	Alternative Alignment
Thickness (cm)	3	3
Peak compressive strength [MPa]	35	35
Shear Strength [MPa]	1	1
Unit Weight (MN/m ³)	0.026	0.026

Figure 7-11 shows the shotcrete detail applied on crown of power house cavern.

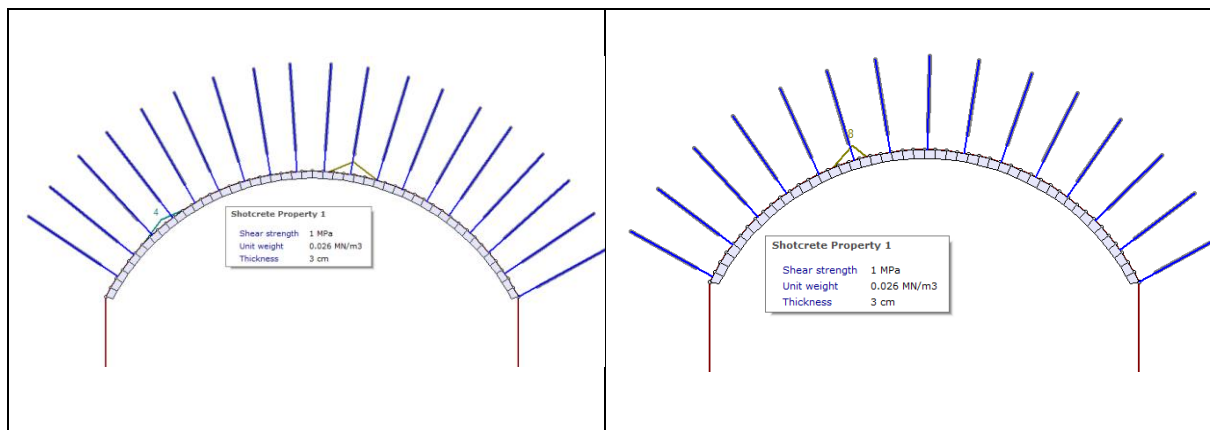


Figure 7-11. Shotcrete detail used in Original Alignment N55°E (Left) & Alternative Alignment N20°E (Right)

Figure 7-12 shows that the minimum factor of safety has increased considerably for the whole roof. All critical wedges, left after applying rock bolts are safe after applying shotcrete.

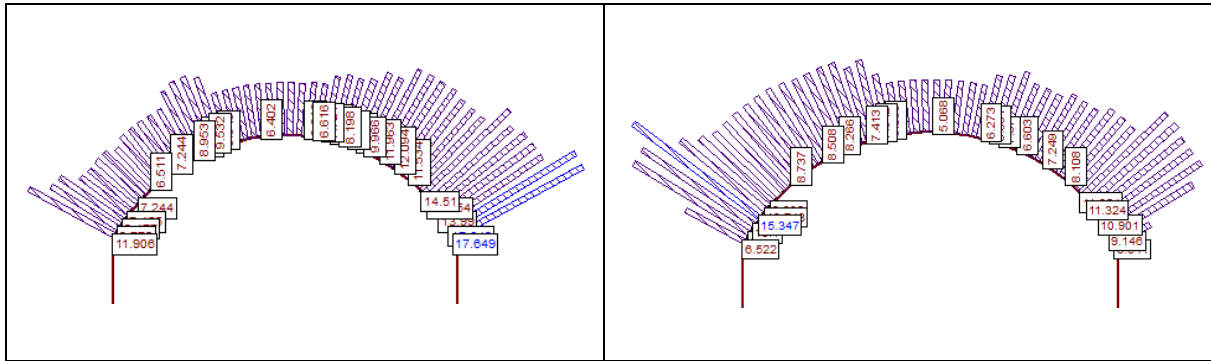


Figure 7-12. Minimum factor of safety in Original Alignment N55°E (Left) & Alternative Alignment N20°E (Right) after providing shotcrete support

Figure 7-13 shows that the probability of failure is zero for the whole cavern roof after application of shotcrete.

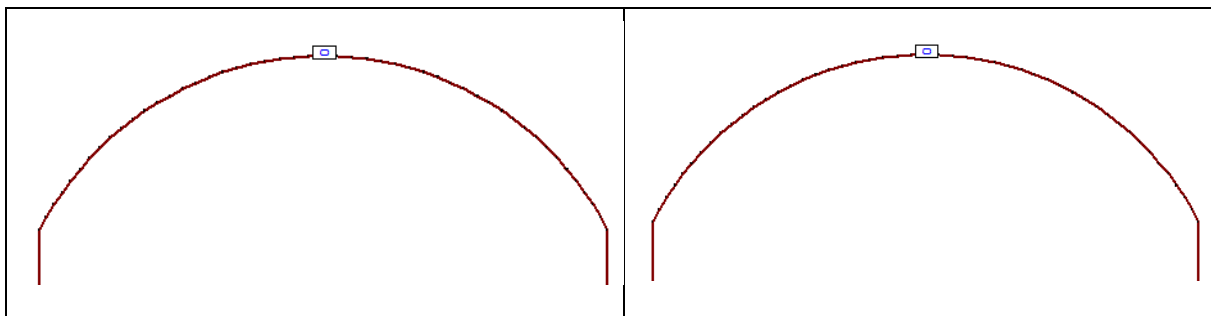


Figure 7-13. . Probability of failure in Original Alignment N55°E (Left) & Alternative Alignment N20°E (Right) after providing shotcrete support

7.1.5 Discussion of model results

The model results are based on the input data. Values for maximum support pressure, wedge weight, wedge depth, minimum factor of safety and probability of failure used in this analysis have low cumulative probability, refer to Appendix K for cumulative plots.

Support design is done for the maximum values with low cumulative probability, keeping in mind the conservative design approach (Section 7.1.1.2) . The final support system will be discussed after performing stress analysis (Chapter 9).

7.2 Phase2 Analysis

The phase2 package from Rocscience is used for numerical modelling. Modelling is carried out as plane strain analysis using Gaussian eliminator as solver type. Both elastic and plastic material properties are applied in the analysis. Redistribution of stresses and strength factor of material is analysed using elastic material. Displacement and rock mass failure is examined using plastic material. Plastic property allows the material to yield.

Two different sets of parameters are used. The first set of parameters belongs to the majority of rock found in the powerhouse cavern area (Section 3.2.4). The second set of parameters use the lowest values from the range of parameters, which can be related to the worst case scenario. Sensitivity analysis is done to check the influence of input parameters on results.

Martin et al. (1999) states that depth of brittle failure is significantly under-predicted when rock mass failure criteria with frictional parameters is used. Brittle parameters are modelled to get a better estimate of the depth of brittle failure.

7.2.1 Model set up and input data

7.2.1.1 Geometry and excavation stages

The cross section of the cavern is simplified slightly as compared to the original cross-sectional geometry (Appendix B) in order to ease the modelling. Bus duct tunnel and draft tube is excluded. Inclusion of these features is insignificant within the scope of Unwedge analysis. Figure 7-14 (right) shows the simplified geometry used in the modelling. The Power house cavern is 126m long, respectively.

In this thesis Phase2 analysis is carried out for cross-section having lowest cover over cavern crown and shorted distance between cavern wall and slope face. Table 7-5 shows total and rock cover over each unit. Some properties have been calculated using the average value of rock cover over the powerhouse cavern crown.

Table 7-5. Rock Cover over the units for both cases under study

Description		Unit-1	Unit-2	Unit-3
Original Alignment	Total	59 m	66 m	75 m
	Rock cover	45 m	46 m	48 m
Alternative Alignment	Total	68 m	66 m	64 m
	Rock Cover	45 m	44 m	45 m

For Phase2 analysis, the cross-section of unit-1 for original alignment and unit-3 for alternative alignment has been used.

Large scale caverns have been excavated in several stages. Figure 7-14 (left) shows general cavern profile and excavation stages.

The scope of performing this task is to find overall stability. Hence, excavation stages have been reduced as compared to the original excavation plan (Figure 7-14 (left)). Order and number of stages used in Phase2 analysis have been shown in Figure 7-14 (right).

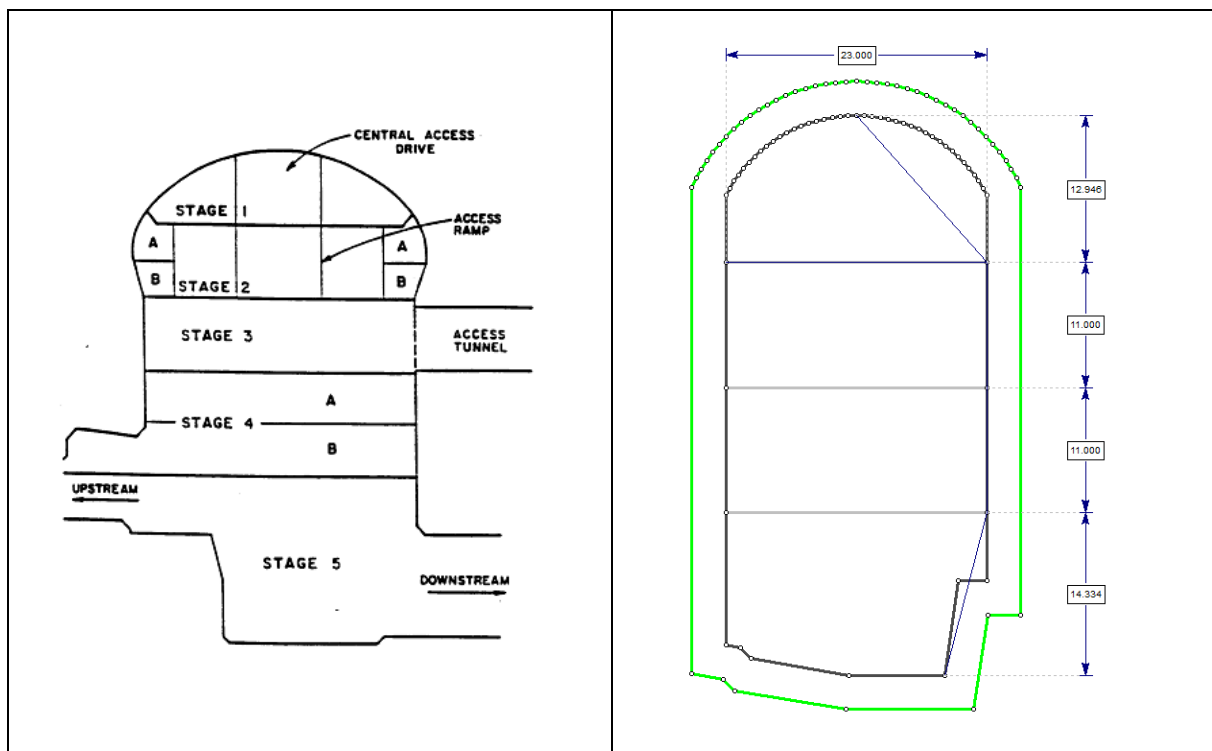


Figure 7-14. Cavern profile and excavation stages (Hoek, 2007) (left), Cavern profile and excavation stages (Phase2) (right)

7.2.1.2 Mesh and displacement

A graded mesh type with 3 noded triangles has been used in modelling. A gradation factor of 0.1 and a number of excavation nodes equal to 110 has been used. Discretization of the excavation boundary is determined by the number of excavation nodes. Discretization of all other boundaries in the model is determined by a gradient factor in conjunction with a number of excavation nodes (RocScience, 2016a).

The external boundary represents the project topography and extent of available rock line. Boundaries in the model are fixed in both x- and y- directions at corners. The upper boundary follows ground topography and is not restricted in any direction. The lower boundary is

restricted in the vertical direction (y-direction) and side boundaries are restricted in the horizontal direction (x-direction).

7.2.1.3 In-situ stresses

Gravitational field stress is chosen for modelling stresses to account for variation of vertical stresses with depth and effect of topography on stress situation. The stress situation is discussed in detail in section 3.3.4. The minor principal stress for both alternatives is calculated using the average of effective cover over the units. Average rock density of 2.72T/m³ is used. Magnitude and directional range of principle stresses powerhouse cavern area are approximated in Table 7-6.

Table 7-6. Magnitude and principle stresses in the area of the powerhouse caverns for both alternatives

Principal Stress	Magnitude (MPa)		Direction
σ_1	10		N50°E to N86°E.
σ_2	5.88		N140°E to N176°E.
σ_3	1.82 (Original Alignment)	1.78 (Alternative Alignment)	

Since Phase2 is a two-dimensional program, projection of horizontal stresses into the relevant cross-section is most important. Eq- 7.1, derived from the equilibrium state in a two-dimensional stress plane (Figure 7-15), is used for the projection of horizontal stresses into the relevant cross-section.

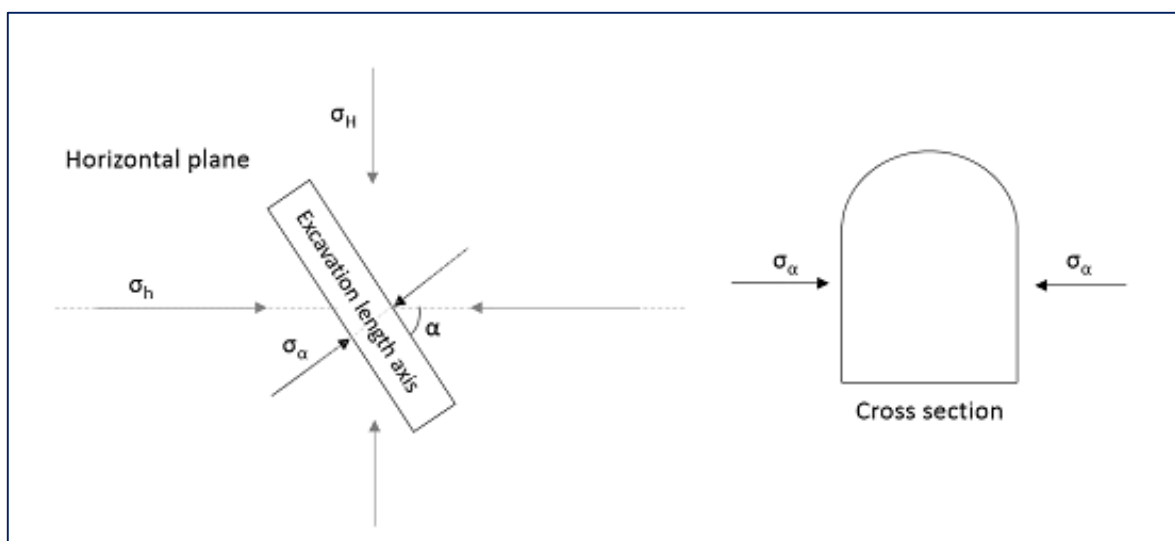


Figure 7-15. Illustration of the use of Eq- 7.1. This analysis disregards shear stresses along with the excavation

$$\sigma_{\alpha} = \sigma_H \cos^2 \alpha + \sigma_h \sin^2 \alpha \quad \text{Eq- 7.1}$$

(Emdal, 2013)

Where σ_{α} is the normal stress on a plane, which in this case will be the excavation contour, σ_H and σ_h are horizontal principle stresses and α is the angle between σ_h and the length axis of excavation.

The cavern orientation deviates from the major principal stress by the range of 5° to 31° for original and 30° to 66° for alternative alignment. Hence, Eq- 7.2 is applicable to calculate stress in the cavern cross section (Table 7-8).

The location of the hydraulic fracturing test in exploratory drift, and both the caverns are same. Hence, in-situ stresses discussed in Table 7-6 are relevant. To set stress parameters, it is necessary to isolate the tectonic stress, which will be locked-in stresses in the model.

$$\sigma_{tec} = \sigma_h - \frac{\nu}{1 - \nu} \sigma_v \quad \text{Eq- 7.2}$$

Where (σ_h) is the magnitude of the horizontal stress, ν is Poisson's ratio, (σ_v) is gravity stress (in this case also the major principle stress) and (σ_{tec}) = tectonic horizontal stress (locked-in stress).

(Panthi, 2012)

Applying the stresses in Table 7-6 to Eq- 7.2 gives locked in stresses (Table 7-7). These locked in stress values are used for stress modelling.

Table 7-7. Locked in stresses calculated from principal stresses in the Power house cavern area

Locked in Stress	
In Plane	Out of plane
5.55	9.66

The modelled section (Figure 7-16) is parallel to the cavern cross section of original alignment. This is in the direction of the access tunnel and approximately parallel to the σ_2 (Table 7-6) direction. A bulk density of 0.018 MN/m^3 is used for modelling overburden (Panthi, 2016). The vertical height above the rock cover is used to calculate overburden and is modelled as distributed load to simulate the field conditions.

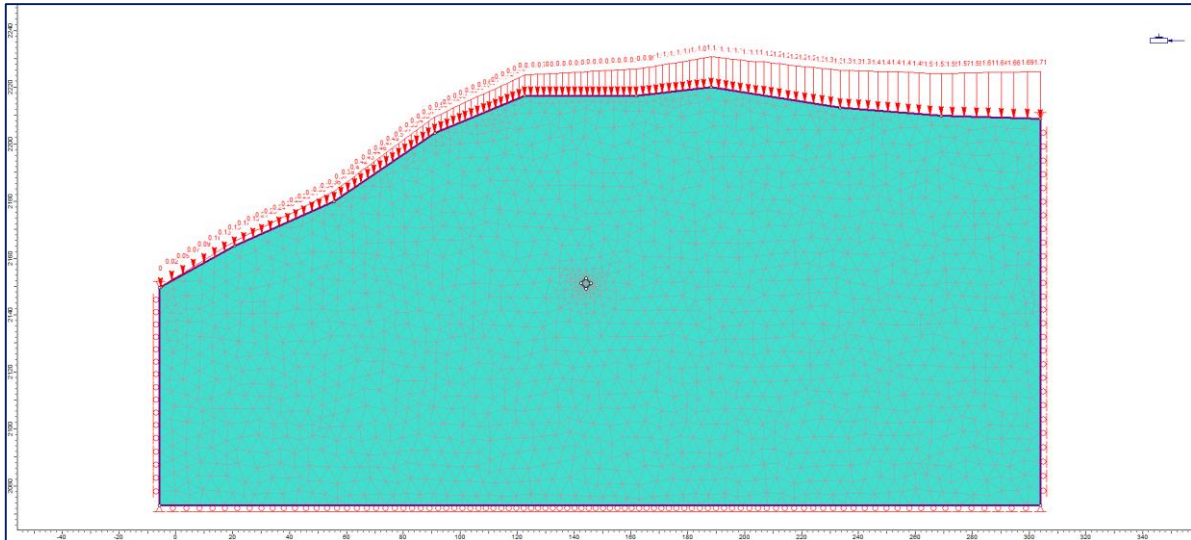


Figure 7-16. Cross section of right bank of valley in a straight line parallel to cavern cross section to model in-situ stresses.

The results are shown in Figure 7-17. The actual input stress ratio obtained from Table 7-6 is used to calibrate the model. Sigma-1 in model is matching minimum horizontal stress from hydraulic fracturing measurements at a depth of approximately 46 m.

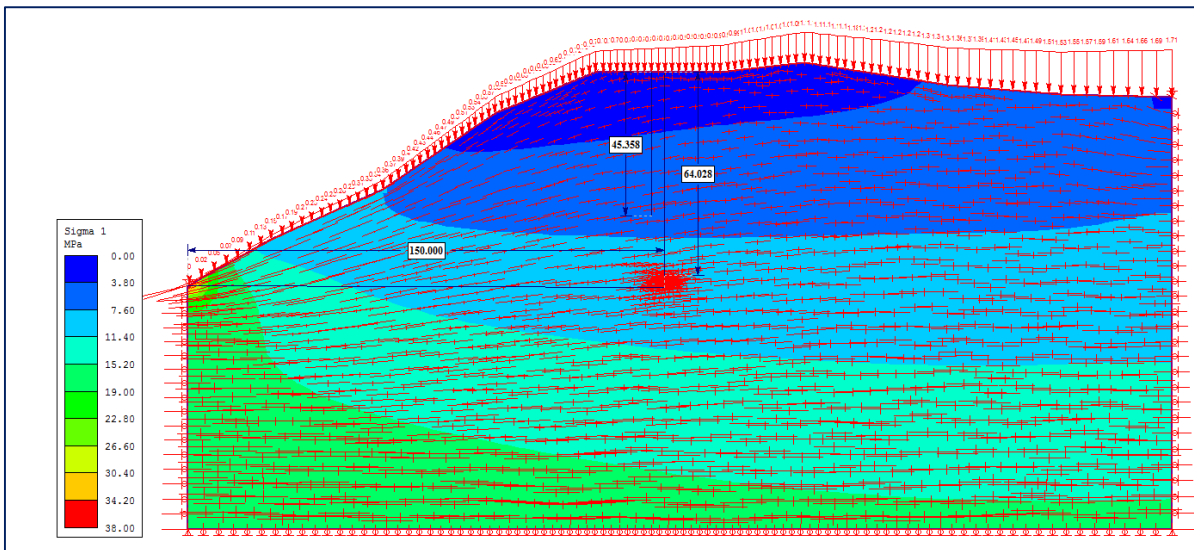


Figure 7-17. Results from the modelling of in-situ stresses.

There are certain contradictions in terms of mesh width and boundary conditions. However, the model shows more natural and matching results with boundaries restrained at a lower external boundary in vertical direction (y direction) and side boundaries in the horizontal direction (x direction). Corners are restrained in both x and y direction. Main objective of terrain modelling in gravitational stress fields is to check if stresses in the location of the cavern are approximately of the same magnitude as measured in the hydraulic fracturing test.

Results show that values are of the same order. Hence, the values from the hydraulic fracturing test are adequate for further use in stability analysis. It is worth noticing that dipping of principle stress is decreasing further into the valley side, becoming almost horizontal at the powerhouse cavern location. The reason might be rock line trace, becoming almost horizontal above cavern location.

Table 7-8 shows range of stress situation that must be applied to the 2D numerical model. As the values range over a small interval, the average of the values in Table 7-9 will be applied to the Phase2 model.

Table 7-8. Stress situation that must be applied in the numerical model

Description	σ_1(MPa)	σ_2(MPa)	σ_3(MPa)
Original Alignment	9.95-8.89 (out of plane)	5.91-6.97 (in plane)	1.60-2.04 (in plane)
Alternative Alignment	8.96-6.55 (out of plane)	6.90-9.31 (in plane)	1.74-1.79 (in plane)

Table 7-9. Stress situation applied in the numerical model in Phase2.

Description	σ_1(MPa)	σ_2(MPa)	σ_3(MPa)
Original Alignment	9.42 (out of plane)	6.44 (in plane)	1.82 (in plane)
Alternative Alignment	7.755 (out of plane)	8.10 (in plane)	1.765 (in plane)

Applying the stress in Table 7-9 to Eq- 7.2 give, locked-in stresses (Table 7-10). These locked in stress values are used as input in original and alternative alignment.

Table 7-10. Locked in stresses calculated from

Description	Locked in Stress	
	<i>In Plane</i>	<i>Out of plane</i>
Original Alignment	5.98	8.96
Alternative Alignment	7.64	7.30

7.2.1.4 *Material properties*

Material input parameters are acquired from laboratory test results and field mapping (Section 4.2.2). GSI is calculated from RMR value using Eq- 5.10 (Table 6-5).

Table 7-11. Material properties obtained from laboratory tests and field mapping (Larsen and Toubro(PDL), 2012a)

Parameters	Value
UCS	83.02 (MPa)
E-Modulus	67.96 (GPa)
Poisson's ratio	0.20
GSI	58

The Hoek-Brown failure criterion is used for the analysis of the cavern. Hoek (2007) said, that these criteria are often preferable in rock masses with several joint sets (Figure 7-18). Zhao (2000) found it applicable to the dynamic strength properties of brittle rock materials.

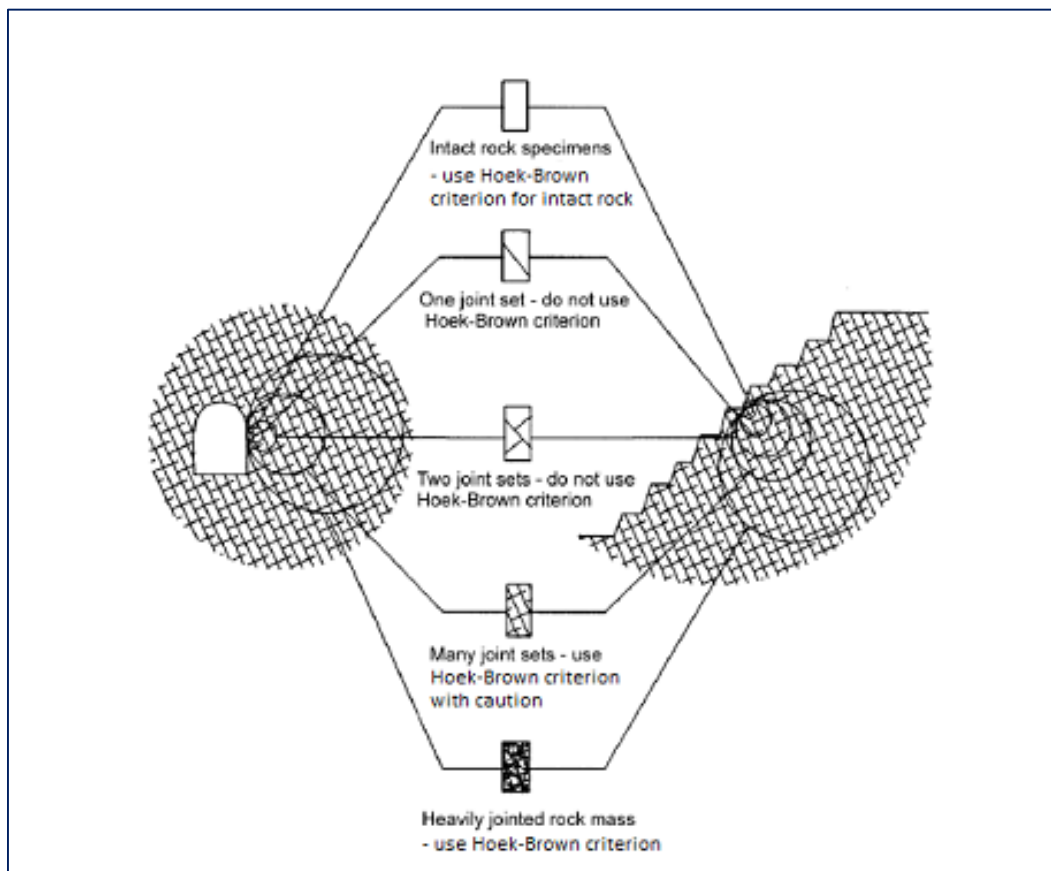


Figure 7-18. Illustration of the area of application for the Hoek-Brown criterion. Modified after Hoek (2007)

RocData calculate Hoek-Brown parameters from UCS, GSI, m_i , and D . m_i is set to 20 (Appendix J). Disturbance factor (D) is set to zero in most of the rock mass apart from the 3-meter radial zone around the excavation contour (Panthi, 2016). A disturbance factor of 0.5 is used to account for the blasting damage (Appendix A). Table 7-12 gives the Hoek-Brown parameters. Furthermore, the rock mass E-modulus (E_{rm}) is calculated from RocData (Table 7-12).

A dilation parameter can be applied for plastic materials. The measure of volume increase in succession to shearing of the material is called Dilatancy (RocScience, 2016a). Dilation is set to zero for most of the rock mass, excluding the disturbed zone. Due to plastic failure in the disturbed zone, dilation is set to 0.05 (Panthi, 2016). This is later proved in the elastic model by examining the area where the strength factor is less than one.

Table 7-12. Rock mass properties applied in the numerical model

Parameter	Undisturbed zone	Disturbed Zone
mb	4.46	2.70
s	0.0094	0.0036
a	0.503	0.503
Dilation	0	0.05
E_{rm} (GPa)	32.25	16.47

Post-peak behaviour of rock mass is modelled by estimating the residual parameters using Eq-2.7 to Eq-2.10 and confirmed by the residual parameter calculator in Phase2. Since there is no GSI value available for the disturbed zone, residual parameters (m_r & s_r) are determined by assuming the GSI value to be 30% of the original GSI (Panthi, 2016). Parameter (a_r) will remain the same as for the undisturbed zone, as it is independent of the blast damage factor (D) (Hoek et al., 2002).

Table 7-13. Residual rock mass parameters applied in the numerical model

Parameter	Undisturbed zone	Disturbed Zone
m_r	1.47	0.38
s_r	0.0003	0.000015
a_r	0.53	0.55

7.2.1.5 Support

Cavern support consists of shotcrete and rock bolts, modified later according to the numerical modelling results. Fully bonded CT rock bolts are used due to their high strength and resistance to corrosion. Bolt diameter is set according to their availability range. 33 mm diameter bar is used to obtain sufficient tensile capacity of 0.38 MN (DSI, 2016). Initial input for the length of the rock bolt is taken by comparing rock support results from Unwedge and empirical analysis. Table 7-14 shows properties of rock bolts applied to the model for both original and alternative alignment. 6 m @ 1.5 m c/c for the roof and 10 m @ 1.5 m c/c for the wall is used (Table 7-14).

Table 7-14. Rock Bolt properties applied in the model

Description	Values
Bolt Type	Fully bonded (CT-bolt)
Length (m)	6-10
Spacing (m × m)	1.5 × 1.5
Diameter (mm)	33 (1)
Bolt Modulus (GPa)	200 (2)
Tensile Capacity (MN)	0.38 (1)
Residual Tensile Capacity (MN)	0.01 (2)
Pre-Tension	-

(1) Values from (VIKØrsta, 2012)

(2) Standard values in Phase2

To simulate shotcrete, standard beam liner is used. It has flexural rigidity (resistance to bending). Timoshenko beam formulation is used for beam elements to account for transverse shear deformation effects (RocScience, 2016a). A starting value of 7 cm for the roof and 12 cm for the wall is used in the analysis for both the alternatives. Roof shotcrete thickness was increased to 15 cm after first initial runs with 7 cm and 12 cm. Wall shotcrete thickness is kept the same (12 cm).

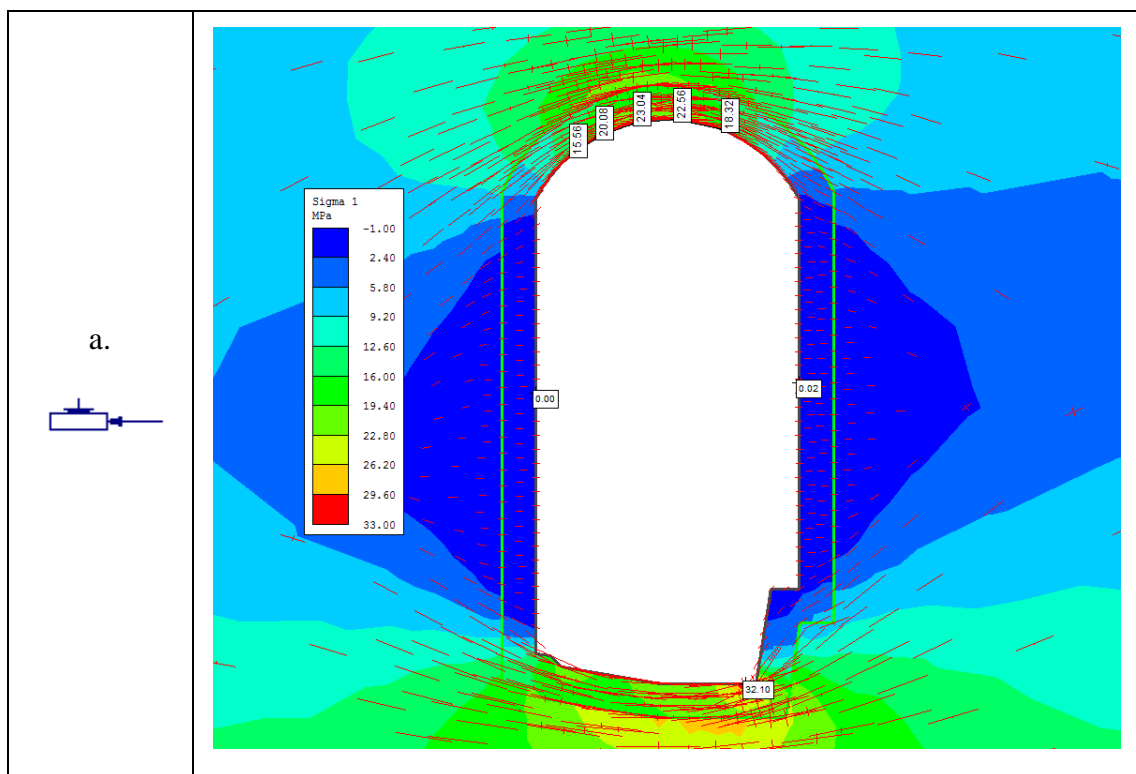
Table 7-15. Liner properties applied in the model. Standard values from Phase2 have been used

Properties	Values
Shotcrete modulus [GPa]	30
Thickness [cm]	15 (roof)
	12(wall)
Poisson's ratio	0.2
Material type	Plastic
Peak compressive strength [MPa]	35
Residual compressive strength [MPa]	5
Peak tensile strength [MPa]	5
Residual tensile strength [MPa]	0
Beam element formulation	Timoshenko

7.2.2 Numerical Modelling Results

7.2.2.1 Stress distribution

Stress distribution around the powerhouse cavern is shown in Figure 7-19. The disturbed zone has lower E_{rm} than the rest of the rock mass. Hence, stresses are distributed in transition of disturbed zone to the rest of the rock mass.



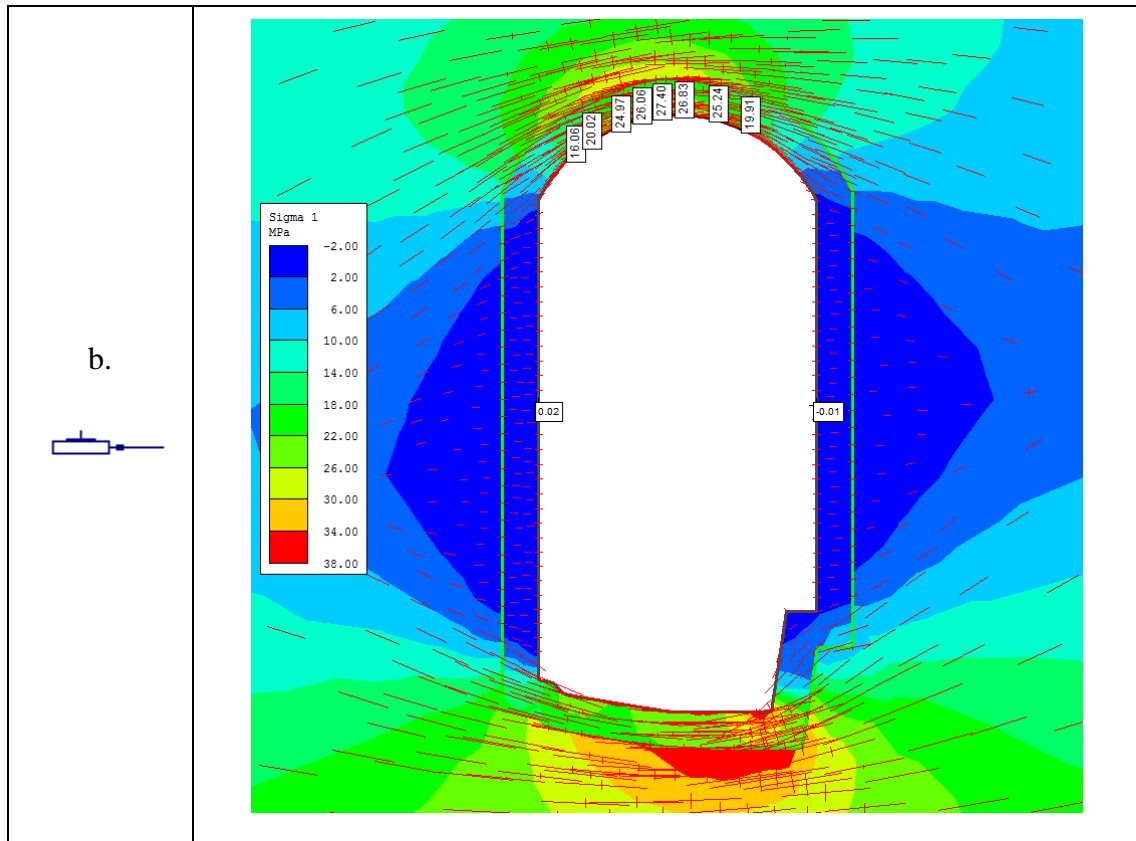


Figure 7-19. Stress distribution (Sigma 1) with trajectories, original alignment (a) & alternative alignment (b). Maximum stress in the roof is labelled [MPa] (elastic model).

Maximum values of redistributed stress in roof are given in Table 7-16.

Table 7-16. Maximum tangential stress in the cavern roofs and their ratio with UCS. Values over 0.4 indicates spalling.

Description	$\sigma_{\theta max}$ [MPa]	$\sigma_{\theta max}/UCS$
Original Alignment	23.04	0.28
Alternative Alignment	27.40	0.33

Negative stresses will cause stability problems due to tension. Zones with negative stresses are shown in Figure 7-20. Vertical tension cracks will be generated at the crest of the slope and minor shear failure could occur near the toe for both alignments. Hoek and Moy (1993) after observing such failures in slopes with weak rock mass, said that once formed, the tensional cracks are not a big cause of concern as they are local in nature. It results in stress relief and re-establishment of equilibrium.

Tension due to negative stresses might cause some stability problems in caverns. Concentration of negative stresses in the cavern wall might be the reason for problems. The geometry of cavern and the direction and magnitude of stresses are the reasons for negative stresses. The critical zone of negative stress is more extensive in alternative alignment than in original alignment.

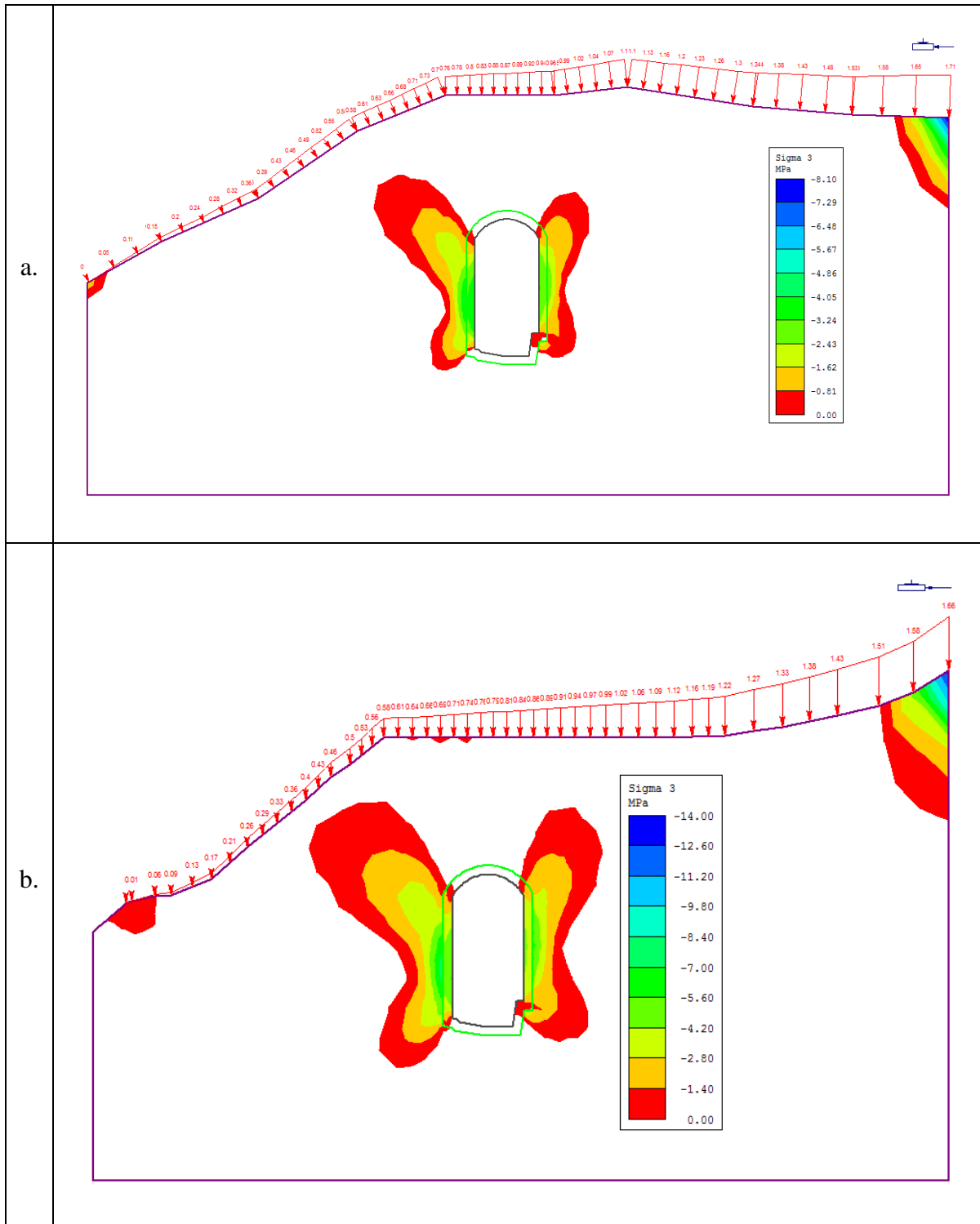
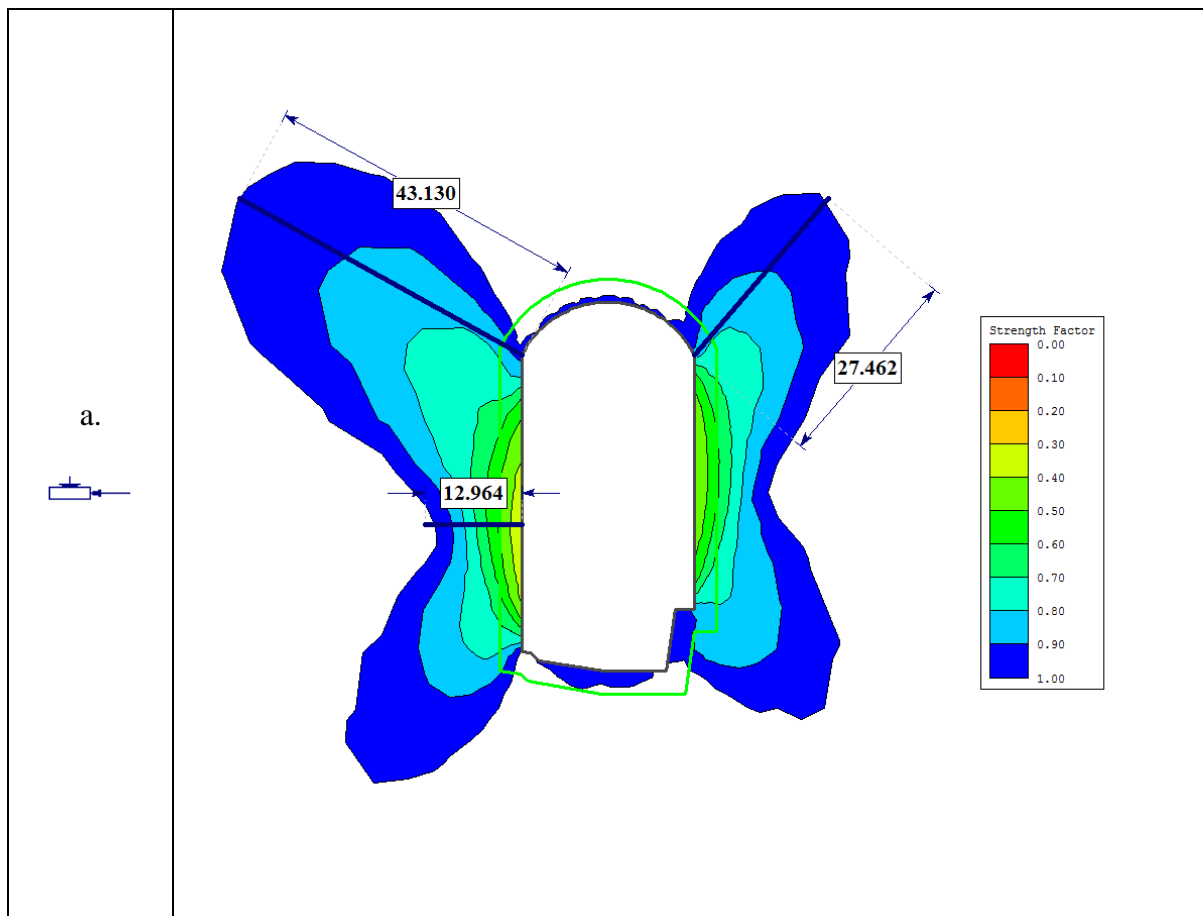


Figure 7-20. Areas with negative stresses for the original alignment (a) and the alternative alignment (b) (elastic model)

7.2.2.2 Predicting failure extent

Depth of brittle failure can be modelled by constant deviatoric stress criterion or by examining strength factor using Hoek-Brown brittle parameters (Section 5.3). Deviatoric stress criterion only takes σ_1 & σ_3 into consideration in Phase2, the results are only concentrated in the roof & floor of the powerhouse cavern. However, all three principal stresses have influence on the strength factor (σ_1 , σ_3 and σ_z). Strength factor in Phase2 is 3-dimensional. Hence, results from the strength factor criterion are more useful.

Figure 7-21 shows depth of potential brittle failure (Strength factor <1) with Hoek-Brown brittle parameters. Strength factor contours for both cases look like butterfly wings around the cavern body. Top left, right corner and walls are areas susceptible to stability problems. Alternative alignment is more severe in comparison to original alignment. Properties for disturbed zone are not assigned to this model. Due to low E-modulus, the disturbed zone will transfer more stress, leading to a discontinuous failure zone.



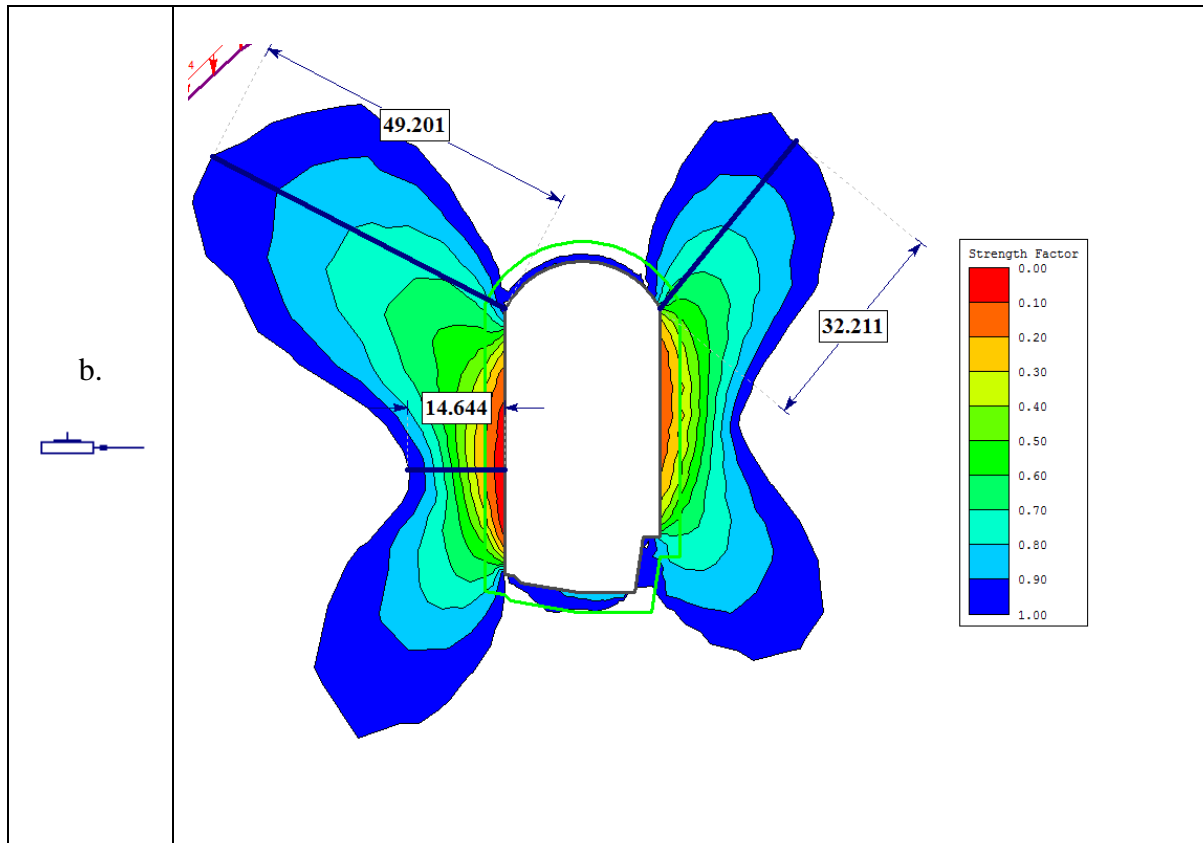


Figure 7-21. Depth of potential brittle failure (Strength factor <1) with Hoek-Brown brittle parameters for the original alignment (a) and the alternative alignment (b) (elastic model)

A plastic model is analysed in Phase2 to assess the degree of damage when the material is allowed to yield. Figure 7-22 shows the extent of the yield elements.

The zone of overstressed rock mass is shown in Figure 7-21 & Figure 7-22. Hoek and Moy (1993) said that in powerhouse caverns, close to the toe slope, overstressed zones could extend to the slope face (Figure 7-22). The case is more severe for alternative alignment.

Overstressed zone that is extended to the slope face can result in local slope instability and formation of a permeable zone between cavern wall and slope face. In addition, the extent and asymmetrical shape of the overstressed zone in rock mass may require long grouted cables to stabilise the rock mass around the cavern (Hoek and Moy, 1993). This will be discussed further in section 7.2.4.

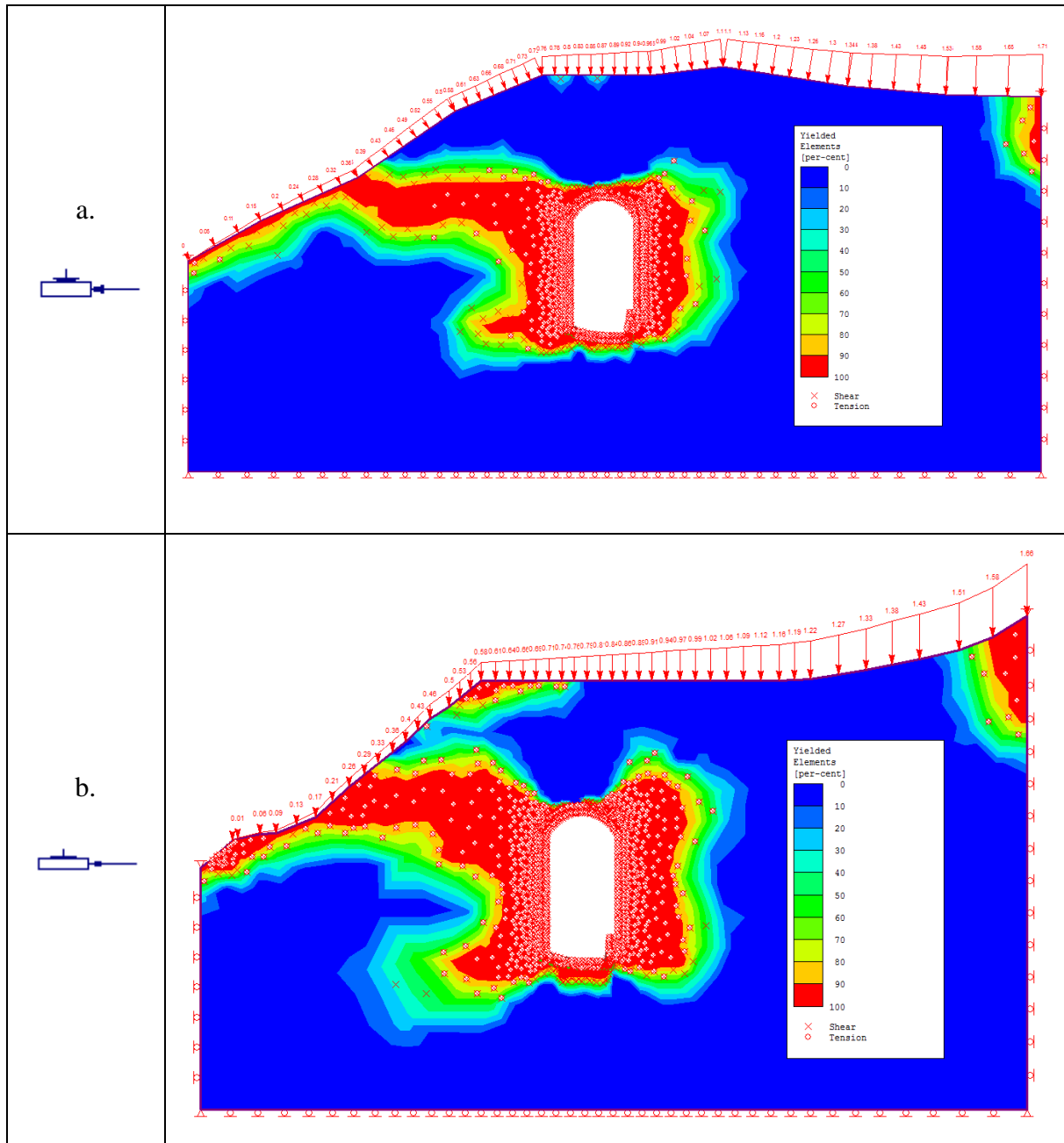


Figure 7-22. Yielded elements in an unsupported state for the original alignment (a) and the alternative alignment (b) (plastic model)

Total deformation is shown in Figure 7-23. Deformation is concentrated in the D-line wall (Appendix B) for both alignments. Total displacement is more favourable in the original alignment than in the alternative alignment. However, the values of total displacement are low, i.e. 5 cm for original and 6 cm for alternative alignment.

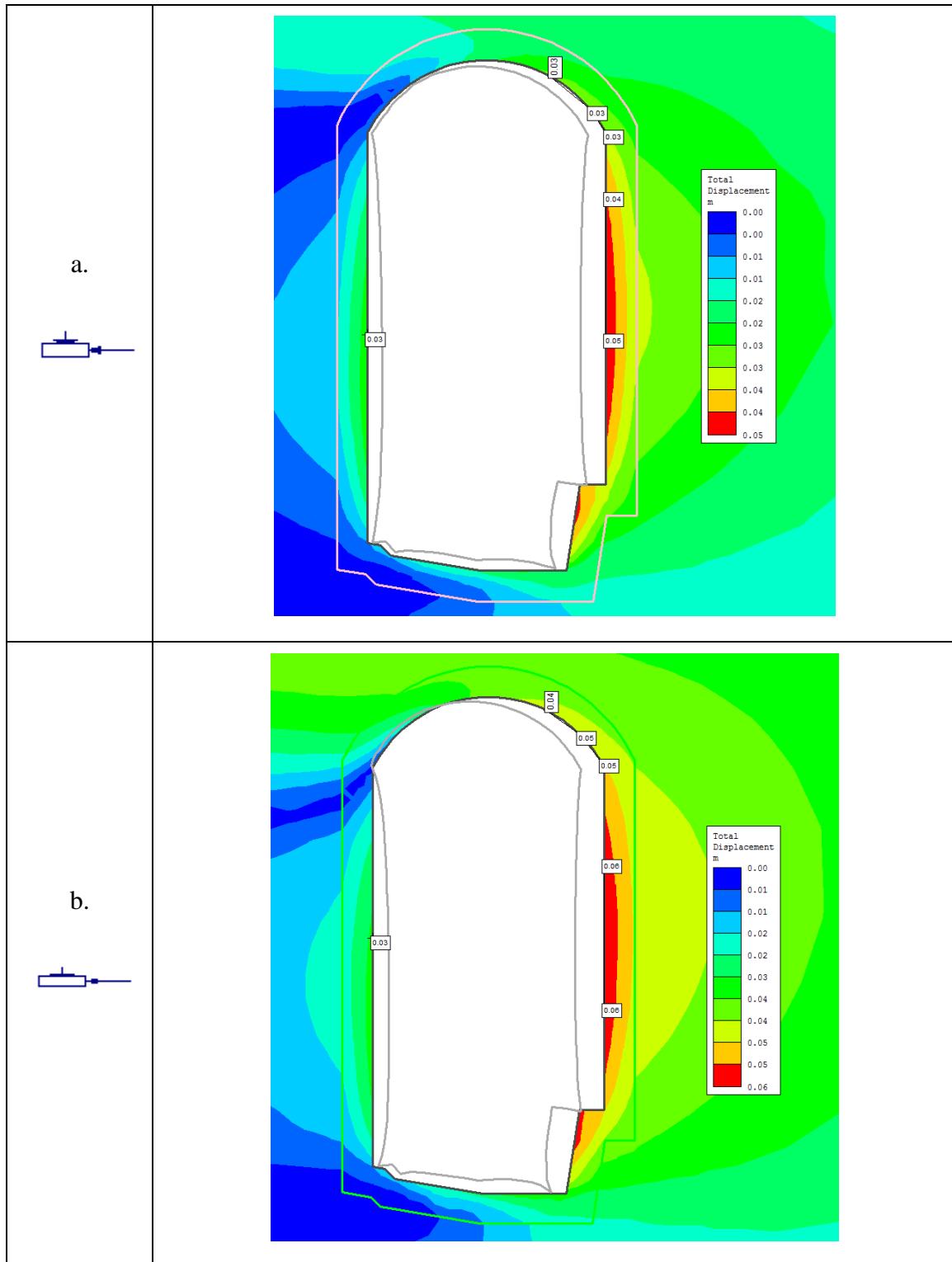


Figure 7-23. Total displacement in unsupported state for the original alignment (a) and alternative alignment (b). Values in crown, walls and floor are labelled [m]. Deformation boundary (scale factor =50) (plastic model)

7.2.2.3 Support

Figure 7-24 shows yielding of bolts in the disturbed zone. The dilation parameter applied to the disturbed area affects deformation and in turn the yielding of elements. Tensile failure of support is the result of increased deformation. Yielding of bolts is almost similar in both cases.

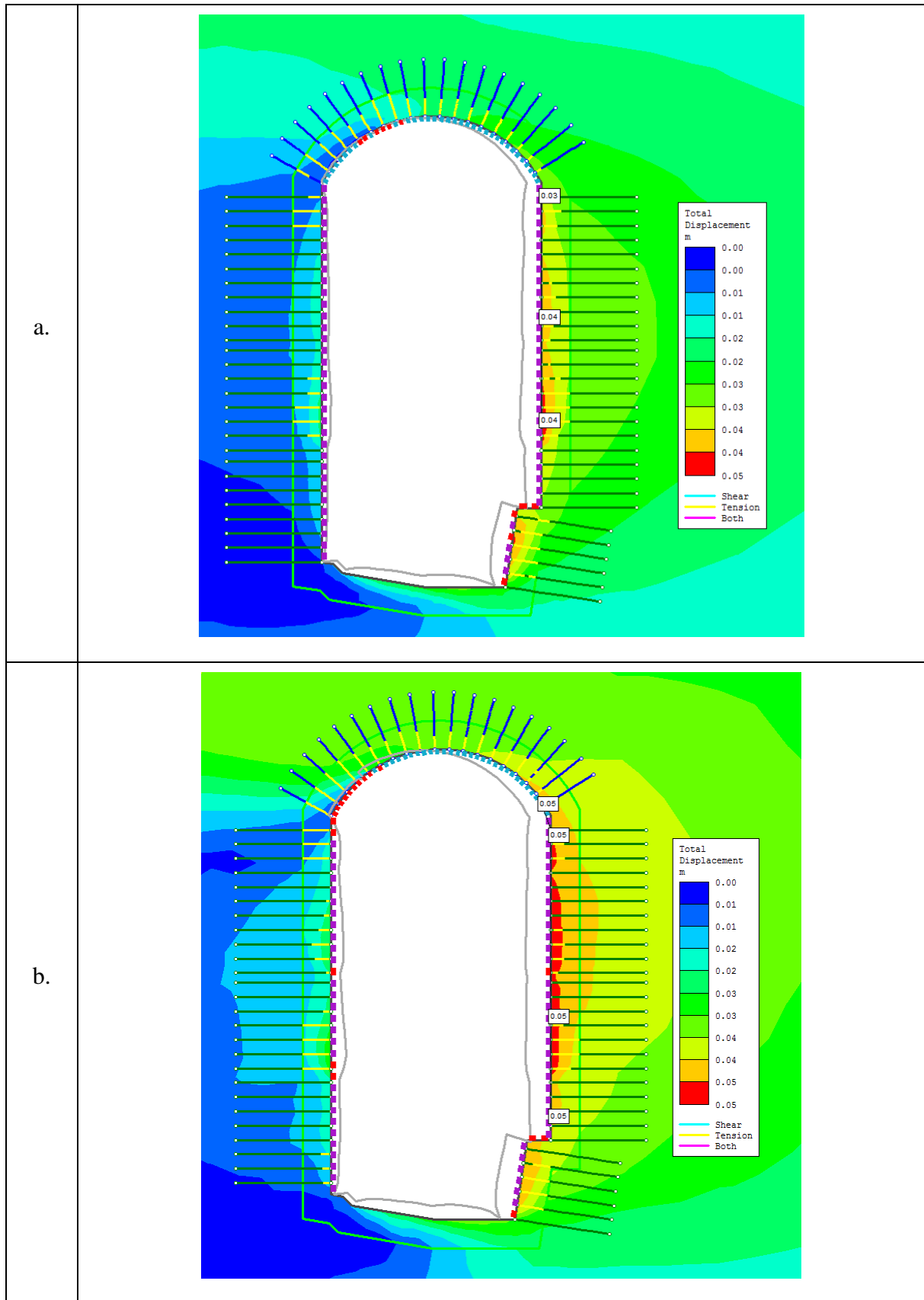


Figure 7-24. Total displacement and installed support for the original alignment (a) and alternative alignment (b). Yielded liner elements (red) and bolt elements (yellow). Values in the roof and walls are labelled [m]. Deformation boundary is scaled 1:50(plastic model).

Liner elements have yielded in the top left side of cavern roof for both alignments. Large span and high horizontal stresses are the reason. The severity is greater in the alternative alignment in the roof and top left corner (Figure 7-24).

Yielded bolt and liner elements are concentrated on the left hand side of the roof due to the concentration of compressive stresses from the slightly tilted stress situation. Both alignments show liner yielding in the walls of the powerhouse cavern due to displacement. Displacement in both alignments has improved by a small margin of 1 cm.

7.2.3 Sensitivity analysis

Numerical models are totally dependent on the quality of input parameters. Hence, it is important to understand that uncertainties in input parameters will lead to inaccuracy in numerical model results. Laboratory results vary in the rock mass (Section 4.2.2). Better values of rock mass found in the powerhouse location is used as input for numerical analysis. Moreover, strength parameters applied in the numerical model are related to the geological strength index (GSI). The GSI itself is a subjective classification instrument and not an exact material property (Section 5.2.3). The Generalized Hoek-Brown criterion is used to calculate strength parameters of the rock mass in the numerical model. Residual parameters used in plastic analysis are calculated from strength parameters using equations dependent on GSI value. There are uncertainties in predicting the disturbance factor due to its dependence on the quality of blasting. The dilation parameter is unconfirmed and used in consultation with the supervisor.

In addition to uncertainties in material properties, the stress situation in the cavern location is estimated and not an exact value, the range varies a lot in hydraulic fracturing test report. Numerical modelling in Phase2 is done based on the best estimate of the prevalent conditions. Regarding all the uncertainties described above, it is interesting to examine the situation with worse parameters (Table 7-17), and the best way to do it is by using sensitivity analysis.

Table 7-17. Parameters examined in the sensitivity analysis.

Parameter	Best Estimate	Worst Case
GSI	58	48
m_i	20	17
UCS (MPa)	83.02	53.54
E-Modulus (GPa)	67.96	45.58
Disturbed Zone (m)	3	5

Table 7-17 shows values that are most likely to occur (Best estimates), and worst case scenario values.

Stress situation values used for sensitivity analysis (Table 7-18) are the major values used from Table 7-8 (Section 7.2.1.3).

Table 7-18. Stress situation applied in the numerical model in Phase2 in sensitivity analysis

Description	σ_1 (MPa)	σ_2 (MPa)	σ_3 (MPa)
Original Alignment	9.95 (out of plane)	6.97 (in plane)	2.04 (in plane)
Alternative Alignment	8.96 (out of plane)	9.31 (in plane)	1.79 (in plane)

Table 7-19. Locked in stresses calculated stress situation from Table 7-18. .

Description	Locked in Stress	
	<i>In Plane</i>	<i>Out of plane</i>
Original Alignment	6.46	9.44
Alternative Alignment	8.86	8.51

Worst values for GSI and E-modulus are taken from Table 6-5 and Table 4-3. The m_i parameter has its standard deviation (Appendix J) implemented in RocData. The extent of the disturbed zone is set in consultation with the supervisor (Panthi, 2016). Hoek-Brown parameters (peak and residual) are calculated as per the procedure and guideline followed earlier in section 7.2.1.4.

Table 7-20. Rock mass properties for the worst case scenario.

Parameter	Undisturbed zone	Disturbed Zone
mb	2.65	1.42
s	0.003	0.0009
a	0.506	0.506
m_r	1.16	0.28
s_r	0.00024	0.00001
a_r	0.531	0.565
E_{rm} (GPa)	12.37	5.87

The yielded support system and the elements for the worst case scenario are shown in Figure 7-25. The yielded zone has increased significantly and proposed support in the section 7.2.1.5 is not sufficient. Both alignments under study clearly represent an unstable situation. Total displacement on cavern contour has increased 4 to 5 times.

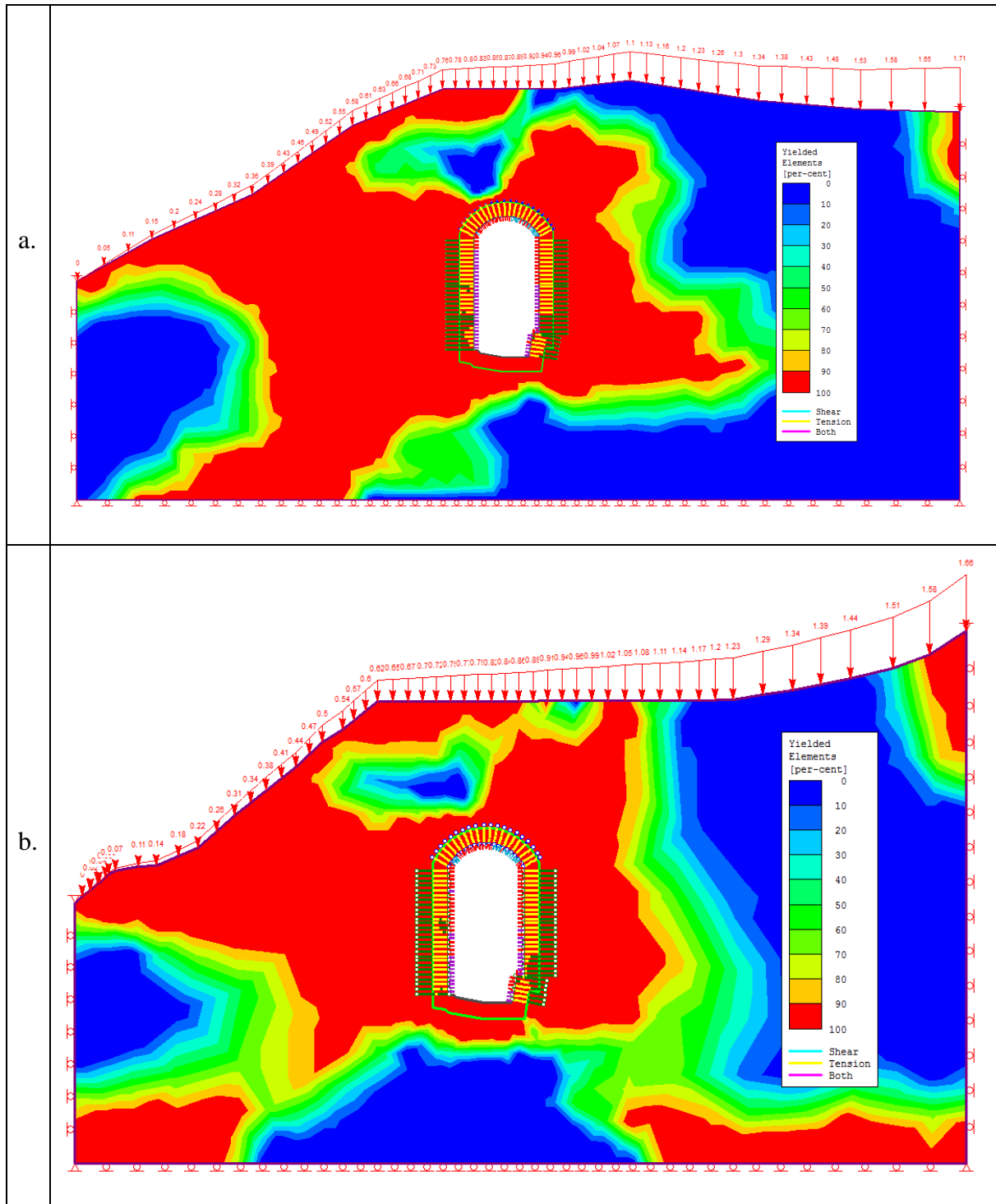


Figure 7-25. Yielding in rock mass and support for worst case scenario. Original alignment (a) and alternative alignment (b) (plastic model)

Sensitivity analysis without support system is carried out in order to see which parameters in Table 7-17 & Table 7-18 influence stability the most. Each parameter is set to worst value one by one, following is the list of parameters:

- GSI
- m_i
- UCS
- E-Modulus
- Extension of Disturbed Zone
- Stresses

Sensitivity of the model is measured by increase in yielded mesh elements and maximum total displacement for unsupported state.

Table 7-21. Sensitivity analysis. Yielded mesh elements and increase of yielded mesh elements from the best estimate in % and maximum total displacement.

Description	Original alignment		Alternative Alignment	
	<i>Yielded mesh elements (% increase)</i>	<i>Maximum total displacement [cm]</i>	<i>Yielded mesh elements (% increase)</i>	<i>Maximum total displacement [cm]</i>
Best estimate	1342	5	1463	6
Worst case	2033 (51)	17	1857 (27)	25
Worst case (Resi. E-modulus)	2176(62)	56	2005(37)	80
GSI	1450 (8)	9	1529 (4.5)	11
m_i	1368 (3)	5	1484 (1.5)	6
UCS (MPa)	1483 (10.5)	5	1554 (6)	6
E-Modulus (GPa)	1340 (0)	7	1465 (0)	9
E-Modulus (Residual)(GPa)	1426(6)	22	1628(11)	24
Disturbed Zone (m)	1474 (10)	5	1612 (10)	8
Stresses	1339 (0)	5	1517 (3.7)	7

Stress levels haven't changed that much, so the influence due to stresses is minimal. GSI and E-modulus show little effect on yielded elements but the influence on the amount of total displacement is much more prominent. UCS and m_i have no effect on total displacement but significant effect on the yielded mesh elements. The disturbed zone has shown effect on yielded mesh elements, total displacement has changed a little for alternative alignment.

For plastic analysis, the option of providing the residual Young's modulus is available in the Phase2 program, it can only be used in analysis if rock mass has yielded and after yielding the rock mass is subjected to alteration in load state. Figure 7-22 shows the yielded zone in both alignments extending towards the toe slope and load redistribution has taken place after excavation. Hence, the residual Young's modulus can be applied. Application of the residual value of Young's modulus in sensitivity analysis shows large change in yielded elements and total displacement. Results are more severe when the residual Young's modulus is used in the worst case scenario.

7.2.4 Discussion of model results

Total closure of powerhouse walls in the best estimate model without installed support for original alignment is at maximum 8 cm, yielding a strain level of 0.35 %. Strain levels of almost 1 % or greater (under worst case scenario) are signs for onset of instability and difficulties in providing suitable support work (Hoek, 2001). On the other hand, in case of the alternative alignment, total closure of powerhouse cavern walls is at maximum 9 cm without installed support corresponding to a strain level of 0.40 %. These levels of total maximum displacements are not alarming, keeping in view the large span of the powerhouse cavern (23 m).

Hoek and Moy (1993) discussed that the yielded zone of powerhouse caverns located close to the toe slope can extend to slope face and result in local slope instability and also result in formation of permeable zone between the slope face and powerhouse cavern wall. Furthermore, extended and asymmetrical shape of yielded zone in rock mass may require long grouted cable bolts to stabilize the rock mass around the powerhouse cavern.

Figure 7-26 shows the scenario discussed by Hoek and Moy (1993), they consider the powerhouse cavern in Figure 7-26(a) to be too close to the toe of the slope and recommend moving it further into the rock mass, which is similar to the situation faced in this thesis.

The situations discussed in Figure 7-26 are according to the geotechnical factors, which itself is not the sole factor in deciding the location of cavern, and other important factor is the length of the tail race tunnel. According to hydraulics tail race tunnel must be kept as short as possible

in order to avoid the need for a downstream surge shaft to take care of pressure fluctuations. Experience gathered from all the underground water conductor systems designed till today show that if the tunnel length approaches 100m or more, the need for a downstream surge shaft has to be considered. In this thesis, the tail race length is in range of the 100 m mark and the project is optimized not to provide downstream surge shaft.

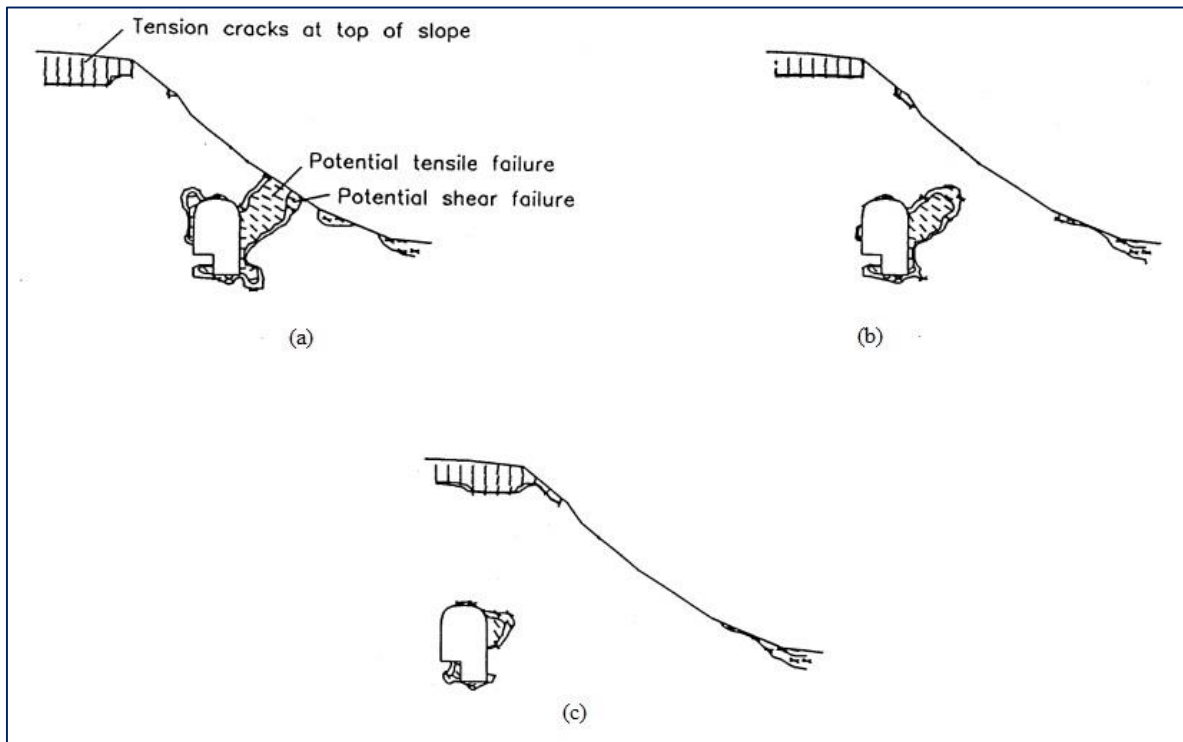


Figure 7-26. Zones of overstress and failure trajectories for underground cavern at different distances from the toe of the slope (Hoek and Moy, 1993).

All yielded bolt elements are restrained within the disturbed zone, which constitutes 1/2 to 1/3 of rock bolt lengths in cavern roof and walls. This is not considered as a critical state for the stability of the caverns (Panthi, 2016). With lower bolt diameters, some of the bolts yielded both in shear and tension, over the whole length in crown and wall. Yielding was not critical but more extensive than 33 mm diameter bolts.

Limited amounts of liner elements yielded due to significant compressive stresses in the roof of the cavern (redistribution of topographical stresses) and total deformation in the wall. The alternative alignment is on the higher side, despite the increase in shotcrete thickness in the cavern roof from 7cm to 15 cm. A compressive strength of 35 MPa for shotcrete is used (Panthi, 2016).

The dilation parameter used in plastic analysis has a large effect on model results. An increase in dilation will add to more displacement and yielding of bolts and shotcrete. On the other hand,

it is observed that increased dilation parameters will somewhat reduce the amount of yielding in the rock mass surrounding the powerhouse cavern. Crowder and Bawden (2004) have suggested dilation values based on the range of GSI values. A dilation value equal to 0.05 is used (Panthi, 2016). There seem to be no definite guidelines to determine the dilation parameter. This input parameter adds uncertainty to the numerical modelling analysis carried out in this thesis.

7.3 RS³ analysis

RS³ package from Rocscience is used for numerical modelling. Modelling is carried out as uncoupled analysis using automatic solver type. Both elastic and plastic material properties are applied in the analysis. Redistribution of stresses and strength factor of material is analysed using elastic material. Displacement and rock mass failure is examined using Plastic material. Plastic property allows the material to yield.

Original alignment is more stable in terms of stresses, strength factor, displacements and extent of yielded zone (Section 7.2.4). Hence, RS³ analysis of only original alignment is carried out in this thesis. Two sets of parameters are used. The best parameters belong to the majority of rock mass in powerhouse cavern area (Section 3.2.4) and the lowest values of the parameters describes the worst case.

7.3.1 Model set up and input data

The model setup and input data provided in section 7.2.1 for Phase2 analysis has been used for RS³ analysis, the only change is in mesh and displacement properties.

A graded mesh type with a 4 noded tetrahedron with gradation parameters, i.e. offset of 2, gradation factor of 0.1 and an external gradation factor of 1 is used. The number of edges on excavation boundaries is 57.

The external boundary represents the project topography, as the cavern lies at shallow depth. There are certain contradictions in terms of mesh width and boundary conditions, but the model shows more natural and matching results with boundary nodes restrained in the xyz-direction, and an external lower boundary surface restrained in the vertical direction (y direction) and side boundaries in the horizontal direction (x direction) and side boundaries along the length restrained in all directions (xyz direction). The top surface following the topography is not restrained in any direction.

A cavern length of 126 m has not been used as slice thickness as the terrain changes after every 3-5 m along the length of the cavern. A centre-to-centre spacing between the units of 21.5 m is used as slice thickness for the cross-section with lowest cover and shortest distance between cavern wall and slope face.

7.3.2 Numerical Modelling Results

7.3.2.1 Stress distribution

The stress distribution around the cavern is shown in Figure 7-27. The maximum stress value in the roof is shown in Table 7-22. The disturbed zone has lower E_{rm} than the rest of the rock mass. Hence, the stress in the distributed zone has transitioned to the rest of the rock mass (Figure 7-27).

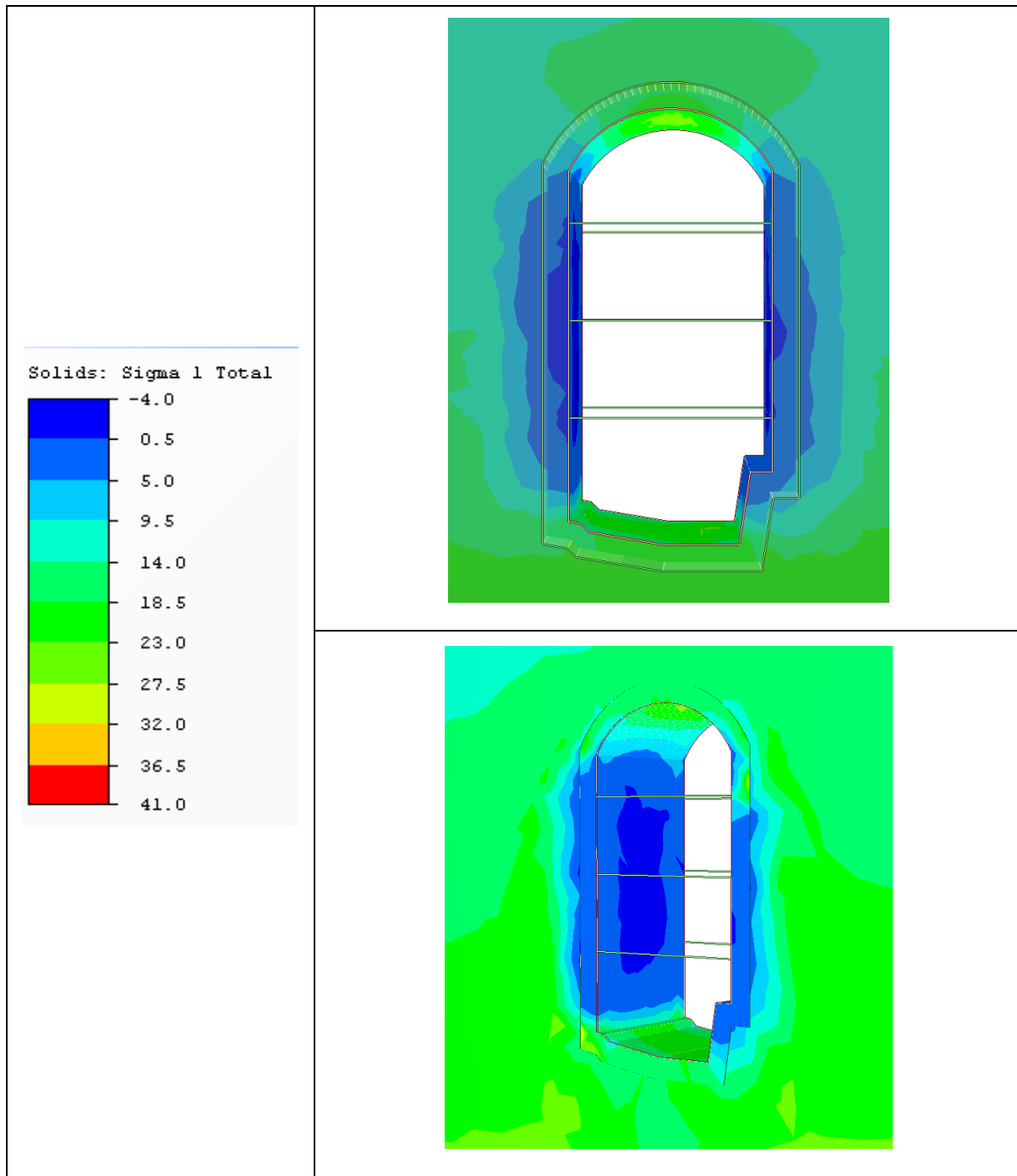
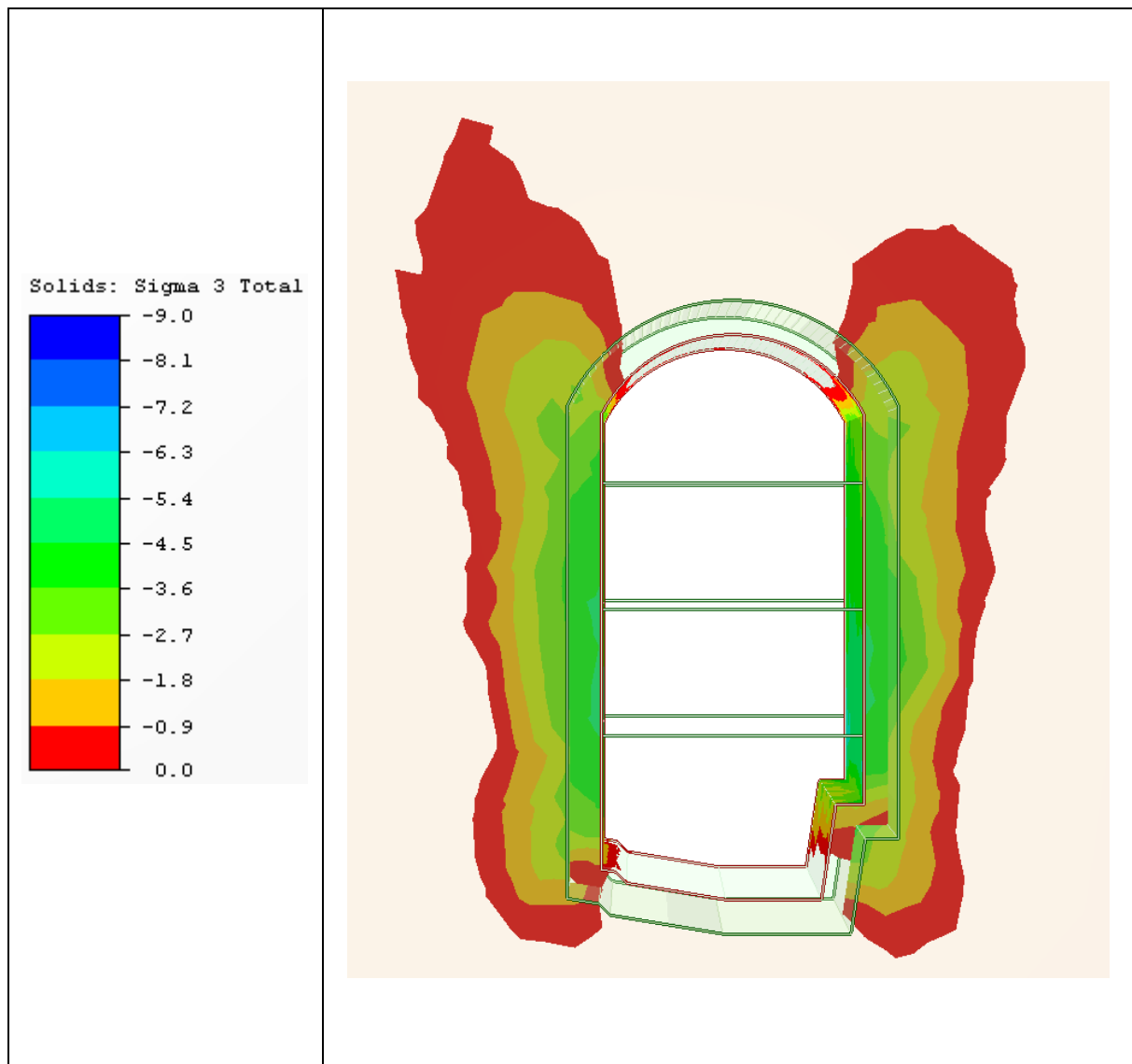


Figure 7-27 Stress distribution (Sigma 1) original alignment, slice view from centre (above) & Perspective view (exterior) (below). Maximum stress in the roof [24.84 MPa] (elastic model)

Table 7-22. Maximum tangential stress in the cavern roofs and their ratio with UCS. Values over 0.4 indicates spalling.

Description	$\sigma_{\theta max}$ [MPa]	$\sigma_{\theta max}/UCS$
Original Alignment	24.84	0.30

A negative stress situation is similar to the situation discussed in section 7.2.2.1 for the original alignment and is more confined as compared to Phase2 analysis results. A slice view from the centre shows a more extended area as compared to the end (exterior) view (Figure 7-28). It can be said that negative stresses are getting confined at the end section of the cavern and converging into the end wall stresses.



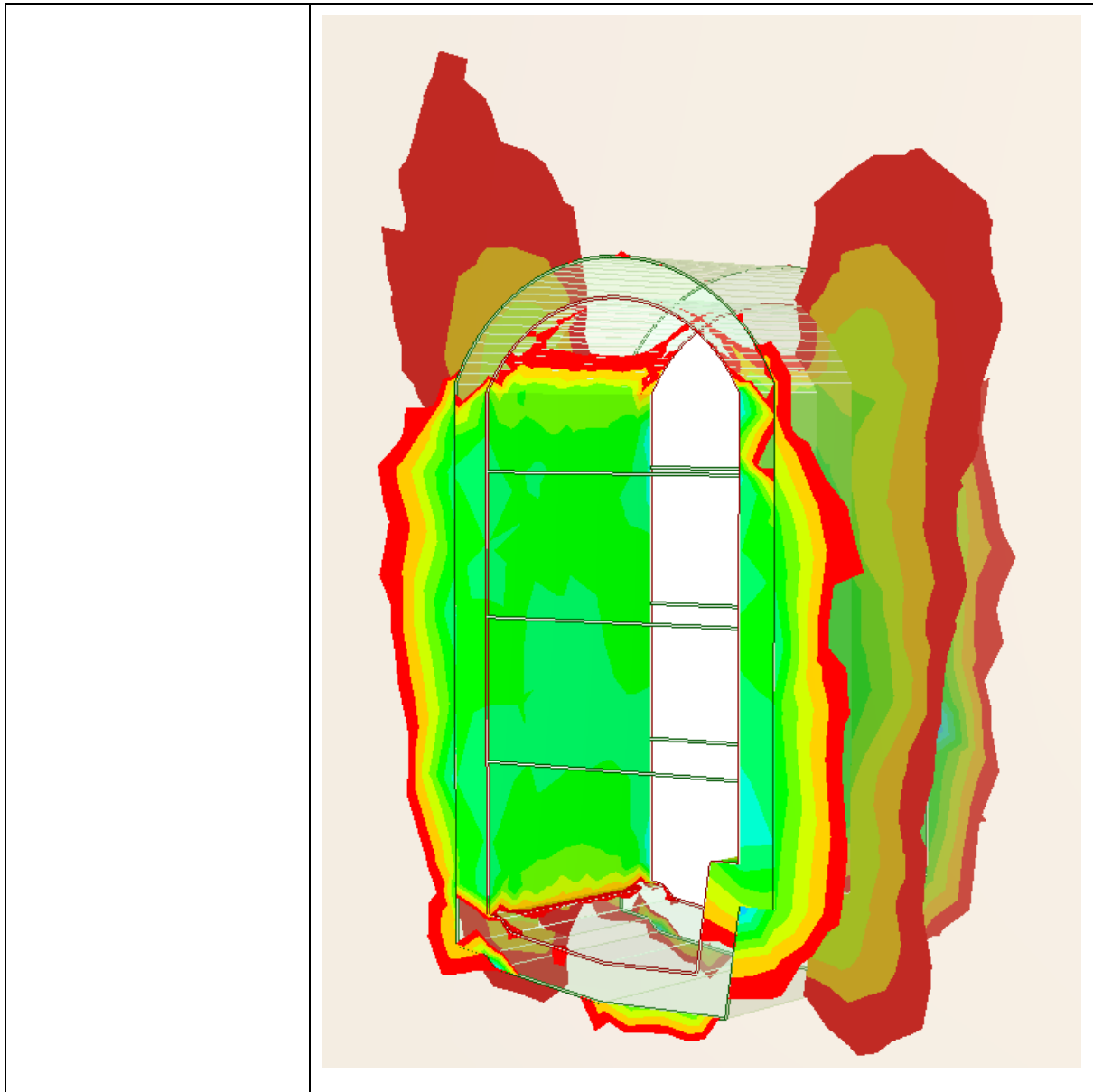


Figure 7-28. Areas with negative stresses for the original alignment, slice view from centre (above) & Perspective view (exterior) (below) (elastic model)

7.3.2.2 *Predicting failure extent*

Figure 7-29 shows the depth of brittle failure. Figure 7-30 & Figure 7-31 show the extent of yielded elements in original alignment. The results are more confined and less critical as compared to the Phase2 analysis results (Section 7.2.2.2).

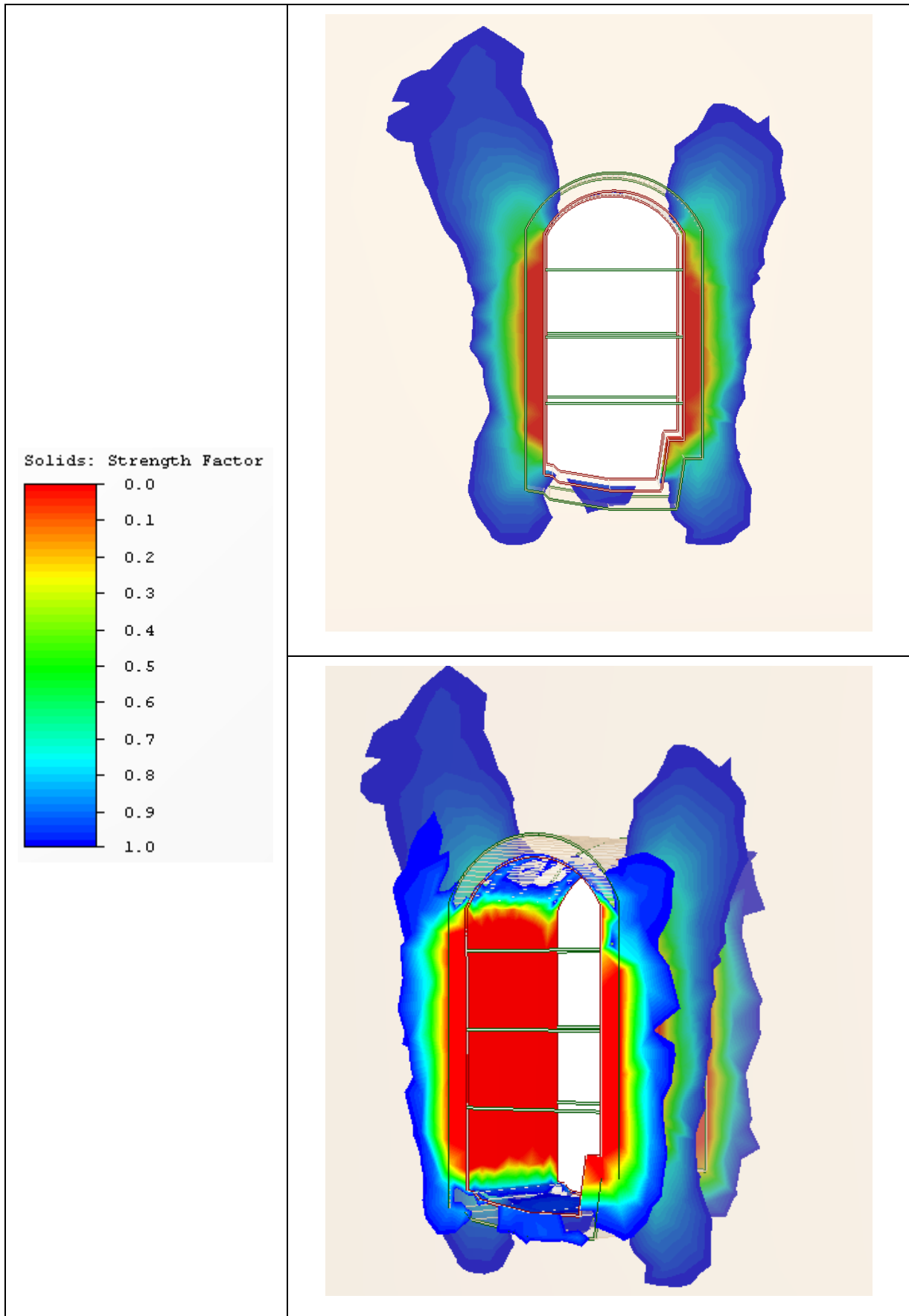


Figure 7-29. Depth of potential brittle failure (Strength factor <1) with Hoek-Brown brittle parameters for the original alignment, slice view from centre (above) & Perspective view (exterior) (below) (elastic model)

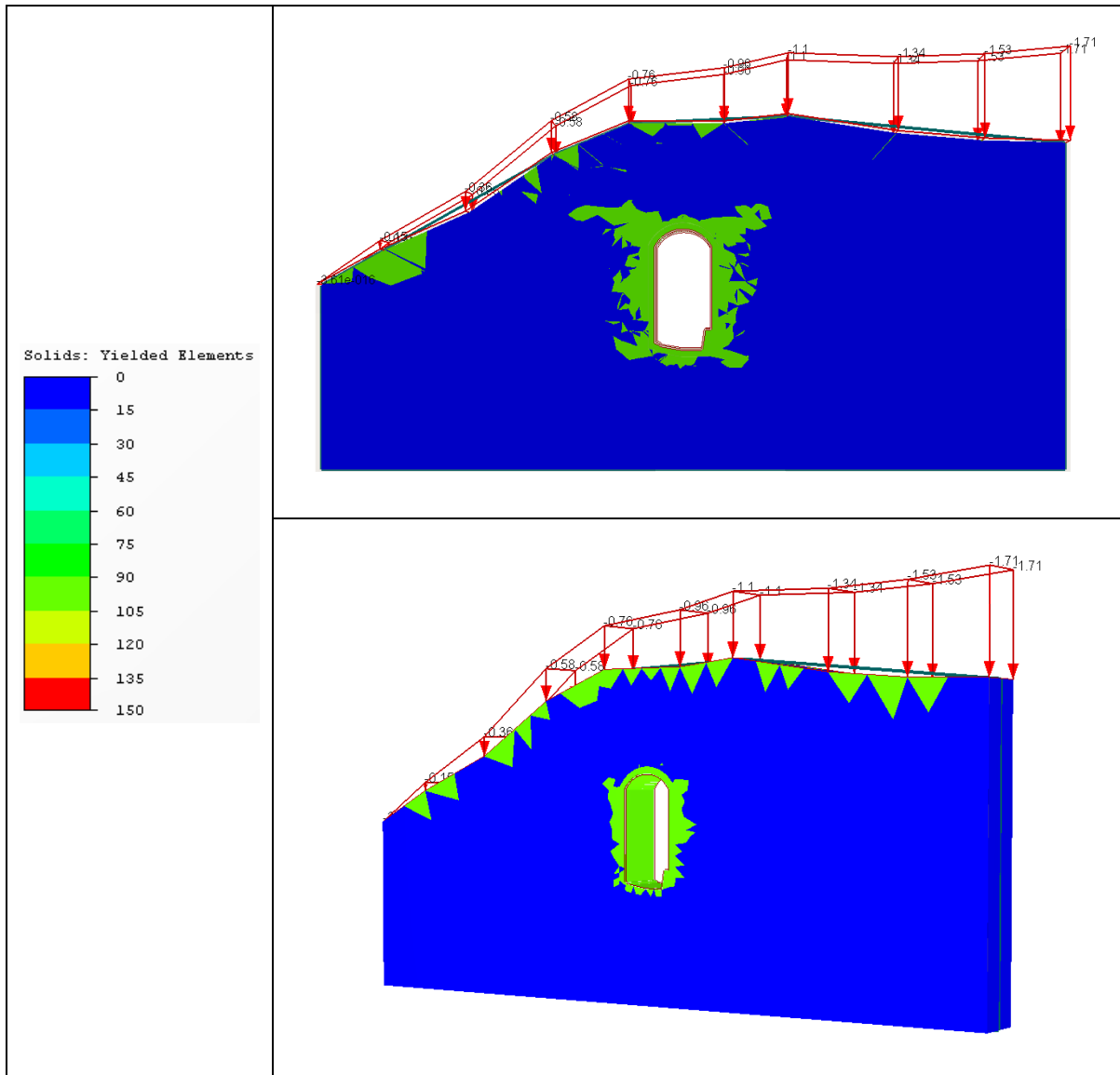


Figure 7-30. Yielded elements in an unsupported state for the original alignment, slice view from centre (above) & Perspective view (exterior) (below) (plastic model)

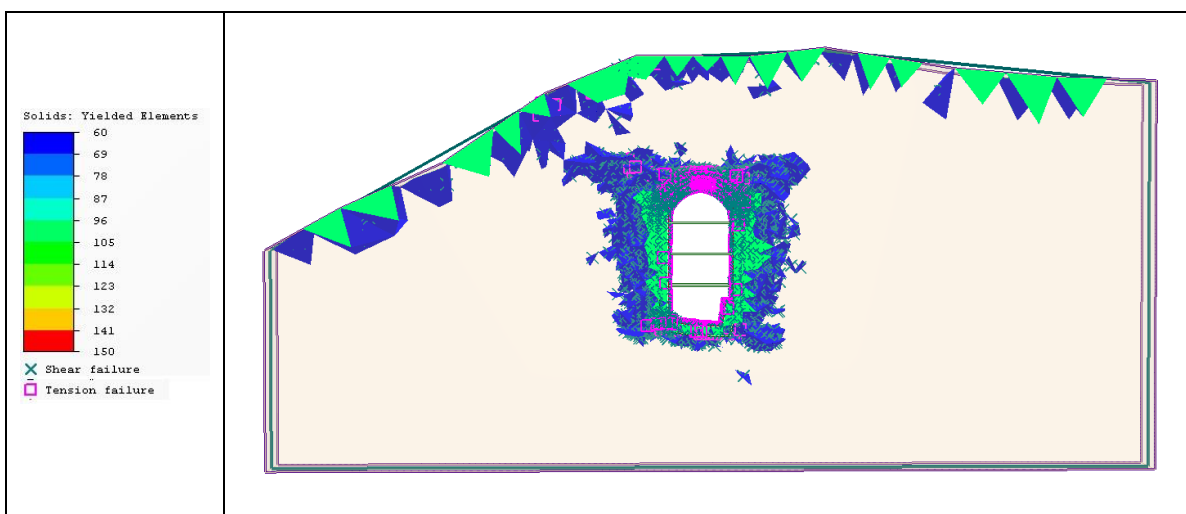


Figure 7-31. Yielded elements in an unsupported state for the original alignment (Slice view), showing tensile and shear failure (Plastic model).

Figure 7-32 shows the total displacement around the cavern. It is in range of 2 to 2.5 cm in roof and wall area. Values of total displacement are less as compared to Phase2 analysis results. The results are not alarming.

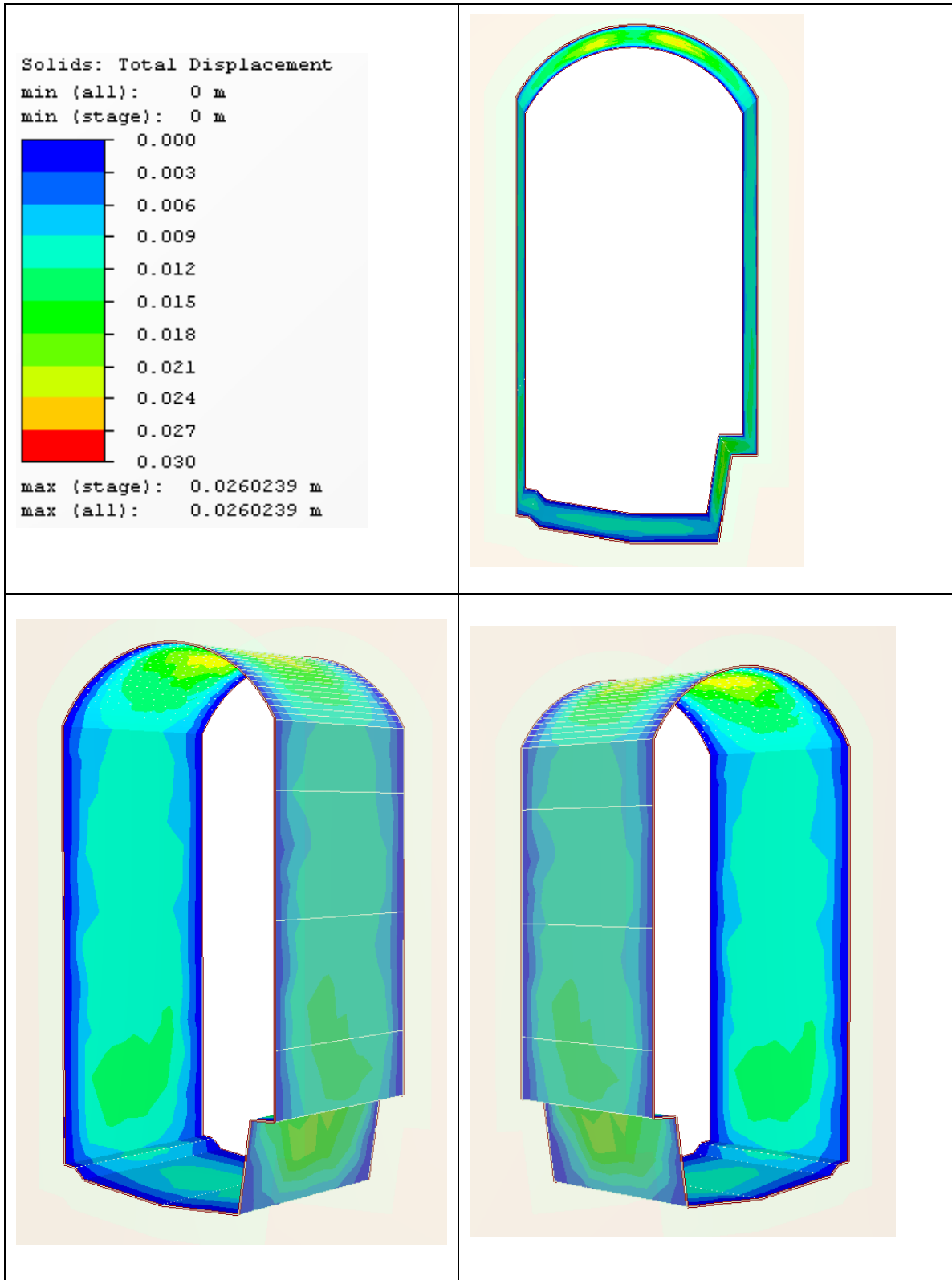


Figure 7-32. Total displacement in unsupported state for the original alignment. (plastic model)

7.3.2.3 Support

Figure 7-33 shows axial force and yield in rock bolts. The dilation parameter applied to disturbed area affects deformation and in turn yielding of elements. Tensile failure of support is the result of increased deformation. Yielding of bolts is similar to yielding in Phase2 analysis. It is concentrated in the roof and some on the walls.

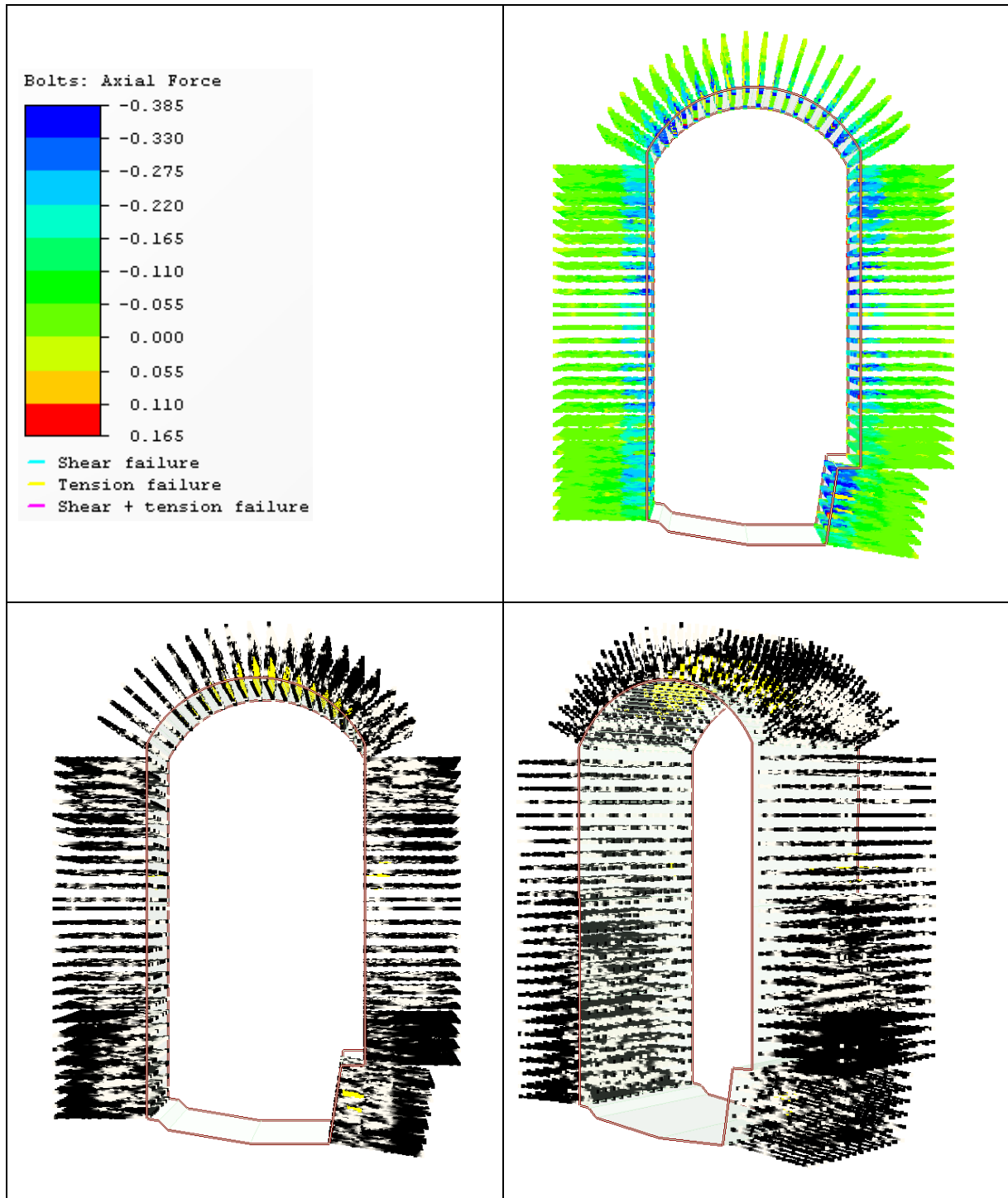


Figure 7-33. Installed rock bolts support for the original alignment. Bolt Axial force (Right-above), Yielded bolt elements (yellow) (below) (plastic model).

No liner element has been yielded in the roof and wall (Figure 7-34) as compared to the results in Phase2 analysis (Section 7.2.2.3). Total displacement has reduced to 1.5 cm maximum in the D-line wall (Appendix B).

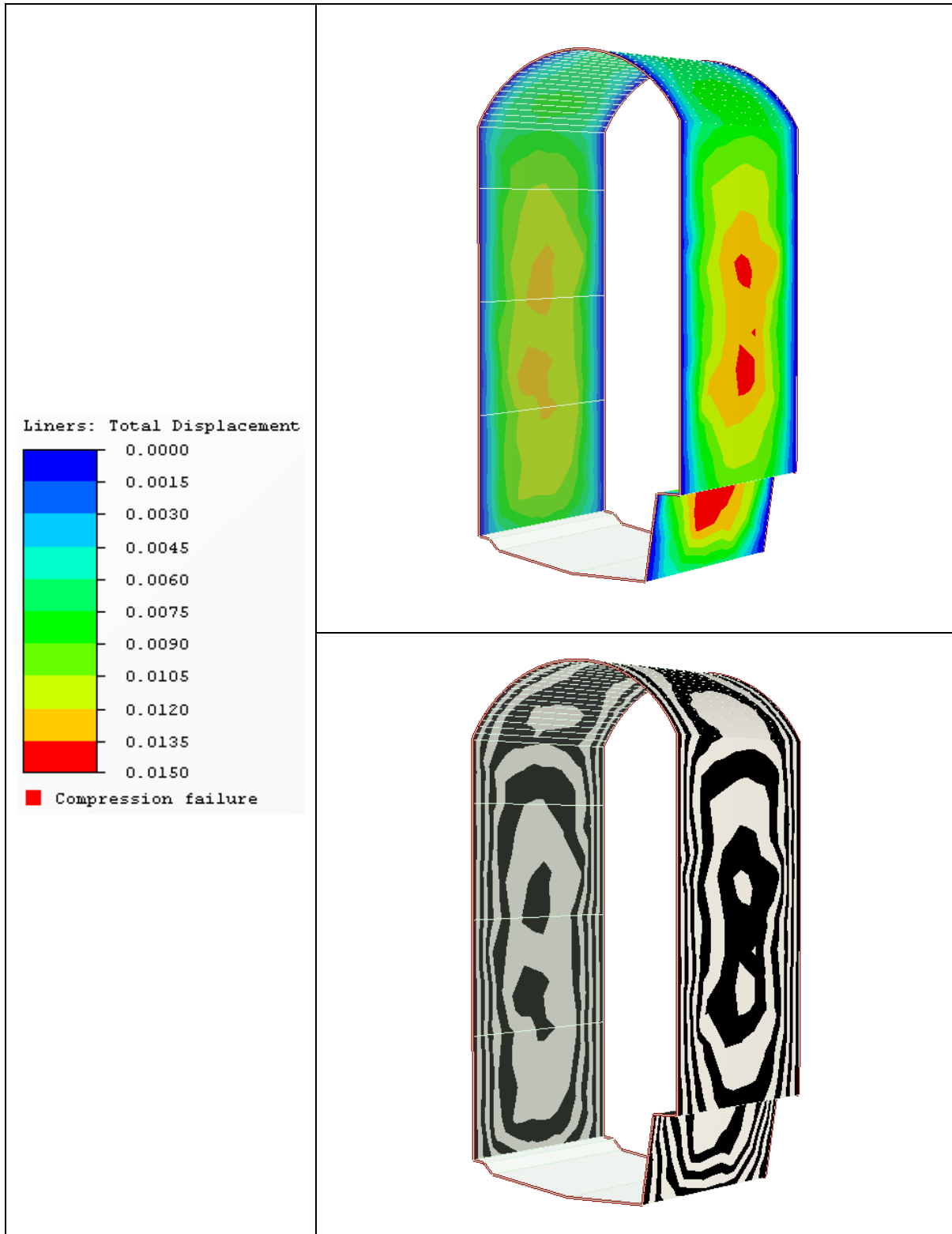


Figure 7-34. Installed shotcrete support for the original alignment. Yielded elements (red) (below) (plastic model).

7.3.2.4 Worst Case Scenario

The RS³ model is analysed for worst values (Section 7.2.3). The results are shown in Figure 7-35, Figure 7-36 & Figure 7-37.

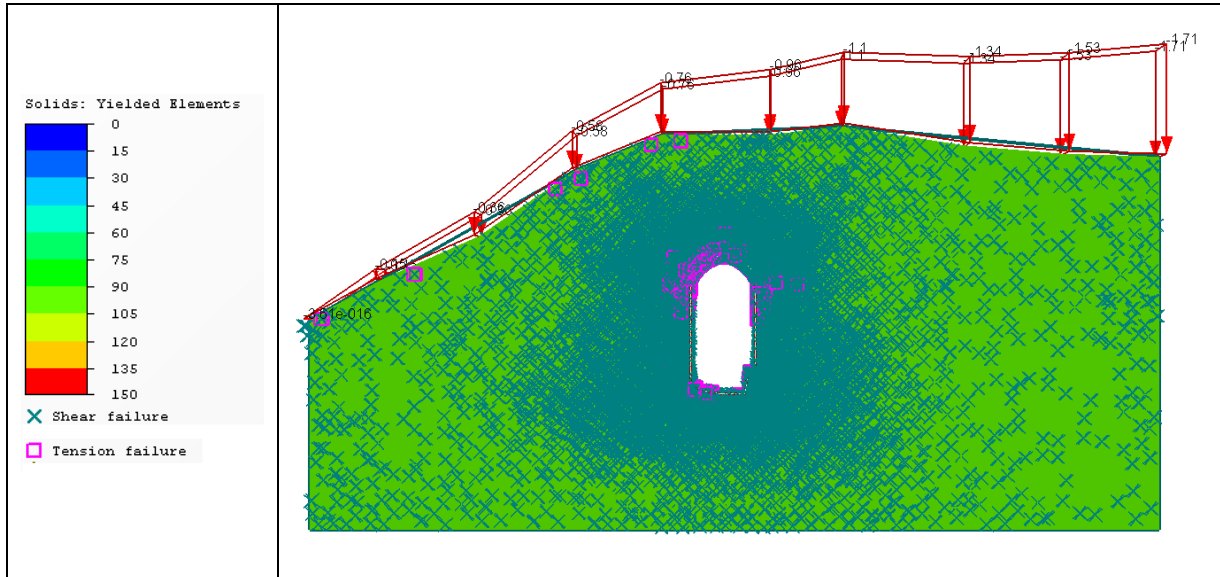
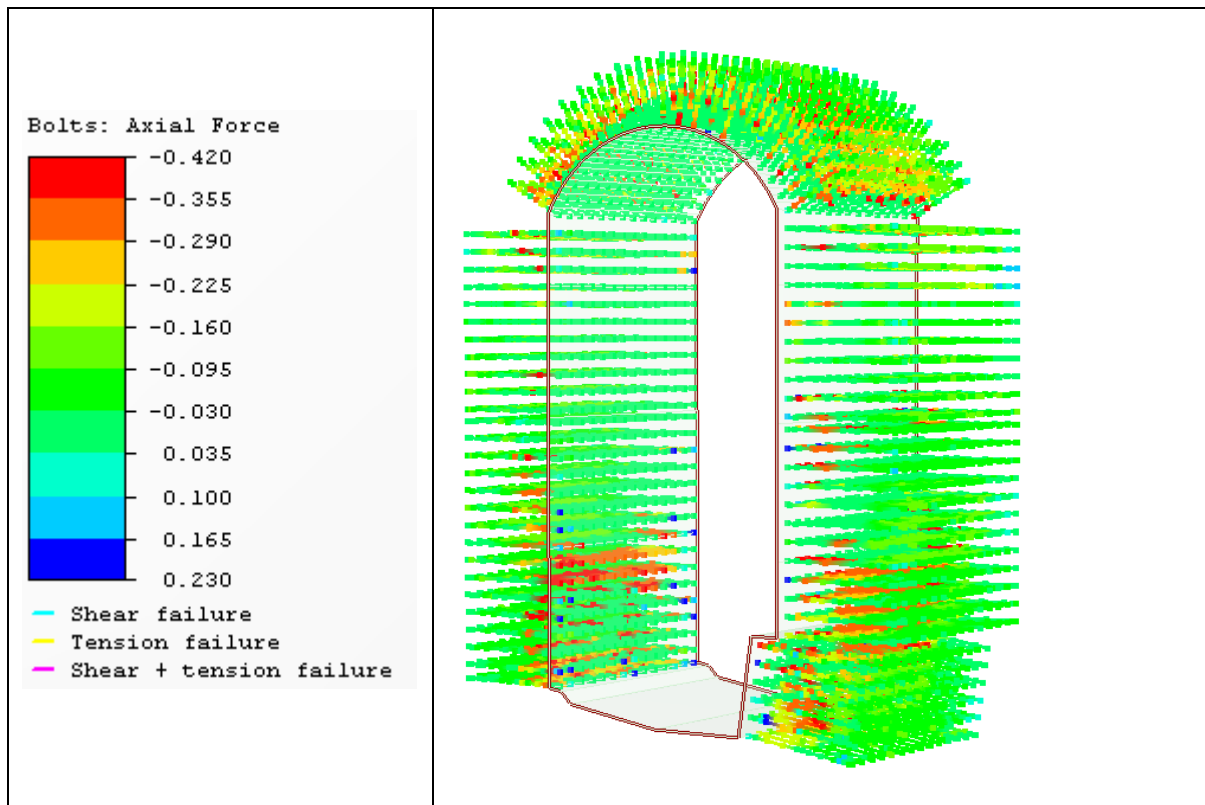


Figure 7-35. . Yielding in rock mass for worst case scenario. Original alignment (plastic model).

Figure 7-35 shows that the rock mass around the cavern has yielded in both shear and tension. The extent of shear failure has increased as compared to Phase2 analysis. It may be due to the boundary conditions chosen for the model. Collapse may occur leading to failure at slope.



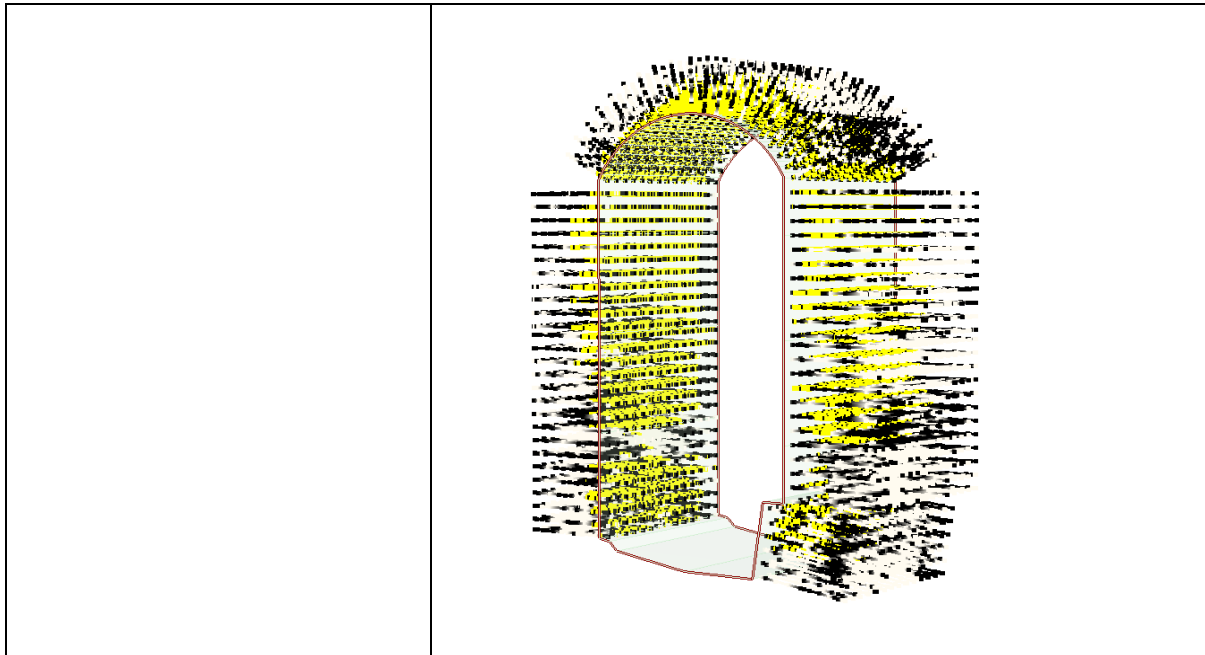
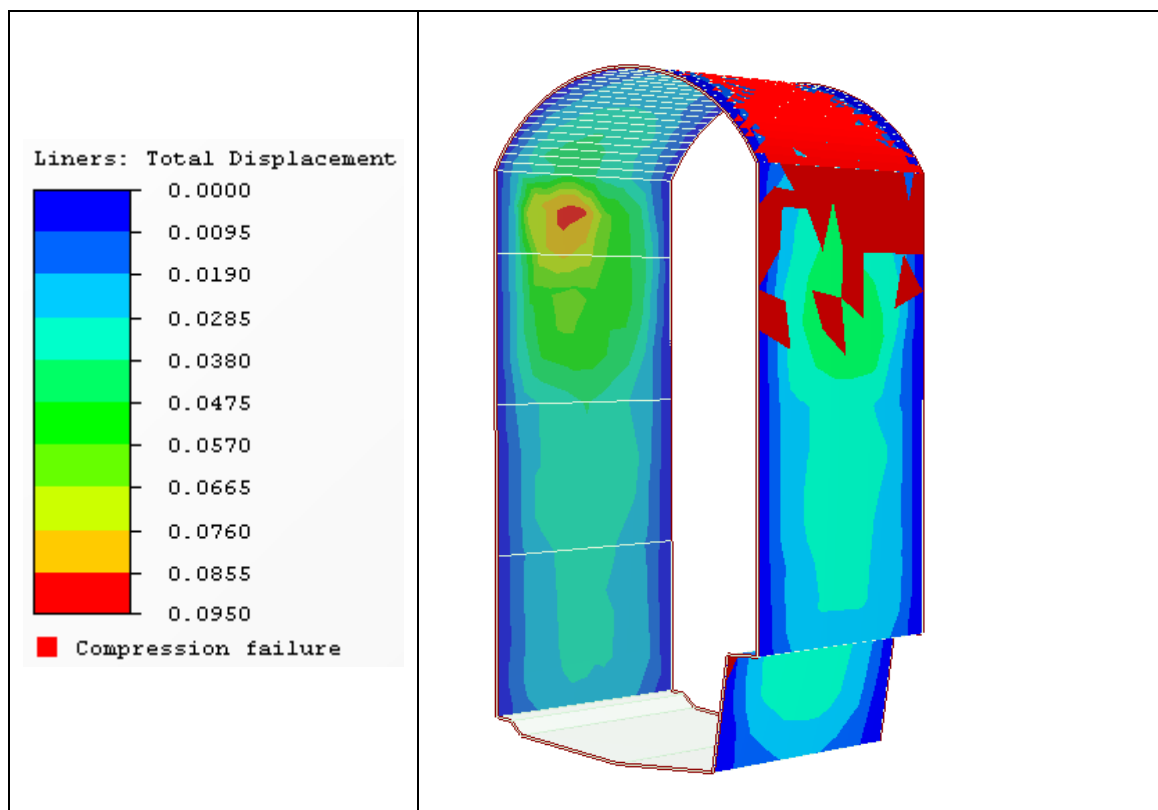


Figure 7-36. Yielding in rock bolts (Yellow) for worst case scenario(below), Original alignment (plastic model).

Figure 7-36 shows axial force and yield in rock bolts. Figure 7-37 shows total displacement and compression failure in the liner elements. Most of the rock bolts have failed under tension in roof and wall. The dilation parameter and an increased radius of the disturbed area affects the deformation and in turn leads to yielding of bolt elements. Liner elements have failed in compression in roof and top side walls (Figure 7-37).



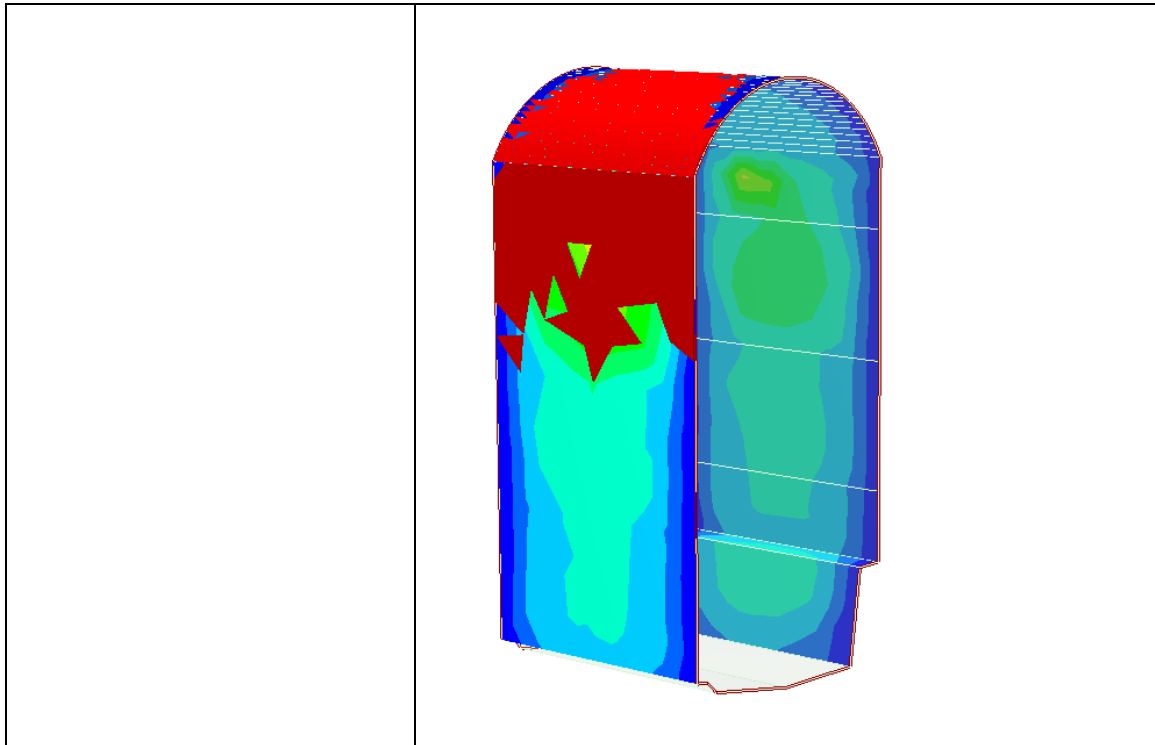


Figure 7-37. Yielding in liner (red) for worst case scenario(below)along with total displacement Original alignment (plastic model).

7.3.3 Discussion of model results

RS³ model results for alternative alignment are not different from the results of Phase2 analysis. Results are more conservative. For the best estimate model without the installed support, the original alignment had a total closure of powerhouse walls at 3 to 4 cm at maximum, yielding a strain level of 0.13 to 0.17 %. Strain level are within the stable limit of 1 % (Hoek, 2001).

Yielding of rock bolts and liner elements is similar to results from Phase2 analysis (Section 7.2.4).

All inputs in Phase2 analysis i.e. geometry, material properties, loading are similar to RS³ model. Hence, results have not varied significantly, although a 3D model shows better results. The reason can be the 3-dimensional aspect of the modelling and stress application.

The effect of dilation parameter is large on the modelling results in both Phase2 and RS³ model.

8 DISCUSSION

8.1 Stress situation

The quality of stability analysis depends critically on predicting the stress. When the cavern is excavated, the magnitude and direction of distributed in-situ stresses directly influence the behaviour of rock mass. Although in our case, the stress situation doesn't show a wide variation. Recommended values from the hydraulic fracturing test agency have been used (Section 4.2.1). The failure zone that forms around the cavern is a function of far-field stresses, strength of rock mass and geometry of the opening (Kaiser et al., 2000; Martin et al., 1999). Hence, uncertainty in input values applied to the stability analysis is always significant (Section 7.2.3). Additionally, there is uncertainty involved in verification of the results by stress modelling in section 7.2.1.3.

Eq- 7.1 used for the projection of horizontal stresses into the relevant cross section is questionable as it disregards shear stresses. Stress values are adjusted by 0.04 to 1.1 MPa after applying Eq- 7.1 for original alignment. The values are almost in line with the major principal horizontal stress from hydraulic fracturing tests. Compared to already existing uncertainties, this is a small adjustment. The reason is the angle between the length axis of the original alignment of the cavern, the major principal stress varies between 5° to 31° (Section 7.2.1.3). In the alternative alignment, stress values are adjusted by a significant amount of 1.03 to 3.44 MPa. The reason is the angle between the length axis and major principal stresses, which varies from 30° to 66° (Section 7.2.1.3).

Gravitational field stress is used for modelling stresses to account for variation of vertical stresses with depth and effect of topography on stress situation.

8.2 Placement and Orientation of caverns

In this thesis, the analysis uses the same location of the cavern for both alignments. The reason is that; land acquisition has already been completed for the project. The project has been conceptualized as a dam toe project with an underground powerhouse after studying four different alternative options with different layouts (Appendix L).

This leaves behind the option to check orientation and lateral movement, i.e. movement of the location deeper into the mountain. The orientation is discussed in detail (Section 8.2.1). Lateral movement is discussed in detail in section 7.2.4.

8.2.1 Orientation

The rosette plot in Figure 3-11 shows that the original and alternative alignments have a favourable orientation with respect to the major dominating joint set. The original alignment is nearly normal to the major dominating joint set and parallel to the second one. The alternative alignment is close to the bi-section of the angle between two major dominating joint sets. The alternative orientation is more favourable in terms of avoiding structurally induced instabilities (Section 2.6.3).

The original alignment is aligned nearly parallel to a major horizontal stress direction (Figure 3-11). It is optimal to avoid stress concentration in the roof, but tensional jointing might develop along the length axis. The orientation of the length axis is with major horizontal stress direction and may varied over an angle range of 5° to 31°. The alternative alignment is aligned at an intersection of directional range of major and minor horizontal principal stresses (Figure 3-11), This is not optimal regarding the concentration of projected stresses (Section 7.2.1.3) in the roof of the cavern. Although, high horizontal stresses will contribute to the confining pressure and thereby stabilize the cavern against wedge failure. The original alignment is more stable regarding stress induced instability (Section 2.6.3).

The main advantage of the alternative alignment is the reduction in length of the main access tunnel, tail race tunnel and bus duct tunnel. This saves cost and time. However, a slight change in pressure shaft orientation will result in an increase of steel liner length, balancing the cost advantage. Intake location and pressure shaft alignment are not discussed in detail in this thesis the for alternative case.

A tilted stress situation in the cross section of the cavern due to topographical effects can result in concentration of stresses in the part of the roof facing valley side, leaving the other side of the roof stress relieved, and block fall failure will increase, calling for extra carefulness.

8.3 Stability analysis

8.3.1 Stress distribution

With empirical and analytical methods, it is relatively difficult to achieve accurate calculations of the stress distribution. The irregular cavern shape and the angle between the principal stresses and the horizontal and vertical axes are the main reasons for such difficulties. Therefore, these results should merely be an indication rather than the exact values of stress magnitudes.

Table 8-1 shows the stress distribution around the excavated cavern calculated by different methods.

The topographical effect on stresses is seen clearly in numerical model results, which is not possible in analytical and empirical methods. Kirsch's equation does not take excavation shape into account, it is underestimating the stress values in the roof of the cavern. Rock mass properties that affect radial distribution of secondary stresses is also not taken into account in Kirsch's solution.

Table 8-1. Comparison of calculated stress distribution from analytical, empirical and numerical methods.

Description	Maximum Tangential Stress (MPa)			
	<i>Kirsch's Equation (average) (Table 6-1)</i>	<i>Hoek and Brown (1980) (average) (Table 6-2)</i>	<i>Numerical results (average) (Table 7-16 & Table 7-22)</i>	<i>Numerical results (No disturbed zone)</i>
Original Alignment	17.5	23.57	23.94	30.43
Alternate Alignment	22.55	30.75	27.40	41.55

Hoek and Brown (1980) proposed empirical methods produce stress values that correspond better for both original and alternative alignment with the disturbed zone, however lower than the values for undisturbed zone. The disturbed zone has a lower rock mass E-modulus than the rest of the rock mass, hence it passes some of the stress radially into the less disturbed rock mass. The excavation shapes used in the empirical method are generalized.

8.3.2 Failure and extent

The empirical predictions in section 5.3 propose minor spalling in alternative alignment, however, these predictions are not applicable to this thesis (Section 6.3).

Cai and Kaiser (2014) maintain that the spalling strength of 0.3-0.5 times UCS can only be used to describe field rock strength when the simplified model geometry is used (Section 5.3).

An in-situ spalling strength of 0.4 times UCS has been used in this thesis. Spalling is expected in the alternative alignment of the powerhouse cavern (Table 6-7) according to tangential stresses calculated from equations proposed by Hoek and Brown (1980) (Section 6.3).

The depth of failure calculated from Eq- 5.12 varies with the stress input (Table 6-8). Stress values from Kirsch's equation under-predicts the failure depth compared to numerical analysis. The extent of the failure is calculated only in the roof of the cavern. Table 6-8 shows the results for depth of failure calculated from the equation given by Martin and Christiansson (2009).

Section 7.2.2.2 describes failure extent in numerical analysis. Figure 7-21 and Figure 7-22 show the extent of brittle failure and yielded zone respectively. The numerical model takes into consideration the geometry of the excavation and the topographical effect of stresses.

The comparison table will mislead the reader, questioning the results from numerical model and equation for depth of failure. This study tells the uncertainties involved in predicting failure extent in caverns located at shallow depths and near the toe slope. Hence, the equation for depth of failure should be applied carefully when planning the hydropower cavern near the toe slope of a mountain at planning stage.

General trend of failure extent results from numerical analysis and failure depth equation show that original alignment is more stable as compared to alternative alignment. The study shows that to minimize the impact of brittle failure in caverns close to the toe slope, it is favourable to align the cavern length axis almost parallel to the major horizontal principal stress such that the horizontal stresses decrease in the cross section. Other measures can be to change the shape of the cavern, which could ease stress concentration in the roof such as reducing height/span ratio or adopting an elliptical shape. Due to practical reasons this is rarely an option used.

Rock mass failure due to low secondary stresses is only done through numerical analysis (Figure 7-20) in this thesis. Areas with negative tangential stresses are detected in walls of the powerhouse for both alignments (Figure 7-20). The largest extension of the negative stress zone occurs in the alternative alignment in comparison to the original alignment (Figure 7-28). This zone has a range of around 50 m approximately into the slope face measured diagonally from the cavern corner for alternative alignment, and the range is around 35 m for original alignment. Failure in this zone can be assumed to be consisting of diagonal joints extending to the slope face due to large horizontal virgin stresses. This is the reason rock bolts in the wall are proposed normal to the excavation surface for both alignments under study in this thesis.

The Hoek and Brown (1980) method used for estimation of tangential stresses for the cavern wall predicts negative tangential stresses in the power house wall for both alignments (Table 6-2). The values are in range with the numerical analysis. It is observed that results from methods predicted by Hoek and Brown (1980) are in acceptable range if used in the early stage of planning underground structures.

8.3.3 Rock mass quality and rock support

From the classification based on the Q-system, rock mass can be characterized as fair rock. RMR calculated from bore log and exploratory drift data also classifies the rock as fair rock. The GSI value calculated from RMR also describes rock mass as blocky and fair rock. GSI value used in modelling is on the conservative side (Table 6-4 & Table 6-5).

The support system estimated from RMR is limited, since it is developed for a 10m span horse shoe rock tunnel. Estimation by RMR system is not suitable for the Sach Khas HEP powerhouse cavern (23 m span). Q-system support chart is more appropriate because of its higher level of details. Q-system is a primary rock mass classification system used by the project authorities. It is more appropriate to use Q-system at planning stage along with RMR and GSI. There are always certain uncertainties involved, as rock mass classification systems are more applicable for stability problems caused by block fall, and not high stresses (Palmström and Stille, 2010). Bolt lengths proposed by the Q-system support chart (Table 6-13) correspond well with the bolt lengths estimated from empirical formulas (Table 6-10) and Unwedge probabilistic analysis (Table 7-2) for the roof.

All three methods suggest 6 m bolts for the roof. Q-system and empirical formulas (Table 6-10) suggest a 10 m bolt for the wall. Proposed bolt lengths in the numerical model are based on these initial values. Numerical analysis shows that bolt a length of 6 m for the roof is seen sufficient (Section 7.2.4). This justifies 6 m rock bolt length for roof from stress and block failure point of view. 10 m long bolts seem to be enough to deal with tensional yielding zone in wall according to numerical analysis. Bolt spacing used in numerical analysis is c/c: 1.5×1.5 m (Table 7-14), which is lower than spacing proposed by Q-system.

Shotcrete thickness proposed by Q-System support chart ranges from 7 to 12 cm (Table 6-13). To avoid extensive yielding of the beam elements in the roof, the thickness in the numerical model is increased to 15 cm for the roof in both cases. The compressive strength of shotcrete normally does not exceed the value of 35 MPa (Panthi, 2016). Therefore, shotcrete thickness in the roof is increased to minimise the yielding.

In comparison, support estimated from the numerical modelling results offer a much better idea about the kind of support system required for caverns near the toe slope and low cover. The support system estimated from numerical modelling is low as compared to the recommendations made by Hoek and Moy (1993) (Section 7.2.4).

A similar support system is used for better comparison of results in both alignments in numerical modelling.

9 CONCLUSION, RECOMMENDATIONS AND LIMITATIONS

9.1 Conclusions

Considering the location and importance of the powerhouse complex, it becomes important to provide a safe, secure and cost-effective design. This involves placement, orientation and overall stability of the cavern. Identifying potential challenges and developing a support plan according to these challenges is the prime objective of stability assessment. Stability assessment of Sach Khas HEP cavern shows brittle failure in the cavern roof due to high horizontal stresses. Secondary stresses causing tensile fracturing and shear failure in the cavern walls (Figure 7-22) propagating towards toe slope. Propagation of the yielded zone to the slope face is the main issue.

Assessment of location and orientation of the cavern is carried out in this thesis. Both alignments have advantages and disadvantages regarding orientation and location. The assessment of location and orientation are concluded as follows:

- Original Alignment
 - It is more stable in case of stress induced instability (Section 6.3, 7.3.3 & 8.2.1).
 - It has more favourable overburden, although the difference is very less (Table 7-5).
 - It is also safe for structurally induced stability after application of support (Section 7.1.5).
- Alternative Alignment
 - It is more favourable in terms of avoiding structurally induced instability (Section 7.1.5 and 8.2.1).

Analytical, empirical and numerical modelling methods are used in this thesis to document stability issues and evaluate rock support. The conclusions are summarized as follows:

- Alternative alignment will suffer from a large extent of brittle failure in cavern roof due to higher compressive stresses.
- Numerical calculation for depth of brittle failure does not correspond to results from empirical equation for spalling depth impact.
- The yielded zone for both the original and alternative alignment extend to the slope face (Figure 7-22). Original alignment has better location and orientation (Section 8.2 & 8.3), confirmed by RS³ modelling results (Section 7.3.3).

- Q-system and empirical formulas, both suggest bolt length of 6 m bolt for the roof and 10 m bolt for the wall. Similar lengths of bolts for the roof and the wall are provided in Numerical model but with different spacing, and further recommended (Section 8.3.3).
- 15 cm shotcrete thickness is recommended after analysing the numerical model for the trial thickness of 7, 12 and 15 cm. The shotcrete thickness is wall is kept same as 12 cm. This is applicable to both the alignments for better comparison.
- The results from worst case scenario are not acceptable for the cavern with such a large span (23 m). Hence, it is important to make sure that stress condition and rock mass properties are better than the worst case before the excavation commences in future.
- The situation regarding lateral placement of cavern i.e. deep in the rock is discussed in detail in section 7.2.4. The location of the cavern is kept same in this thesis.

Discussions of the results and conclusions tells the strength and weaknesses of the methods applied in this thesis. It is important to know the uncertainties involved, and caution should be taken in assessing the results (Section 7.2.3). A combination of several methods and their results are needed to build a strong foundation for a conclusion and building up a strong case for high-quality stability analysis. This can be achieved by minimising the error in input parameters. Without proper input parameters the analysis tool is worthless.

From the assessment of all the results from empirical, analytical and numerical modelling using different Rocscience packages, it is advisable to keep the alignment to its original state i.e. N55°E. This will result in saving both cost and time and avoid more critical stress situations. Furthermore, these finding must be updated with latest correct stress values and rock material properties. This will give a clearer view and understanding to the decision-makers and future construction planners.

Moving the cavern location further deep into the rock is a choice between geotechnical factors and water conductor hydraulics. Also length of bus duct tunnels will increase putting in picture the need for transformer cavern.

Keeping in view all factors discussed in conclusions, it is recommended to keep the location and orientation of the cavern same as original conceived by the project authorities.

9.2 Recommendations

Further work recommended on the basis of the studies carried out in this thesis:

- Bus duct tunnels will pass through yielded zone. Detailed analysis should be carried out in Examine3D to get the overall picture of the stress situation that will be generate

around the opening and its influence on the cavern and slope stability and challenges that will be faced during construction.

- Slope stability analysis should be carried out to study the effect of stress redistribution due to cavern excavation. Properties of the overburden should be studied in detail in regard to this study.
- Documentation and study of similar projects around the world should be done with respect to caverns located near the toe slope with low cover, and guidelines for numerical modelling should be made for analysis under gravitational field stress. Not much work is done except from Hoek and Moy (1993).
- When additional stress measurements are available, numerical analysis should be updated to increase the level of accuracy.

9.3 Limitations

Following are the limitations observed during the course of write-up for this thesis:

- The frequency of major joints noted in the exploratory drifts and rock out crop were not documented properly. This could have helped to plot a clearer joint rosette and do deterministic Unwedge analysis
- Major and minor principal horizontal stress values are taken from the recommendation in the test report. The basis for these recommendations is not properly documented in the test reports.
- The External boundaries used in Phase2 and RS3 analysis are based on the extent of the available rock line. Dizaji et al. (2015) in his study concluded the expansion factor for modelling tunnels or underground structures equal to 7 must be used, but the analysis carried out by him are for constant field stress condition. No study regarding boundary expansion factor for analysis under gravitational field stress is provided.
- Boundary conditions used in the RS³ are different from the ones used in used in Phase2 analysis. Only the surface-fixing conditions match the Phase2 analysis, corners and edges are fixed in all directions. This can be a reason for slight differences in results.

10 BIBLIOGRAPHY

- AECS Engineering and Geotechnical Services Pvt. Ltd, 2014. Report on hydraulic fracturing tests in the power house drift of proposed Sach Khas H.E. Project, Himachal Pradesh.
- Barton, N., 1999. The influence of joint properties in modelling jointed rock masses, 8th ISRM Congress. International Society for Rock Mechanics, pp. 1023-32.
- Barton, N., Bandis, S. and Bakhtar, K., 1985. Strength, deformation and conductivity coupling of rock joints, *International Journal of Rock Mechanics and Mining Sciences & Geomechanics Abstracts*. Elsevier, pp. 121-140.
- Barton, N., Lien, R. and Lunde, J., 1974. Engineering classification of rock masses for the design of tunnel support. *Rock mechanics*, 6(4): pp. 189-236.
- Barton, N., Loser, F., Lien, R. and Lunde, J., 1980. Application of Q-system in design decisions concerning dimensions and appropriate support for underground installations, *ISRM International Symposium-Rockstore 80*. International Society for Rock Mechanics, pp. 553-561.
- Bieniawski, Z., 1978. Determining rock mass deformability: experience from case histories, *International journal of rock mechanics and mining sciences & geomechanics abstracts*. Elsevier, pp. pp. 237-247.
- Bieniawski, Z.T., 1989. *Engineering rock mass classifications: a complete manual for engineers and geologists in mining, civil, and petroleum engineering*. John Wiley & Sons.
- BIS, 2002. IS : '9012 - 1978' - Recommended practice for shotcreting.
- Brudy, M., 1995. Determination of in-situ stress magnitude and orientation to 9 km depth at the KTB site. na.
- Cai, M. and Kaiser, P., 2014. In-situ rock spalling strength near excavation boundaries. *Rock mechanics and rock engineering*, 47(2): pp. 659-675.
- Cai, M., Kaiser, P., Tasaka, Y. and Minami, M., 2007. Determination of residual strength parameters of jointed rock masses using the GSI system. *International Journal of Rock Mechanics and Mining Sciences*, 44(2): pp. 247-265.
- Crowder, J. and Bawden, W., 2004. Review of post-peak parameters and behaviour of rock masses: current trends and research. *Rocnews*, fall: pp. 13.
- Dezes, P., Vannay, J.-C., Steck, A., Bussy, F. and Cosca, M., 1999. Synorogenic extension: Quantitative constraints on the age and displacement of the Zanskar shear zone (northwest Himalaya). *Geological Society of America Bulletin*, 111(3): pp. 364-374.
- Diederichs, M., 2007. The 2003 CGS Geocolloquium Address: Damage and spalling prediction criteria for deep tunnelling. *Can. Geotech. J*, 44(9): pp. 1082-1116.
- Diederichs, M., Carter, T. and Martin, C., 2010. Practical rock spall prediction in tunnels, *Tunnel Vision Towards 2020 (Proc. ITA-AITES World Tunnelling Congress, Vancouver, May)*. Paper No. fin00517 8pp.

- Dizaji, A.M., Hosseinitoudeshki, V. and Gheidari, M.H.N., 2015. Numerical analysis of boundary conditions to tunnels.
- DSI, 2016. Dywidag Systems International , HI-TEN Strand Cable Bolt 23.5mm. Product sheet (https://www.dywidag.co.uk/uploads/media/DSI_Alwag-Systems_DYWIDAG_Cable_Bolts_for_Mining_en_01.pdf).
- Edvardsson, S. and Broch, E., 2003. Underground powerhouses and high pressure tunnels. Norwegian University of Science and Technology, dpt of Hydraulic and Environment Engineering.
- Emdal, A., 2013. Introduksjon til geoteknikk. Institutt for bygg, anlegg og transport, NTNU. Tapir akademisk forlag. pp. 191
- Farmer, I. and Shelton, P., 1980. Factors that affect underground rock bolt reinforcement systems-design. Transactions of the institution of mining and metallurgy section a-mining industry, 89(APR): pp. 68-83.
- Gansser, A., 1964. Geology of the Himalayas, 289 pp. Interscience, New York.
- Goodman, R.E., 1989. Introduction to rock mechanics, 2. Wiley New York.
- Grimstad, E. and Barton, N., 1993. Updating the Q-system for NMT, Proc. int. symp. on sprayed concrete-modern use of wet mix sprayed concrete for underground support, pp. pp. 46-66.
- Haimson, B.C. and Lee, M.Y., 1984. Development of a wireline hydrofracturing technique and its use at a site of induced seismicity, The 25th US Symposium on Rock Mechanics (USRMS). American Rock Mechanics Association, pp. 194–203.
- Hammett, R. and Hoek, E., 1981. Design of large underground caverns for hydroelectric projects with particular reference to structurally controlled failure mechanisms. Recent Developments in Geotechnical Engineering for Hydro Projects.(Edited by Kulhawy FH): pp. 192-206.
- Hoek, E., 1994. Strength of rock and rock masses. ISRM News Journal, 2(2): pp. 4-16.
- Hoek, E., 2000. Large powerhouse caverns in weak rock. Rock engineering for tunnels.
- Hoek, E., 2001. Big Tunnels in Bad Rock: 2000 Terzaghi Lecture. ASCE Journal of Geotechnical and Geoenvironmental Engineering, 127: pp. 726-740.
- Hoek, E., 2007. Practical rock engineering.
- Hoek, E. and Brown, E.T., 1980. Underground excavations in rock.
- Hoek, E. and Brown, E.T., 1997. Practical estimates of rock mass strength. International Journal of Rock Mechanics and Mining Sciences, 34(8): pp. 1165-1186.
- Hoek, E., Carranza-Torres, C. and Corkum, B., 2002. Hoek-Brown failure criterion-2002 edition. Proceedings of NARMS-Tac, 1: pp. 267-273.
- Hoek, E. and Diederichs, M.S., 2006. Empirical estimation of rock mass modulus. International journal of rock mechanics and mining sciences, 43(2): pp. 203-215.






- Hoek, E., Kaiser, P. and Bawden, W., 1995. Support of underground excavations in hard rock AA Balkema Rotterdam 215. 215.
- Hoek, E., Kaiser, P.K. and Bawden, W.F., 2000. Support of underground excavations in hard rock. CRC Press.
- Hoek, E. and Marinos, P., 2007. A brief history of the development of the Hoek-Brown failure criterion. *Soils and rocks*, 2: pp. 1-8.
- Hoek, E. and Moy, D., 1993. Design of large powerhouse caverns in weak rock. *Comprehensive rock engineering*: pp. 85-110.
- Hudson, J. and Harrison, J., 1997. *Engineering rock mechanics: An introduction to the principles*, Imperial College of Science, Technology and Medicine, University of London, UK. Pergamon. Elsevier Science Ltd.
- Hudson, J.A., 1989. *Rock mechanics principles in engineering practice*.
- Hutchinson, D.J. and Diederichs, M.S., 1996. *Cablebolting in underground mines*. BiTech Publishers.
- International energy agency, 2015. *India energy outlook, World energy outlook special report*.
- Kaiser, P., Diederichs, M., Martin, C., Sharp, J. and Steiner, W., 2000. Underground works in hard rock tunnelling and mining, ISRM International Symposium. International Society for Rock Mechanics, pp. 841–926.
- Kaiser, P.K., 1996. *Canadian Rockburst Support Handbook: Prep. for Sponsors of the Canadian Rockburst Research*. Geomechanics Research Centre.
- Karlsrud, K. and Kveldevik, V., 2002. Control of water leakage when tunnelling under urban areas in the Oslo region, *Planning and Engineering for the Cities of Tomorrow. Second International Conference on Soil Structure Interaction in Urban Civil Engineering*.
- Larsen and Toubro(PDL), 2012a. Power Development limited (L&T), Sach Khas HEP (260 +7MW), Detailed Project Report - Geology Report - Lab and Field Test report (Volume III B).
- Larsen and Toubro(PDL), 2012b. Power Development limited (L&T), Sach Khas HEP (260 +7MW), Detailed Project Report - Main Geological Report (Volume III A).
- Larsen and Toubro(PDL), 2012c. Power Development limited (L&T), Sach Khas HEP (260 +7MW), Detailed Project Report - Main Report (Volume I).
- Liu, J., Li, Z. and Zhang, Z., 2004. Stability analysis of block in the surrounding rock mass of a large underground excavation. *Tunnelling and underground space technology*, 19(1): pp. 35-44.
- Marcher, T. and Saurer, E., 2013. *Design and verification challenges of hydropower plant caverns*. ILF Consulting Engineers Ltd.
- Marinos, P. and Hoek, E., 2000. GSI: a geologically friendly tool for rock mass strength estimation, ISRM International Symposium. International Society for Rock Mechanics.

- Marinos, V., Marinos, P. and Hoek, E., 2005. The geological strength index: applications and limitations. *Bulletin of Engineering Geology and the Environment*, 64(1): pp. 55-65.
- Martin, C. and Christiansson, R., 2009. Estimating the potential for spalling around a deep nuclear waste repository in crystalline rock. *International Journal of Rock Mechanics and Mining Sciences*, 46(2): pp. 219-228.
- Martin, C., Kaiser, P. and McCreath, D., 1999. Hoek-Brown parameters for predicting the depth of brittle failure around tunnels. *Canadian Geotechnical Journal*, 36(1): pp. 136-151.
- Martin, C.D., 1997. Seventeenth Canadian geotechnical colloquium: the effect of cohesion loss and stress path on brittle rock strength. *Canadian Geotechnical Journal*, 34(5): pp. 698-725.
- McCutchen, W., 1982. Some elements of a theory for in-situ stress. Technical note: *Int J Rock Mech Min Sci*, V19, N4, Aug 1982, P201–203, *International Journal of Rock Mechanics and Mining Sciences & Geomechanics Abstracts*. Pergamon, pp. 129.
- Ministry of Power, 2016. Annual Report 2014–2015, Government of India, New Delhi.
- Morelli, G.L., 2015. Variability of the GSI index estimated from different quantitative methods. *Geotechnical and Geological Engineering*, 33(4): pp. 983-995.
- Najman, Y., 2006. The detrital record of orogenesis: A review of approaches and techniques used in the Himalayan sedimentary basins. *Earth-Science Reviews*, 74(1): pp. 1-72.
- Nilsen, B. and Broch, E., 2009. *Ingeniørgeologi-berg grunnkurskompendium*. NTNU, Institutt for geologi og bergteknikk, Trondheim.
- Nilsen, B. and Palmström, A., 2000. *Engineering Geology and Rock Engineering: Handbook*. Norwegian Group for Rock Mechanics.
- Nilsen, B. and Thidemann, A., 1993. *Rock Engineering, Hydropower Development Vol. 9*. Norwegian Institute of Technology (NTH).
- Oreste, P. and Cravero, M., 2008. An analysis of the action of dowels on the stabilization of rock blocks on underground excavation walls. *Rock mechanics and rock engineering*, 41(6): pp. 835-868.
- Palmstrom, A. and Broch, E., 2006. Use and misuse of rock mass classification systems with particular reference to the Q-system. *Tunnelling and underground space technology*, 21(6): pp. 575-593.
- Palmstrom, A. and Stille, H., 2010. *Rock engineering*.
- Palmström, A. and Stille, H., 2010. *Rock Engineering*. sl. Thomas Telford.
- Panthi, K., 2006. Analysis of engineering geological uncertainties related to tunneling in Himalayan rock mass conditions. Doctoral theses at NTNU 2006: 41, Department of Geology and Mineral Resources Engineering, Norwegian University of Science and Technology (NTNU), Norway. Norwegian University of Science and Technology (NTNU), Trondheim. ISBN: pp. 82-471.

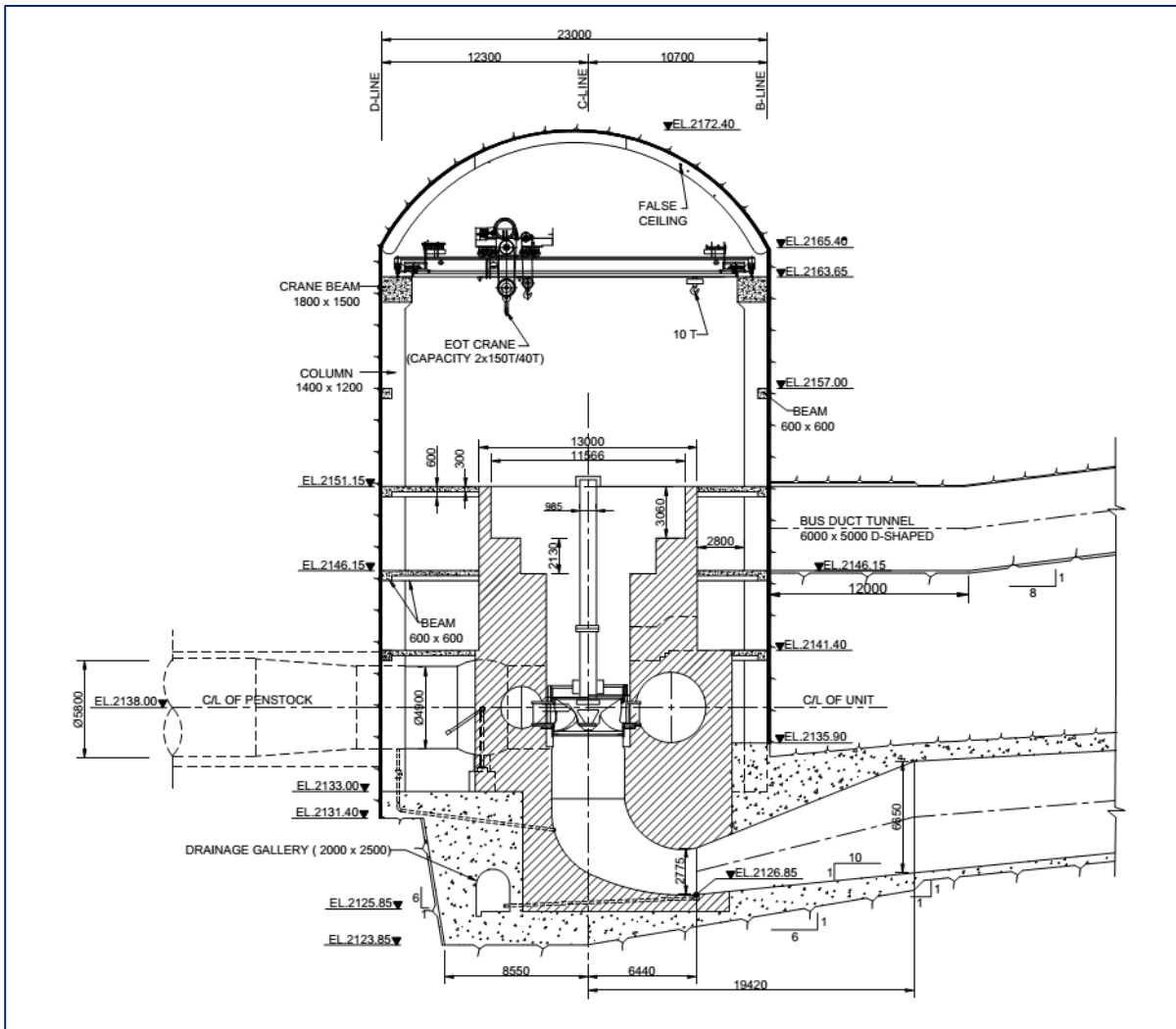
- Panthi, K., 2012. Evaluation of rock bursting phenomena in a tunnel in the Himalayas. *Bulletin of Engineering Geology and the Environment*, 71(4): pp. 761-769.
- Panthi, K., 2016. Personal correspondence with supervisor.
- RocScience, 2016a. Phase2 v9.0 webhelp.
- RocScience, 2016b. Unwedge v. 4.0 Tutorial-1, Quick Start.
- Shanker, R., Kumar, G. and Saxena, S., 1989. A Reappraisal. Special Publication Geological Survey of India, Geology and tectonics of the Himalaya, pp. pp. 1-60.
- VIKØrsta, 2012. CT-Bolt M33. Product sheet (<http://vikorsta.no/en/Products/Rock-support/CT-Bolt1/CT-Bolt-M33/>).
- www.dsiningproducts.com, 2016. DSI-Dywidag System International, Product-Rocks Bolts/Solid Bars/High Strength Bar.
- Zhao, J., 2000. Applicability of Mohr–Coulomb and Hoek–Brown strength criteria to the dynamic strength of brittle rock. *International Journal of Rock Mechanics and Mining Sciences*, 37(7): pp. 1115-1121.

ANNEXURES

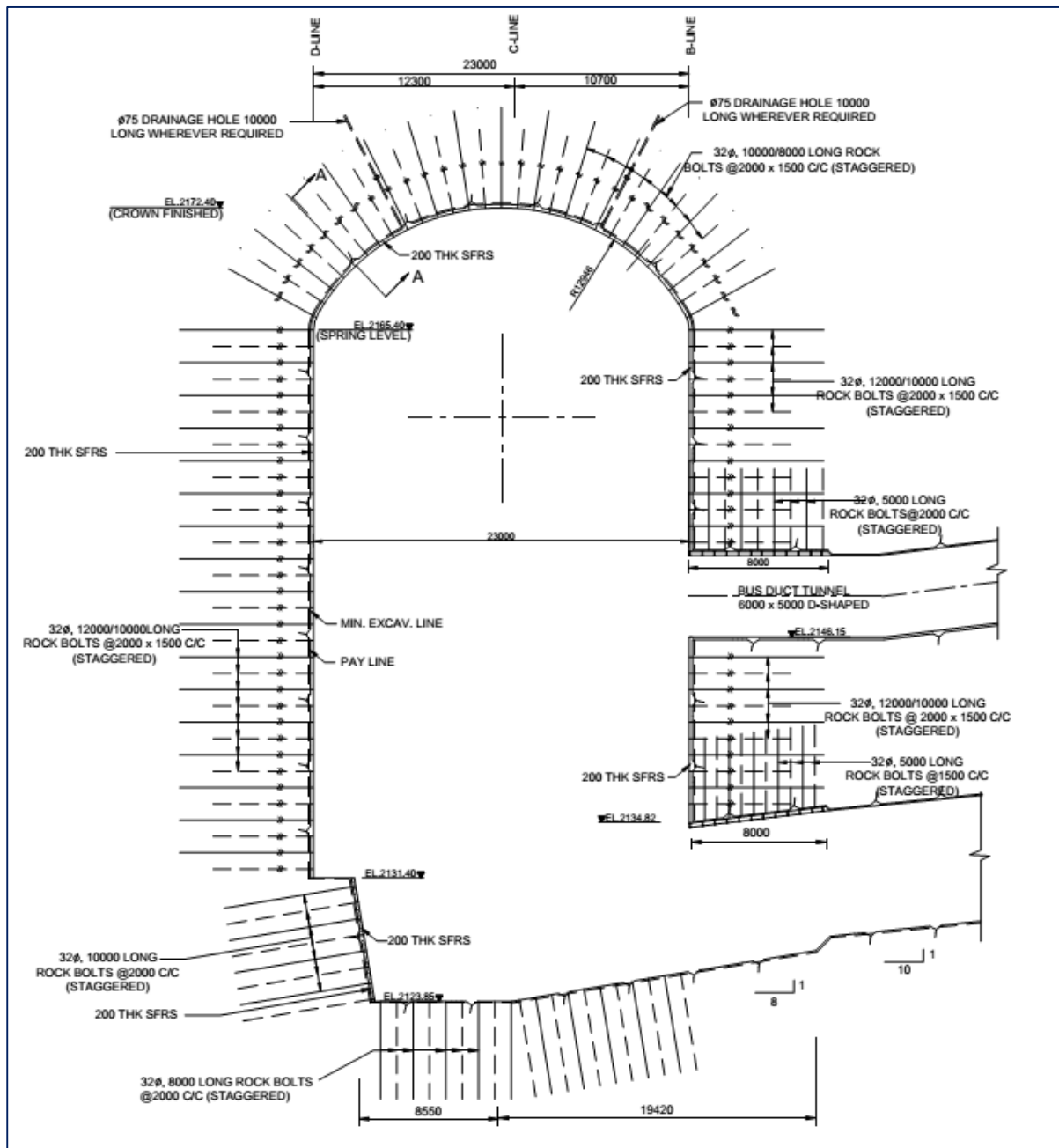
Appendix A: Guidelines for estimating disturbance factor D (Hoek, 2016)

Appearance of rock mass	Description of rock mass	Suggested value of <i>D</i>
	Excellent quality controlled blasting or excavation by Tunnel Boring Machine results in minimal disturbance to the confined rock mass surrounding a tunnel.	$D = 0$
	Mechanical or hand excavation in poor quality rock masses (no blasting) results in minimal disturbance to the surrounding rock mass. Where squeezing problems result in significant floor heave, disturbance can be severe unless a temporary invert, as shown in the photograph, is placed.	$D = 0$ $D = 0.5$ No invert
	Very poor quality blasting in a hard rock tunnel results in severe local damage, extending 2 or 3 m, in the surrounding rock mass.	$D = 0.8$
	Small scale blasting in civil engineering slopes results in modest rock mass damage, particularly if controlled blasting is used as shown on the left hand side of the photograph. However, stress relief results in some disturbance.	$D = 0.7$ Good blasting $D = 1.0$ Poor blasting
	Very large open pit mine slopes suffer significant disturbance due to heavy production blasting and also due to stress relief from overburden removal. In some softer rocks excavation can be carried out by ripping and dozing and the degree of damage to the slopes is less.	$D = 1.0$ Production blasting $D = 0.7$ Mechanical excavation

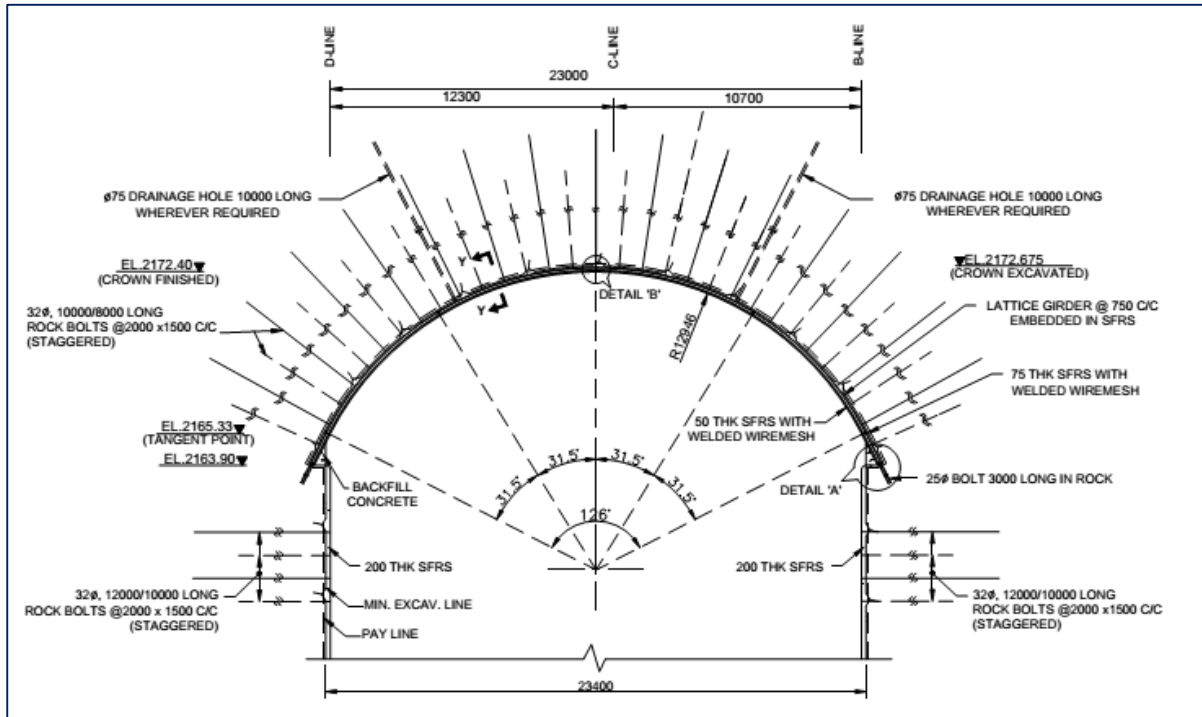
Appendix B : Cross section of the powerhouse cavern, Sach Khas HEP (Larsen and Toubro(PDL), 2012)



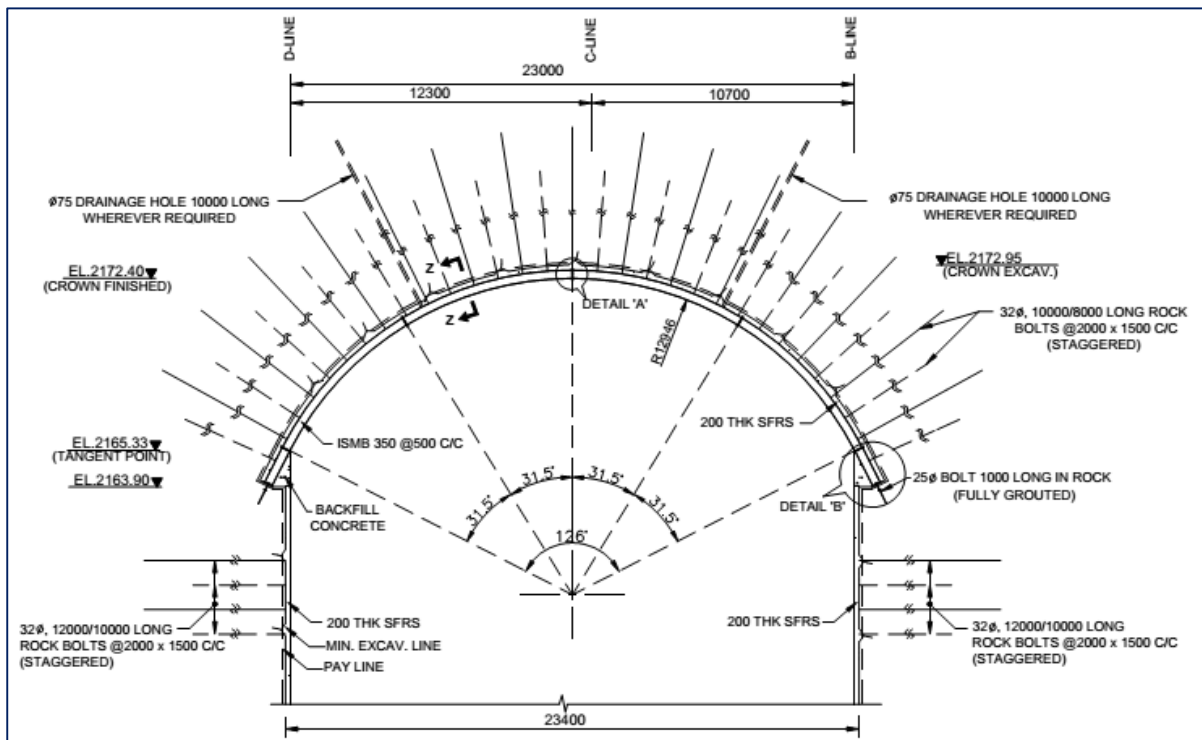
Appendix C : Proposed support in a cross section of the powerhouse cavern (Typical)
(Larsen and Toubro(PDL), 2012)



Appendix D: (I) Proposed support for crown only (Poor rock) (Larsen and Toubro(PDL), 2012)



Appendix D: (II) Proposed support for crown only (Very Poor rock)(Larsen and Toubro(PDL), 2012)



Appendix E: Drill holes used for Underground Cavern exploration study

DRILL HOLES	CODE	REMARKS
Three on the centre line of the power house cavern.	DH-21(abandoned), DH-21A, DH-20 and DH-19	The drill hole DH-18 encountered overburden up to the depth of 28m, DH-23, DH-13 and DH-5 encountered overburden thickness of (35m) (12m) (6m) respectively.
Two on the pressure shafts have been drilled.	DH-18 and DH-23	The drill hole DH-19 located on power house cavern has encountered overburden thickness of (16m) whereas 21A has overburden thickness of (48m).
Drill hole in the vicinity of dam and underground pressure shafts	DH-13	The hole DH-21 was abandoned at the depth of (36m) due to drilling problem.
One drilled in first stage programme.	DH-5	The sub surface exploration by drilling has confirmed the rock mass cover on the power house cavern is of the order of 45m excluding the overburden cover, which varies from (48m) in DH-21A and (17m) in DH-19 and DH-20 respectively

Appendix F: Prominent joint sets-Sach Khas underground power house cavern along with joint characteristics

Strike	Dip Angle	Dip Direction	Joint Characteristics	Remarks	cohesion (c) (MPa)	and friction angle (Φ)
N125 ⁰ - 120 ⁰ E	76 ⁰ -80 ⁰	215-210	Smooth undulating spacing 5-30cm; continuity >1m	The joint is parallel or sub parallel to the bedding and foliation; 5-15cm shear seams with rock flour or clay gouge are present especially at the contact of quartzite with phyllite. Upstream dipping joint.	0.38	31
N20 ⁰ - 30 ⁰ E	25 ⁰ -50 ⁰	110-120	Smooth planar, spacing 50-100cm; continuity >3m	Prominent joint set	0.03-0.08	32
N40 ⁰ E	50 ⁰	310	Smooth planar, spacing 50-100cm; continuity >3m, sub parallel to the valley	Prominent joint set. Needs specific treatment near the river edge.	0.03-0.08	32
N100 ⁰ E	50 ⁰	10	Smooth planar, spacing 100-200cm, continuity 5-7m	Prominent joint set.	0.03-0.08	32
N60 ⁰ E	76 ⁰	330	Smooth planar, spacing 50-100cm, continuity 3-5m	Downstream dipping joint set; 5-10cm thick shear seams with rock flour sub parallel to this joint set.	0.38	31
N153 ⁰ E	30 ⁰	243	Smooth planar, spacing 100-200cm, continuity 5-7m	Upstream valley ward dipping Rock flour/clay coating observed.	0.61-0.74	41
East	48 ⁰	0	Smooth planar, spacing 100-300cm, continuity 5-7m	Rock flour/clay coating observed	0.61-0.74	41

Appendix H: The RMR-system and guidelines for support (Hoek, 2016)

A. CLASSIFICATION PARAMETERS AND THEIR RATINGS									
Parameter		Range of values							
1	Strength of intact rock material	Point-load strength index	>10 MPa	4 - 10 MPa	2 - 4 MPa	1 - 2 MPa	For this low range - uniaxial compressive test is preferred		
		Uniaxial comp. strength	>250 MPa	100 - 250 MPa	50 - 100 MPa	25 - 50 MPa	5 - 25 MPa	1 - 5 MPa	< 1 MPa
		Rating	15	12	7	4	2	1	0
2	Drill core Quality RQD		90% - 100%	75% - 90%	50% - 75%	25% - 50%	< 25%		
	Rating		20	17	13	8	3		
3	Spacing of		> 2 m	0.6 - 2 . m	200 - 600 mm	60 - 200 mm	< 60 mm		
	Rating		20	15	10	8	5		
4	Condition of discontinuities (See E)		Very rough surfaces Not continuous No separation Unweathered wall rock	Slightly rough surfaces Separation < 1 mm Slightly weathered walls	Slightly rough surfaces Separation < 1 mm Highly weathered walls	Slickensided surfaces or Gouge < 5 mm thick or Separation 1-5 mm Continuous	Soft gouge >5 mm thick or Separation > 5 mm Continuous		
	Rating		30	25	20	10	0		
5	Groundwater	Inflow per 10 m tunnel length (l/m)	None	< 10	10 - 25	25 - 125	> 125		
		(Joint water press)/ (Major principal σ)	0	< 0.1	0.1, - 0.2	0.2 - 0.5	> 0.5		
	General conditions		Completely dry	Damp	Wet	Dripping	Flowing		
	Rating		15	10	7	4	0		
B. RATING ADJUSTMENT FOR DISCONTINUITY ORIENTATIONS (See F)									
Strike and dip orientations		Very favourable	Favourable	Fair	Unfavourable	Very Unfavourable			
Ratings	Tunnels & mines	0	-2	-5	-10	-12			
	Foundations	0	-2	-7	-15	-25			
	Slopes	0	-5	-25	-50				
C. ROCK MASS CLASSES DETERMINED FROM TOTAL RATINGS									
Rating	100 ← 81		80 ← 61	60 ← 41	40 ← 21	< 21			
Class number	I		II	III	IV	V			
Description	Very good rock		Good rock	Fair rock	Poor rock	Very poor rock			
D. MEANING OF ROCK CLASSES									
Class number	I		II	III	IV	V			
Average stand-up time	20 yrs for 15 m span		1 year for 10 m span	1 week for 5 m span	10 hrs for 2.5 m span	30 min for 1 m span			
Cohesion of rock mass (kPa)	> 400		300 - 400	200 - 300	100 - 200	< 100			
Friction angle of rock mass (deg)	> 45		35 - 45	25 - 35	15 - 25	< 15			
E. GUIDELINES FOR CLASSIFICATION OF DISCONTINUITY conditions									
Discontinuity length (persistence)	< 1 m		1 - 3 m	3 - 10 m	10 - 20 m	> 20 m			
Rating	6		4	2	1	0			
Separation (aperture)	None		< 0.1 mm	0.1 - 1.0 mm	1 - 5 mm	> 5 mm			
Rating	6		5	4	1	0			
Roughness	Very rough		Rough	Slightly rough	Smooth	Slickensided			
Rating	6		5	3	1	0			
Infilling (gouge)	None		Hard filling < 5 mm	Hard filling > 5 mm	Soft filling < 5 mm	Soft filling > 5 mm			
Rating	6		4	2	2	0			
Weathering	Unweathered		Slightly weathered	Moderately weathered	Highly weathered	Decomposed			
Rating	6		5	3	1	0			
F. EFFECT OF DISCONTINUITY STRIKE AND DIP ORIENTATION IN TUNNELLING**									
Strike perpendicular to tunnel axis				Strike parallel to tunnel axis					
Drive with dip - Dip 45 - 90°		Drive with dip - Dip 20 - 45°		Dip 45 - 90°		Dip 20 - 45°			
Very favourable		Favourable		Very unfavourable		Fair			
Drive against dip - Dip 45-90°		Drive against dip - Dip 20-45°		Dip 0-20 - Irrespective of strike°					
Fair		Unfavourable		Fair					

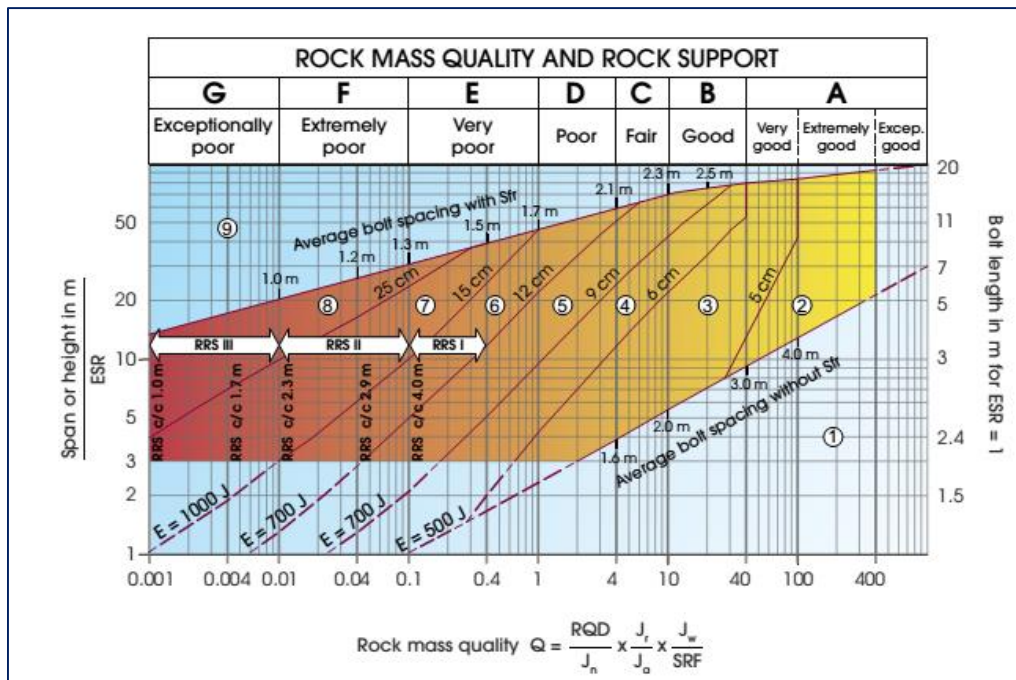
* Some conditions are mutually exclusive . For example, if infilling is present, the roughness of the surface will be overshadowed by the influence of the gouge. In such cases use A.4 directly.

** Modified after Wickham et al (1972).

Guidelines for excavation and support of 10 m span rock tunnels in accordance with the *RMR* system (After Bieniawski 1989)

Rock mass class	Excavation	Rock bolts (20 mm diameter, fully grouted)	Shotcrete	Steel sets
I - Very good rock <i>RMR</i> : 81-100	Full face, 3 m advance.	Generally no support required except spot bolting.		
II - Good rock <i>RMR</i> : 61-80	Full face , 1-1.5 m advance. Complete support 20 m from face.	Locally, bolts in crown 3 m long, spaced 2.5 m with occasional wire mesh.	50 mm in crown where required.	None.
III - Fair rock <i>RMR</i> : 41-60	Top heading and bench 1.5-3 m advance in top heading. Commence support after each blast. Complete support 10 m from face.	Systematic bolts 4 m long, spaced 1.5 - 2 m in crown and walls with wire mesh in crown.	50-100 mm in crown and 30 mm in sides.	None.
IV - Poor rock <i>RMR</i> : 21-40	Top heading and bench 1.0-1.5 m advance in top heading. Install support concurrently with excavation, 10 m from face.	Systematic bolts 4-5 m long, spaced 1-1.5 m in crown and walls with wire mesh.	100-150 mm in crown and 100 mm in sides.	Light to medium ribs spaced 1.5 m where required.
V – Very poor rock <i>RMR</i> : < 20	Multiple drifts 0.5-1.5 m advance in top heading. Install support concurrently with excavation. Shotcrete as soon as possible after blasting.	Systematic bolts 5-6 m long, spaced 1-1.5 m in crown and walls with wire mesh. Bolt invert.	150-200 mm in crown, 150 mm in sides, and 50 mm on face.	Medium to heavy ribs spaced 0.75 m with steel lagging and forepoling if required. Close invert.

Appendix I: The Q-system (NGI, 2013)



Support categories

- ① Unsupported or spot bolting
- ② Spot bolting, **SB**
- ③ Systematic bolting, fibre reinforced sprayed concrete, 5-6 cm, **B+Sfr**
- ④ Fibre reinforced sprayed concrete and bolting, 6-9 cm, **Sfr (E500)+B**
- ⑤ Fibre reinforced sprayed concrete and bolting, 9-12 cm, **Sfr (E700)+B**
- ⑥ Fibre reinforced sprayed concrete and bolting, 12-15 cm + reinforced ribs of sprayed concrete and bolting, **Sfr (E700)+RRS I +B**
- ⑦ Fibre reinforced sprayed concrete >15 cm + reinforced ribs of sprayed concrete and bolting, **Sfr (E1000)+RRS II+B**
- ⑧ Cast concrete lining, **CCA** or **Sfr (E1000)+RRS III+B**
- ⑨ Special evaluation

Bolts spacing is mainly based on Ø20 mm

E = Energy absorption in fibre reinforced sprayed concrete

ESR = Excavation Support Ratio

Areas with dashed lines have no empirical data

RRS - spacing related to Q-value

I Si30/6 Ø16 - Ø20 (span 10m)

D40/6+2 Ø16-20 (span 20m)

II Si35/6 Ø16-20 (span 5m)

D45/6+2 Ø16-20 (span 10m)

D55/6+4 Ø20 (span 20m)

III D40/6+4 Ø16-20 (span 5m)

D55/6+4 Ø20 (span 10m)

Special evaluation (span 20m)

Si30/6 = Single layer of 6 rebars,
30 cm thickness of sprayed concrete

D = Double layer of rebars

Ø16 = Rebar diameter is 16 mm

c/c = RRS spacing, centre - centre

1 RQD (Rock Quality Designation)			RQD
A	Very poor	(> 27 joints per m ³)	0-25
B	Poor	(20-27 joints per m ³)	25-50
C	Fair	(13-19 joints per m ³)	50-75
D	Good	(8-12 joints per m ³)	75-90
E	Excellent	(0-7 joints per m ³)	90-100

Note: i) Where RQD is reported or measured as ≤ 10 (including 0) the value 10 is used to evaluate the Q-value
ii) RQD-intervals of 5, i.e. 100, 95, 90, etc., are sufficiently accurate

2 Joint set number		J_n
A	Massive, no or few joints	0.5-1.0
B	One joint set	2
C	One joint set plus random joints	3
D	Two joint sets	4
E	Two joint sets plus random joints	6
F	Three joint sets	9
G	Three joint sets plus random joints	12
H	Four or more joint sets, random heavily jointed "sugar cube", etc	15
J	Crushed rock, earth like	20
Note: i) For tunnel intersections, use $3 \times J_n$ ii) For portals, use $2 \times J_n$		

3 Joint Roughness Number		J_r
a) Rock-wall contact, and b) Rock-wall contact before 10 cm of shear movement		
A	Discontinuous joints	4
B	Rough or irregular, undulating	3
C	Smooth, undulating	2
D	Slickensided, undulating	1.5
E	Rough, irregular, planar	1.5
F	Smooth, planar	1
G	Slickensided, planar	0.5
Note: i) Description refers to small scale features and intermediate scale features, in that order		
c) No rock-wall contact when sheared		
H	Zone containing clay minerals thick enough to prevent rock-wall contact when sheared	1
Note: ii) Add 1 if the mean spacing of the relevant joint set is greater than 3 m (dependent on the size of the underground opening) iii) $J_r = 0.5$ can be used for planar slickensided joints having lineations, provided the lineations are oriented in the estimated sliding direction		

4 Joint Alteration Number		Φ_r approx.	J_a
a) Rock-wall contact (no mineral fillings, only coatings)			
A	Tightly healed, hard, non-softening, impermeable filling, i.e., quartz or epidote.		0.75
B	Unaltered joint walls, surface staining only.	25-35°	1
C	Slightly altered joint walls. Non-softening mineral coatings; sandy particles, clay-free disintegrated rock, etc.	25-30°	2
D	Silty or sandy clay coatings, small clay fraction (non-softening).	20-25°	3
E	Softening or low friction clay mineral coatings, i.e., kaolinite or mica. Also chlorite, talc gypsum, graphite, etc., and small quantities of swelling clays.	8-16°	4
b) Rock-wall contact before 10 cm shear (thin mineral fillings)			
F	Sandy particles, clay-free disintegrated rock, etc.	25-30°	4
G	Strongly over-consolidated, non-softening, clay mineral fillings (continuous, but <5 mm thickness).	16-24°	6
H	Medium or low over-consolidation, softening, clay mineral fillings (continuous, but <5 mm thickness).	12-16°	8
J	Swelling-clay fillings, i.e., montmorillonite (continuous, but <5 mm thickness). Value of J_a depends on percent of swelling clay-size particles.	6-12°	8-12
c) No rock-wall contact when sheared (thick mineral fillings)			
K	Zones or bands of disintegrated or crushed rock. Strongly over-consolidated.	16-24°	6
L	Zones or bands of clay, disintegrated or crushed rock. Medium or low over-consolidation or softening fillings.	12-16°	8
M	Zones or bands of clay, disintegrated or crushed rock. Swelling clay. J_a depends on percent of swelling clay-size particles.	6-12°	8-12
N	Thick continuous zones or bands of clay. Strongly over-consolidated.	12-16°	10
O	Thick, continuous zones or bands of clay. Medium to low over-consolidation.	12-16°	13
P	Thick, continuous zones or bands with clay. Swelling clay. J_a depends on percent of swelling clay-size particles.	6-12°	13-20

5 Joint Water Reduction Factor		J_w
A	Dry excavations or minor inflow (humid or a few drips)	1.0
B	Medium inflow, occasional outwash of joint fillings (many drips/"rain")	0.66
C	Jet inflow or high pressure in competent rock with unfilled joints	0.5
D	Large inflow or high pressure, considerable outwash of joint fillings	0.33
E	Exceptionally high inflow or water pressure decaying with time. Causes outwash of material and perhaps cave in	0.2-0.1
F	Exceptionally high inflow or water pressure continuing without noticeable decay. Causes outwash of material and perhaps cave in	0.1-0.05
<p>Note: i) Factors C to F are crude estimates. Increase J_w if the rock is drained or grouting is carried out</p> <p>ii) Special problems caused by ice formation are not considered</p>		

6 Stress Reduction Factor			SRF	
a) Weak zones intersecting the underground opening, which may cause loosening of rock mass				
A	Multiple occurrences of weak zones within a short section containing clay or chemically disintegrated, very loose surrounding rock (any depth), or long sections with incompetent (weak) rock (any depth). For squeezing, see 6L and 6M		10	
B	Multiple shear zones within a short section in competent clay-free rock with loose surrounding rock (any depth)		7.5	
C	Single weak zones with or without clay or chemical disintegrated rock (depth $\leq 50\text{m}$)		5	
D	Loose, open joints, heavily jointed or "sugar cube", etc. (any depth)		5	
E	Single weak zones with or without clay or chemical disintegrated rock (depth $> 50\text{m}$)		2.5	
Note: i) Reduce these values of SRF by 25-50% if the weak zones only influence but do not intersect the underground opening				
b) Competent, mainly massive rock, stress problems		σ_c / σ_1	σ_θ / σ_c	SRF
F	Low stress, near surface, open joints	>200	<0.01	2.5
G	Medium stress, favourable stress condition	200-10	0.01-0.3	1
H	High stress, very tight structure. Usually favourable to stability. May also be unfavourable to stability dependent on the orientation of stresses compared to jointing/weakness planes*	10-5	0.3-0.4	0.5-2 2-5*
J	Moderate spalling and/or slabbing after > 1 hour in massive rock	5-3	0.5-0.65	5-50
K	Spalling or rock burst after a few minutes in massive rock	3-2	0.65-1	50-200
L	Heavy rock burst and immediate dynamic deformation in massive rock	<2	>1	200-400
Note: ii) For strongly anisotropic virgin stress field (if measured): when $5 \leq \sigma_1 / \sigma_3 \leq 10$, reduce σ_c to $0.75 \sigma_c$. When $\sigma_1 / \sigma_3 > 10$, reduce σ_c to $0.5 \sigma_c$, where σ_c = unconfined compression strength, σ_1 and σ_3 are the major and minor principal stresses, and σ_θ = maximum tangential stress (estimated from elastic theory)				
iii) When the depth of the crown below the surface is less than the span; suggest SRF increase from 2.5 to 5 for such cases (see F)				
c) Squeezing rock: plastic deformation in incompetent rock under the influence of high pressure		σ_θ / σ_c	SRF	
M	Mild squeezing rock pressure	1-5	5-10	
N	Heavy squeezing rock pressure	>5	10-20	
Note: iv) Determination of squeezing rock conditions must be made according to relevant literature (i.e. Singh et al., 1992 and Bhasin and Grimstad, 1996)				
d) Swelling rock: chemical swelling activity depending on the presence of water			SRF	
O	Mild swelling rock pressure		5-10	
P	Heavy swelling rock pressure		10-15	

7 Type of excavation		ESR
A	Temporary mine openings, etc.	ca. 3-5
B	Vertical shafts*: i) circular sections ii) rectangular/square section * Dependant of purpose. May be lower than given values.	ca. 2.5 ca. 2.0
C	Permanent mine openings, water tunnels for hydro power (exclude high pressure penstocks) water supply tunnels, pilot tunnels, drifts and headings for large openings.	1.6
D	Minor road and railway tunnels, surge chambers, access tunnels, sewage tunnels, etc.	1.3
E	Power houses, storage rooms, water treatment plants, major road and railway tunnels, civil defence chambers, portals, intersections, etc.	1.0
F	Underground nuclear power stations, railways stations, sports and public facilities, factories, etc.	0.8
G	Very important caverns and underground openings with a long lifetime, ≈ 100 years, or without access for maintenance.	0.5

NOTE: It is recommended to use ESR = 1.0 when $Q \leq 0.1$ for the types of excavation B, C and D. The reason for that is that the stability problems may be severe with such low Q-values, perhaps with risk for cave-in.

In addition to the span (or wall height) ESR gives the "Equivalent dimension" in the following way:

$$\frac{\text{Span or height in m}}{\text{ESR}} = \text{Equivalent dimension}$$

Conversion from actual Q-values to adjusted Q-values for design of wall support

In rock masses of good quality	$Q > 10$	Multiply Q-values by a factor of 5.
For rock masses of intermediate quality	$0.1 < Q < 10$	Multiply Q-values by a factor of 2.5. In cases of high rock stresses, use the actual Q-value.
For rock masses of poor quality	$Q < 0.1$	Use actual Q-value.

Appendix J: Values of the constant m_i for intact rock (Hoek, 2016)

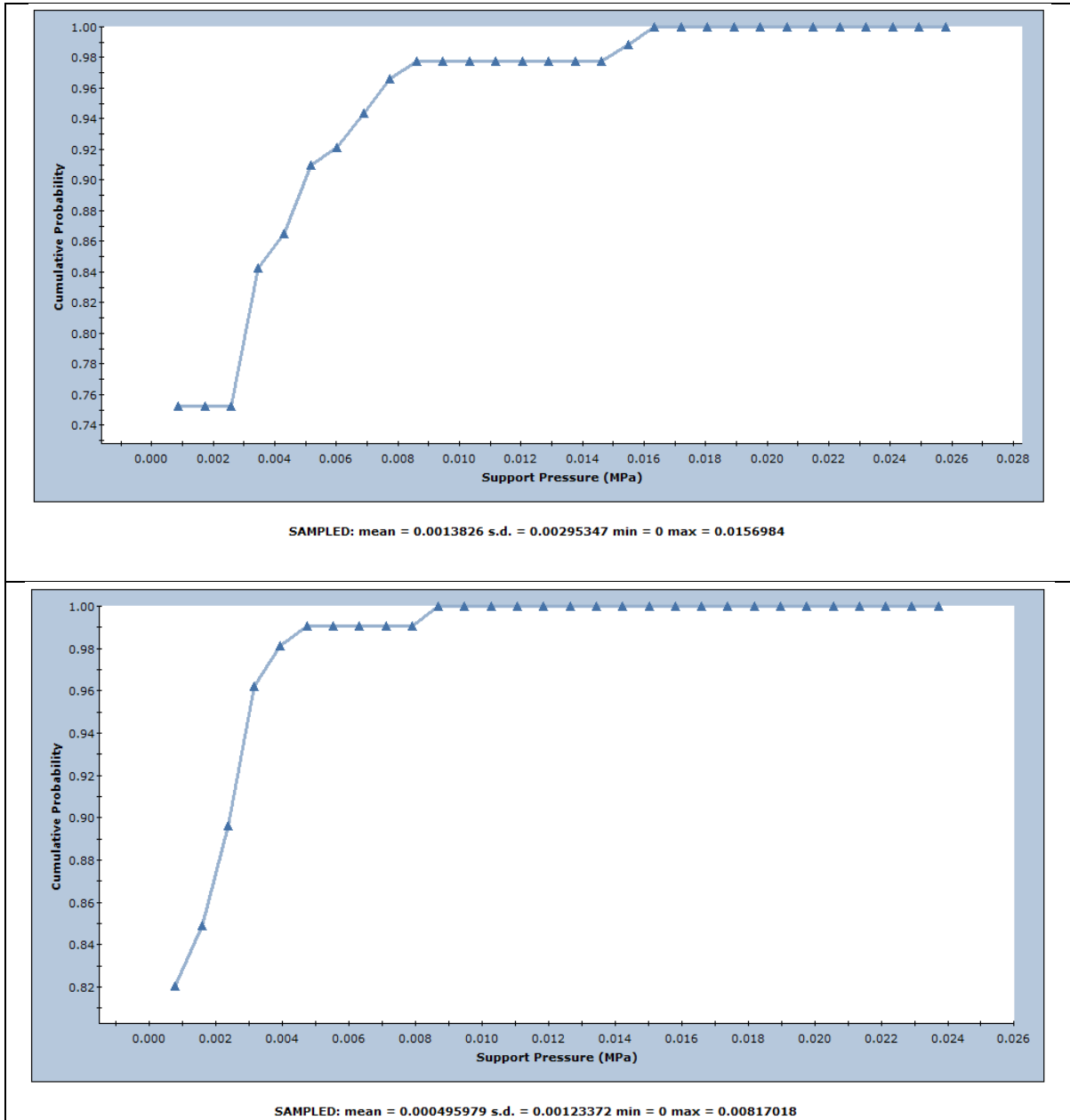
Rock type	Class	Group	Texture			
			Coarse	Medium	Fine	Very fine
SEDIMENTARY	Clastic		Conglomerates* (21 ± 3)	Sandstones 17 ± 4	Siltstones 7 ± 2	Claystones 4 ± 2
			Breccias (19 ± 5)		Greywackes (18 ± 3)	Shales (6 ± 2)
	Non-Clastic	Carbonates	Crystalline Limestone (12 ± 3)	Sparitic Limestones (10 ± 2)	Micritic Limestones (9 ± 2)	Dolomites (9 ± 3)
		Evaporites		Gypsum 8 ± 2	Anhydrite 12 ± 2	
		Organic			Chalk 7 ± 2	
METAMORPHIC	Non Foliated		Marble 9 ± 3	Hornfels (19 ± 4) Metasandstone (19 ± 3)	Quartzites 20 ± 3	
	Slightly foliated		Migmatite (29 ± 3)	Amphibolites 26 ± 6		
	Foliated**		Gneiss 28 ± 5	Schists 12 ± 3	Phyllites (7 ± 3)	Slates 7 ± 4
IGNEOUS	Plutonic	Light	Granite 32 ± 3 Granodiorite (29 ± 3)	Diorite 25 ± 5		
		Dark	Gabbro 27 ± 3 Norite 20 ± 5	Dolerite (16 ± 5)		
	Hypabyssal		Porphyries (20 ± 5)		Diabase (15 ± 5)	Peridotite (25 ± 5)
	Volcanic	Lava		Rhyolite (25 ± 5) Andesite 25 ± 5	Dacite (25 ± 3) Basalt (25 ± 5)	Obsidian (19 ± 3)
		Pyroclastic	Agglomerate (19 ± 3)	Breccia (19 ± 5)	Tuff (13 ± 5)	

* Conglomerates and breccias may present a wide range of m_i values depending on the nature of the cementing material and the degree of cementation, so they may range from values similar to sandstone to values used for fine grained sediments.

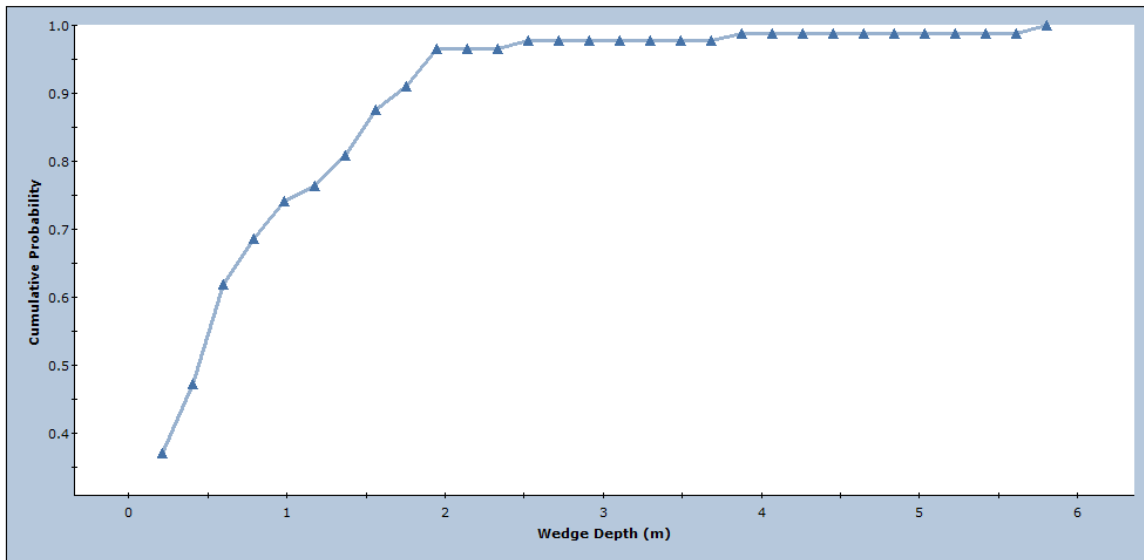
** These values are for intact rock specimens tested normal to bedding or foliation. The value of m_i will be significantly different if failure occurs along a weakness plane.

Appendix K: Cumulative frequency plots of Probability view Unwedge analysis

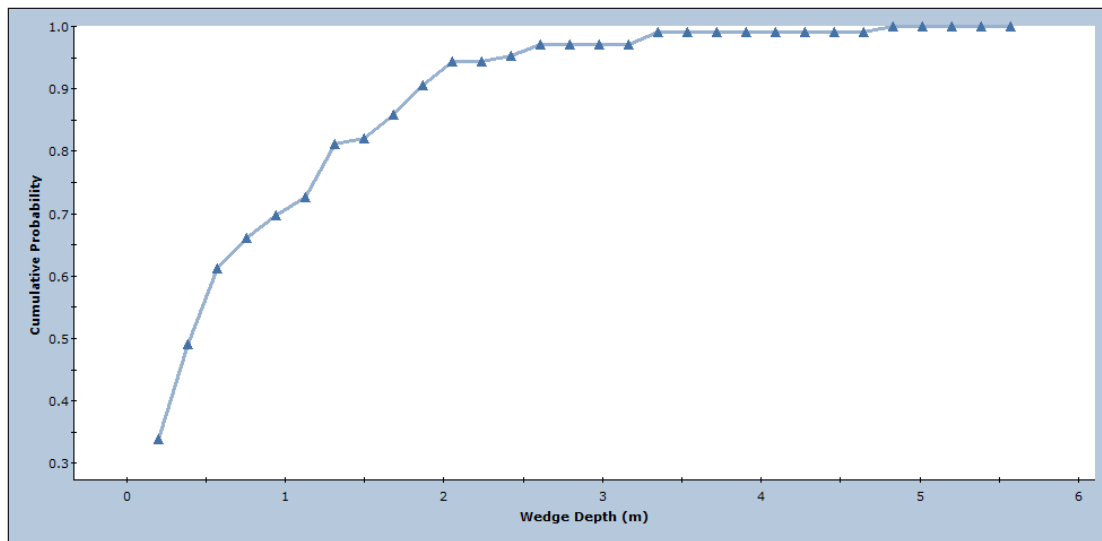
Cumulate Probability 1: Maximum support pressure (MPa) cumulative probability plot for each segment of cavern roof for Original Alignment N55°E(Top) & Alternative Alignment N20°E (Bottom)



Cumulate Probability 2: Maximum wedge depth (m) cumulative probability plot for each segment of cavern roof for Original Alignment N55°E(Top) & Alternative Alignment N20°E (Bottom)

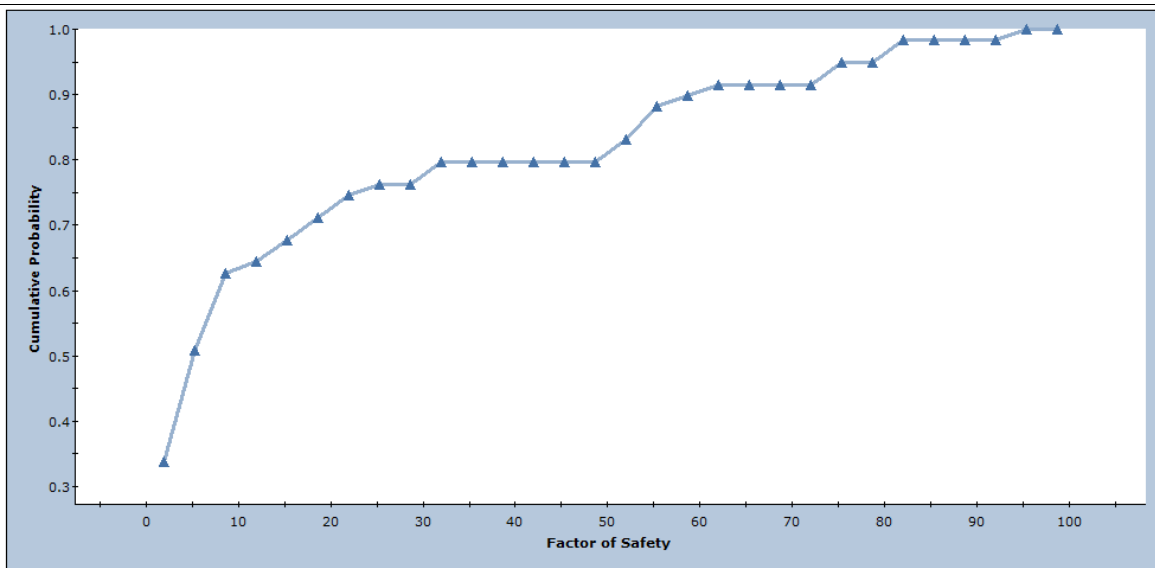
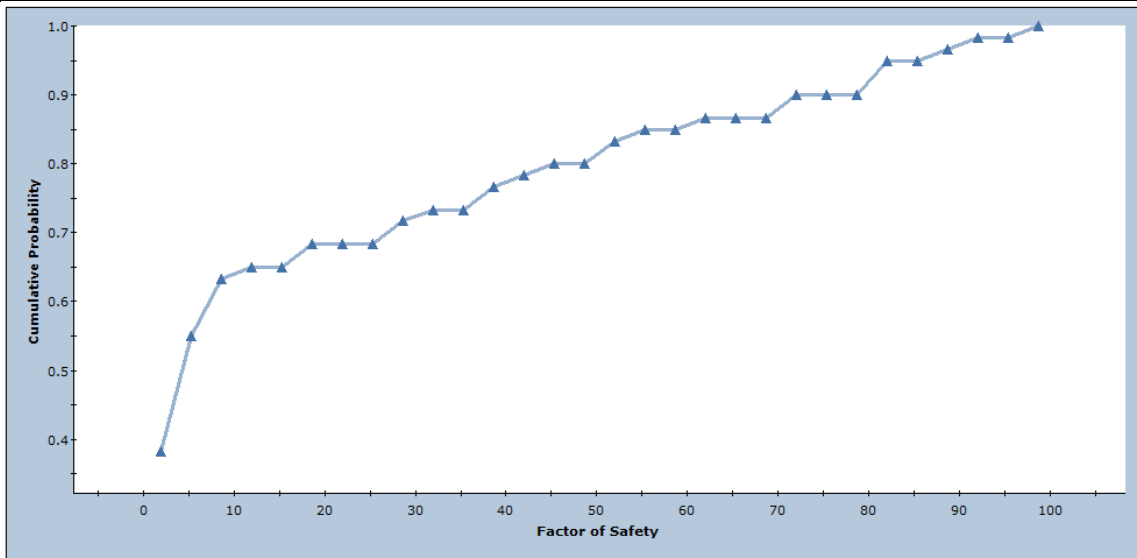


SAMPLED: mean = 0.716429 s.d. = 0.856079 min = 0.0216329 max = 5.80237

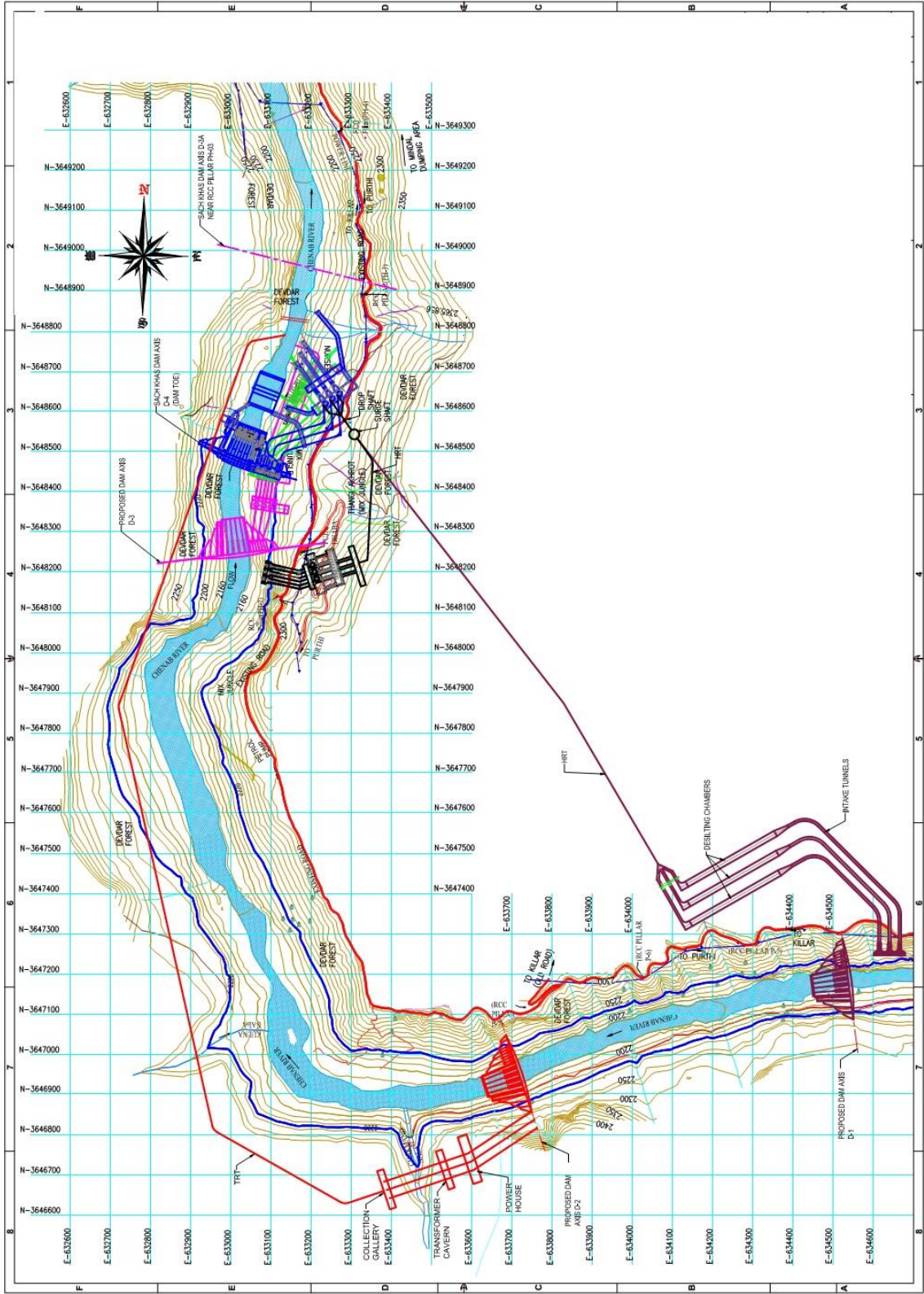


SAMPLED: mean = 0.74757 s.d. = 0.82438 min = 0.0197884 max = 4.75841

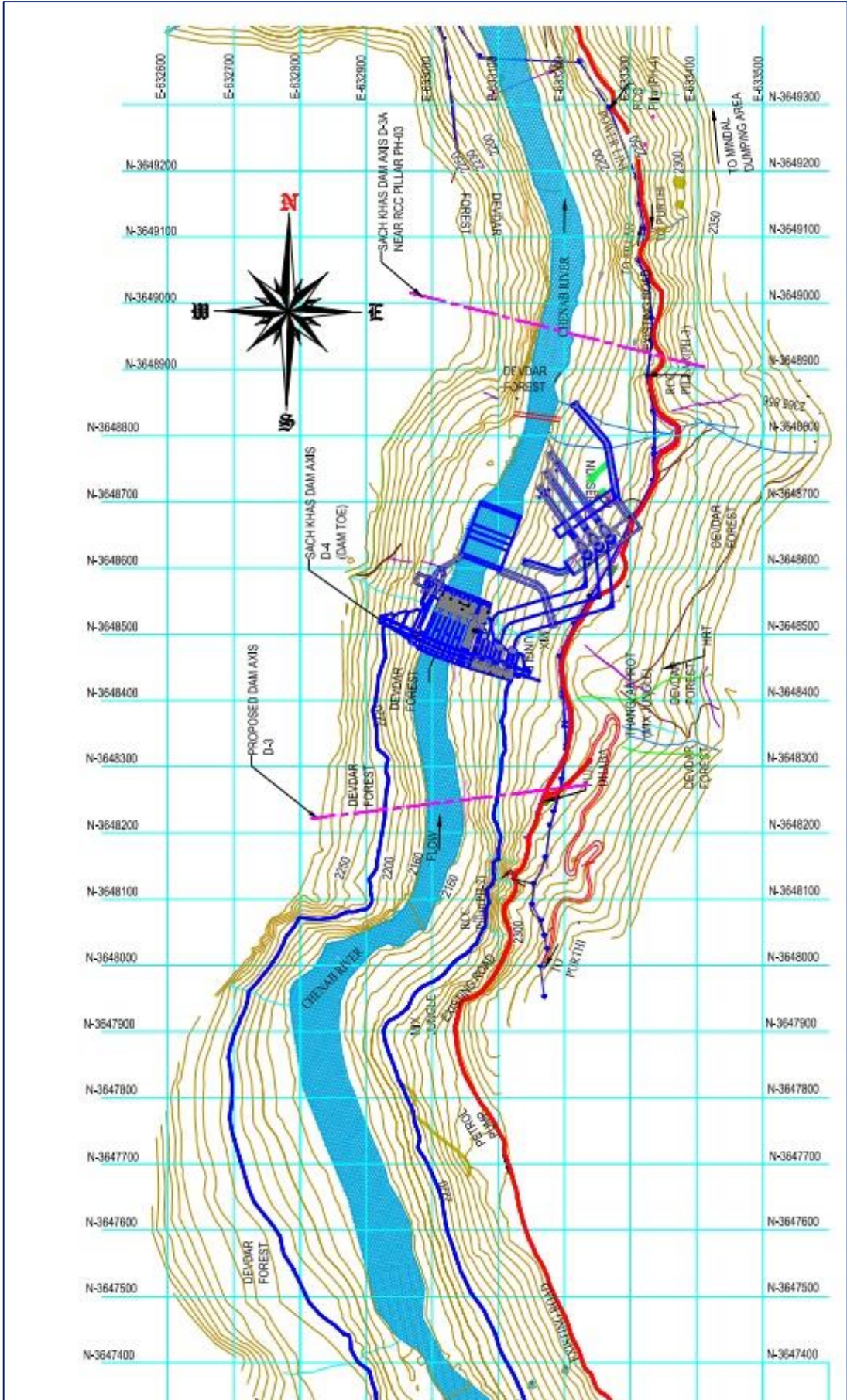
Cumulate Probability 3: Minimum factor of safety (Probabilistic) cumulative probability plot for each segment of cavern roof for Original Alignment N55°E(Top) & Alternative Alignment N20°E (Bottom)



Appendix L: Alternative sites - layouts and selection (Final Layout in Blue)



APPENDIX M: Layout plan underground power house cavern (Final)



APPENDIX N: Project Layout features

Concrete Gravity Dam	
Height	90.00 m (From assumed deepest foundation level)
Dam Length at top	251.5 m
Sluice Spillway	
Sluice size	7.5m (W) x 12.3m (H)
Intakes	
Number (Primary, on right non-overflow blocks)	3 (142.707 cumec each)
Gate Size	6.6m (W) x 5.8m (H).
Secondary Intake Number (on Left Non-Overflow Block)	1 (12 cumec)
Gate Size	2.2m (W) x 2.5m (H)
Pressure Shafts	
Number (Primary)	3
Diameter	5.8 m
Length Avg.	300m
Number secondary pressure shaft	1
Diameter	2.5m up to bifurcation , 1.75m after
Length Avg.	92 m up to bifurcation , 33.5m & 28m after bifurcation
Underground power house	
Dimensions	126m (L) x 23m (W) x 48.5m (H)
Power units	3 x 86.7 MW
Secondary surface power house	
Dimensions	52m (L) x 15m (W) x 32m (H)
Power units	7.5MW (2 units, one standby)
Tail Race Tunnels	
Number	3 (D-shaped)
Lengths	99.75m, 113.13m & 132.35m

**APPENDIX O: Shear strength of filled discontinuities and filling materials
(After Barton (1975))**

Rock	Description	Peak c' (MPa)	Peak ϕ°	Residual c' (MPa)	Residual ϕ°
Basalt	Clayey basaltic breccia, wide variation from clay to basalt content	0.24	42		
Bentonite	Bentonite seam in chalk	0.015	7.5		
	Thin layers	0.09-0.12	12-17		
	Triaxial tests	0.06-0.1	9-13		
Bentonitic shale	Triaxial tests	0-0.27	8.5-29		
	Direct shear tests			0.03	8.5
Clays	Over-consolidated, slips, joints and minor shears	0-0.18	12-18.5	0-0.003	10.5-16
Clay shale	Triaxial tests	0.06	32		
	Stratification surfaces			0	19-25
Coal measure rocks	Clay mylonite seams, 10 to 25 mm	0.012	16	0	11-11.5
Dolomite	Altered shale bed, \pm 150 mm thick	0.04	1(5)	0.02	17
Diorite, granodiorite and porphyry	Clay gouge (2% clay, P1 = 17%)	0	26.5		
Granite	Clay filled faults	0-0.1	24-45		
	Sandy loam fault filling	0.05	40		
	Tectonic shear zone, schistose and broken granites, disintegrated rock and gouge	0.24	42		
Greywacke	1-2 mm clay in bedding planes			0	21
Limestone	6 mm clay layer			0	13
	10-20 mm clay fillings	0.1	13-14		
	<1 mm clay filling	0.05-0.2	17-21		
Limestone, marl and lignites	Interbedded lignite layers	0.08	38		
	Lignite/marl contact	0.1	10		
Limestone	Marlaceous joints, 20 mm thick	0	25	0	15-24
Lignite	Layer between lignite and clay	0.014-0.03	15-17.5		
Montmorillonite	80 mm seams of bentonite (montmorillonite) clay in chalk	0.36	14	0.08	11
Bentonite clay		0.016-0.02	7.5-11.5		
Schists, quartzites and siliceous schists	100-15- mm thick clay filling	0.03-0.08	32		
	Stratification with thin clay	0.61-0.74	41		
	Stratification with thick clay	0.38	31		
Slates	Finely laminated and altered	0.05	33		
Quartz / kaolin / pyrolusite	Remoulded triaxial tests	0.042-0.09	36-38		